Petrology of platinum-group element mineralization in the Koillismaa intrusion, Finland

Jon Gustafsson

Dissertations in Geology at Lund University,
Master's thesis, no 576
(45 hp/ECTS credits)

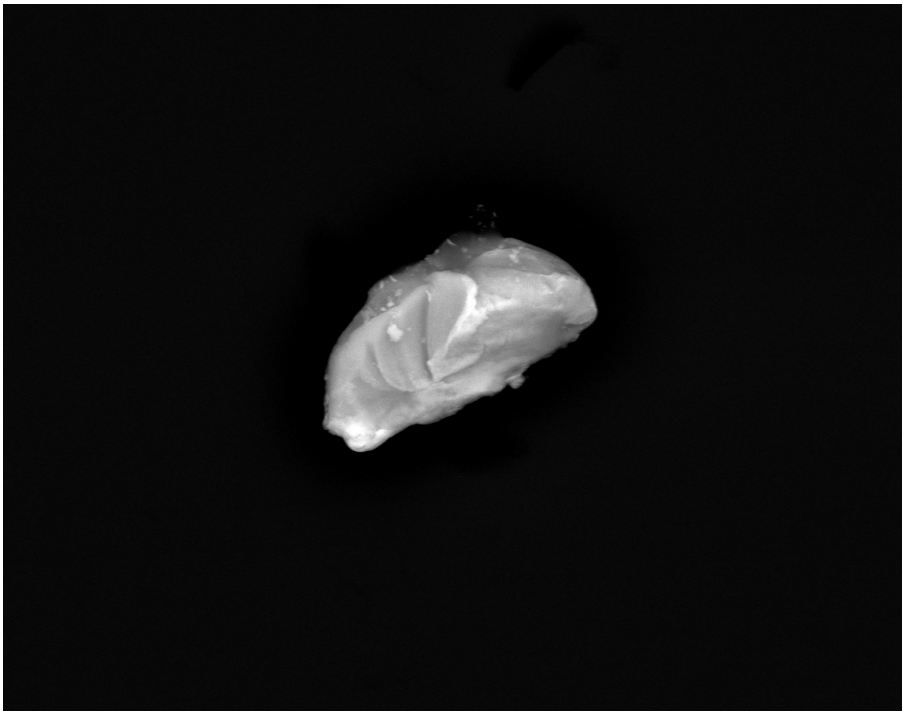

Department of Geology
Lund University
2019

Petrology of platinum-group element mineralization in the Koillismaa intrusion, Finland

Master's thesis
Jon Gustafsson

Department of Geology
Lund University
2019

Contents

Cover Picture Jon Gustafsson: SEM-EDS image of a platinum-group mineral grain (AuPd-alloy) in a silicate matrix, from the Marginal Series of the Koillismaa intrusion. The grain is approximatley 10µm in length.

Petrology of platinum-group element mineralization in the Koillismaa intrusion, Finland

JON GUSTAFSSON

Gustafsson, J., 2019: Petrology of PGE mineralization in the Koillismaa intrusion, Finland . *Dissertations in Geology at Lund University*, No. 576 71 pp. 45 hp (45 ECTS credits) .

Abstract: The 2.44 Ga Koillismaa intrusion of the Koillismaa-Näränkävaara Layered Complex, in northeastern Finland, has been studied in order to assess the formation processes involved during platinum-group element (PGE) mineralization. The layered series is host to the reef-type mineralization called Rometölväs Reef, and the marginal series contains contact-type mineralization. This MSc-project, besides giving an in-depth review of PGE mineralization in layered intrusions, tries to elucidate the origin of PGE mineralization in the Koillismaa intrusion, via SEM-EDS mapping of platinum-group minerals (PGM) and $\delta^{34}S$ in-situ laser ablation of base-metal sulfides (BMS). The sulfide assemblages of both the Marginal Series (MS) and the Rometölväs Reef (RT) are solely disseminated in character. Most BMS are heavily altered and display a speckled porous appearance and are distinctly associated with hydrosilicates. The dominant host-phase of the PGM are silicates (MS 81% and RT 76%), whereas sulfide-related grains are significantly less prevalent. The PGM of the Marginal Series were, in order of abundance, (1) merenskyite-moncheite-melonite ($PdTe_2$-$PtTe_2$-$NiTe_2$), (2) sperrylite ($PtAs_2$), (3) kotulskite-sobolevskite-sudburyite (PdTe-PdBi-PdSb), and (4) keithconnite-telluropalladinite ($Pd_{3-x}Te$-Pd_9Te_4). In the Rometölväs Reef the PGM were; (1) merenskyite-moncheite-melonite, (2) sperrylite, (3) kotulskite-sobolevskite-sudburyite, and (4) PGE -alloy. The findings are similar to other coeval Fennoscandian PGE mineralizations, suggested to have formed in a low-temperature hydrothermal setting, but contrasts with many of the global PGE occurrences of which are dominated by PGM sulfides and Fe alloys. The $\delta^{34}S$ data obtained from Rometölväs Reef (-0.40 to +1.80‰) and the Marginal Series (-0.94 to +2.19‰) suggests that crustal sulfur played no significant role in the generation of the PGE mineralization of the Koillismaa intrusion. The PGE mineralizations are proposed to have been generated by hydrothermal fluids, either in a late magmatic stage, or later-stage during the Svecofennian orogeny. The Rometölväs Reef is proposed to have formed from a primary metasomatic event, in association with microgabbronoritic bodies. On the other hand, the Marginal Series is suggested to have formed in an orthomagmatic setting due to sialic contamination during interaction with the footwall.

Keywords: layered intrusions, PGE mineralization, base-metal sulfides, Koillismaa-Näränkävaara Complex, Paleoproterozoic, platinum-group minerals, orthomagmatic, hydrothermal, sulfur isotopes, Finland

Supervisors: Anders Scherstén, Shenghon Yang & Eero Hanski

Subject: Bedrock Geology

Jon Gustafsson, Department of Geology, Lund University, Sölvegatan 12, SE-223 62 Lund, Sweden. E-mail: jonsandramail@gmail.com

Petrologisk studie av platinagrupp-mineralisering i Koillismaaintrusionen, Finland

JON GUSTAFSSON

Gustafsson, J., 2019: Petroglogisk studie av platinagrupp-mineralisering i Koillismaaintrusionen, Finland . *Dissertations in Geology at Lund University*, No. 576, 71 pp. 45 hp.

Sammanfattning: Koillismaaintrusionen (2,44 Ga) tillhörande Koillismaa-Näränkävaara Layered Complex, i nordöstra Finland, har studerats i avseende att utröna de processer involverande vid platinagrupp (PGE) mineraliseringens bildande. Den lagrade serien hyser ”reef-type”-mineraliseringen Rometölväs Reef, och den marginella serien ”contact-type”-mineralisering. Det här MSc-arbetet ger en djupgående teoretisk genomgång av PGE-mineralisering i lagrade intrusioner, samt försöker belysa bildandet av PGE-mineraliseringen i Koillismaaintrusionen. Förmedelst SEM-EDS-kartläggning av platinagrupp-mineral (PGM), samt $\delta^{34}S$ *in-situ* laserablation av basmetallsulfider (BMS). Sulfiderna i Marginal Series (MS) och Rometölväs Reef (RT) är disseminerade i karaktär och majoriteten är kraftigt modifierade, samt har ett fläckigt poröst utseende, associerat med hydrosilikater. Silikater utgör majoriteten av värdmineralen för PGM (MS 81% och RT 76%), BMS-relaterade PGM-mineral är utmärkande mindre prevalent. PGM i Marginal Series-mineraliseringen är baserat på förekomst, (1) merenskyite-moncheite-melonite ($PdTe_2$-$PtTe_2$-$NiTe_2$), (2) sperrylite ($PtAs_2$), (3) kotulskite-sobolevskite-sudburyite (PdTe-PdBi-PdSb), samt (4) keithconnite-telluropalladinite ($Pd_{3-x}Te$-Pd_9Te_4). Beträffande Rometölväs Reef-mineraliseringen är fynden av PGM, (1) merenskyite-moncheite-melonite, (2) sperrylite, (3) kotulskite-sobolevskite-sudburyite och (4) PGE-legering. Resultaten är överensstämmande med andra samtida PGE-mineraliseringar i Fennoscandia som tidigare föreslagits ha bildats i en lågtempererad hydrotermal miljö. Till skillnad frånb många andra globala PGE-förekomster som domineras av PGM-sulfider och Fe-legeringar. Svavelisotopdata ($\delta^{34}S$) från Rometölväs Reef (-0.40 till +1.80‰) och Marginal Series (-0.94 till +2.19‰) tyder på att krustalt svavel inte hade någon betydande roll i bildandet av PGE-mineraliseringarna i Koillismaaintrusionen. PGE-mineraliseringarna föreslås ha bildats i association med hydrotermala fluider, antingen i ett magmatisk stadie eller ett senare post-magmatiskt stadie i samband med den Svecofeniska orogenesen. Rometölväs Reef-mineraliseringen föreslås ha bildats i ett primärt metasomatiskt skede i samband med mikrogabbronoritiska intrusioner. Marginal Series-mineraliseringen föreslås däremot ha bildats orthomagmatisk genom sialisk kontaminering, i samband med integrering av liggväggen.

Nyckelord: layered intrusions, PGE mineralization, base-metal sulfides, Koillismaa-Näränkävaara Complex, Paleoproterozoic, platinum-group minerals, orthomagmatic, hydrothermal, sulfur isotopes, Finland

Handledare: Anders Scherstén, Shenghon Yang & Eero Hanski

Ämnesinriktning: Berggrundsgeologi

Jon Gustafsson, Geologiska institutionen, Lunds Universitet, Sölvegatan 12, 223 62 Lund, Sverige. E-post: jonsandramail@gmail.com

1 Introduction

The origin of PGE mineralization remains poorly understood and controversial (Cawthorn et al. 2005; Maier et al. 2013). Two opposing views, an orthomagmatic and a metasomatic, have circulated on behalf of explaining the formation processes for more than 30 years (cf. Mungall & Naldrett 2008; Maier et al. 2013; Godel 2015), often referred to as "downers" and "uppers". The orthomagmatic model involves the role of PGE collection via a magmatic immiscible sulfide liquid, separated from the magma which then percolate downwards through the cumulate pile, hence the term "downers". The metasomatic model, involves the transportation and collection of PGE and metals via upwards percolating Cl-rich fluids, released from the semi-consolidating cumulate pile, hence the term "uppers".

The 2.44 Ga Koillismaa-Näränkävaara Complex is one of many Paleoproterozoic layered intrusions in the Fennoscandian shield (Amelin & Semenov 1996; Huhma et al. 2011). Located in northern Finland, approx. 150 km northeast of the city of Oulu, the complex consists of two separate but related intrusions, the Koillismaa and the Näränkävaara intrusions, connected by a strong gravity anomaly zone (Alapieti 1982). The Koillismaa intrusion consists of several severed blocks, which host both reef- and contact-type platinum-group element (PGE) mineralizations (Karinen 2010). The Koillismaa intrusion consists of a layered- and a marginal series; the layered series is host to the reef-type mineralization called Rometölväs Reef, and the marginal series contains contact-type mineralization. In keeping with the generally poor understanding of PGE mineralization on a global scale (and through time), the origin of PGE mineralization in the Koillismaa-Näränkävaara Complex remains equally unclear.

Besides giving a review on PGE mineralizations in layered intrusions in general, the aim of this MSc-project is to contribute to the understanding of the origin of PGE mineralization in the Koillismaa intrusion by focusing on two main questions:

1). Was external crustal sulfur involved in the formation of PGE sulfide mineralization?

2). Were hydrothermal secondary processes involved during the formation of PGE mineralization?

The first question can be answered by the use of in-situ sulfur isotopes in base-metal sulfides (BMS), to determine whether the mineralization types display mantle-derived values or not.

In order to investigate signs of hydrothermal activity, the following working hypotheses were stated: If PGE were enriched by magmatic sulfide processes, the platinum-group minerals (PGM) will tend to be enclosed in BMS or situated at the boundary of BMS. If, on the other hand, hydrothermal fluids were involved, PGM should mainly be associated with secondary silicates. In addition, PGM that formed through secondary processes should have low-temperature compositions. However, low-temperature PGM may form during slow-cooling conditions as well (Holwell & McDonald 2006; Helmy et al. 2007; O'Driscoll & González-Jiménez 2016).

Twenty-two thin sections from the two PGE mineralization types were studied using optical microscopy and scanning electron microscopy-based automated analysis to determine the textural relationships, composition and grain size of PGM. Additionally, in-situ laser ablation for trace elements and sulfur isotopes of primary and secondary BMS were carried out at the facilities of the Geological Survey of Finland.

The structure of this thesis starts with an in-depth review (optional for the acquainted reader) of PGE mineralization in layered intrusions, as well as the principles of sulfur isotopes. This is followed by a geological background-, and methodology chapter. Results of the two PGE mineralization types are subsequently presented and discussed.

2 Review of platinum-group element mineralization

2.1 Introduction

The platinum-group elements (PGE) consist of platinum, palladium, rhodium, ruthenium, iridium, and osmium. They are transition metals that exhibit similar properties (Fig. 1). The PGE can be additionally subdivided, based upon their associations, into iridium-group platinum elements (IPGE; Os, Ir, Ru) and palladium-group platinum elements (PPGE; Rh, Pd, Pt), where gold is often interrelated with the PPGE group (Rollinson 2014). The platinum group elements together with gold and silver are commonly referred to as precious metals.

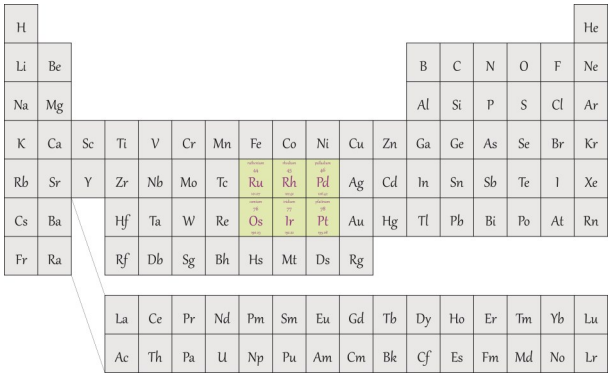

Figure 1. Periodic table showing the platinum-group elements, Ru, Rh, Pd, Os, Ir and Pt.

In modern times, the PGE are of major importance, foremost due to their industrial applications. The PGE are superb catalysts, have resilient electrical properties, and are resistant to wear and chemical alteration. They are used in the automobile industry, in the medical sector, and for high-tech products, such as electrical conductors, but also as jewelry. Platinum, palladium and rhodium are additionally used both as physical and financial assets (Zientek et al. 2017).

2.1.1 Resources and production

The PGE market did not take off until the 1960's, when industrial purposes for the metals were developed. Currently, the market is controlled by South Africa, Russia, and Canada (Prevec 1997; Zientek et al. 2017). The world's estimated resources are approximately 100,000 tons, and in 2012 the world's annual production of PGE was 450 tons ((Zientek et al. (2017) and references therein). Ten percent of the deposits account for 80% of the world's resources, and 30% of the deposits contain 97% of all the resources. There are three mining camps that dominate the resources (Fig. 2): The Bushveld Complex in South Africa, the Noril'sk-Talnakh Complex in Russia and the Great Dyke Complex in Zimbabwe. It has been estimated that 72% of the resources are associated with reef-type and contact-type deposits in the Bushveld Complex. The reef-type, contact-type and conduit-type deposits account for 69%, 20% and 11% of the resources, respectively. The current supply of PGE in combination with recycled PGE (approx. 24% of Pt and Pd; (Butler 2012)) meets the world's demand and are thought to last for the nearby decades. However,

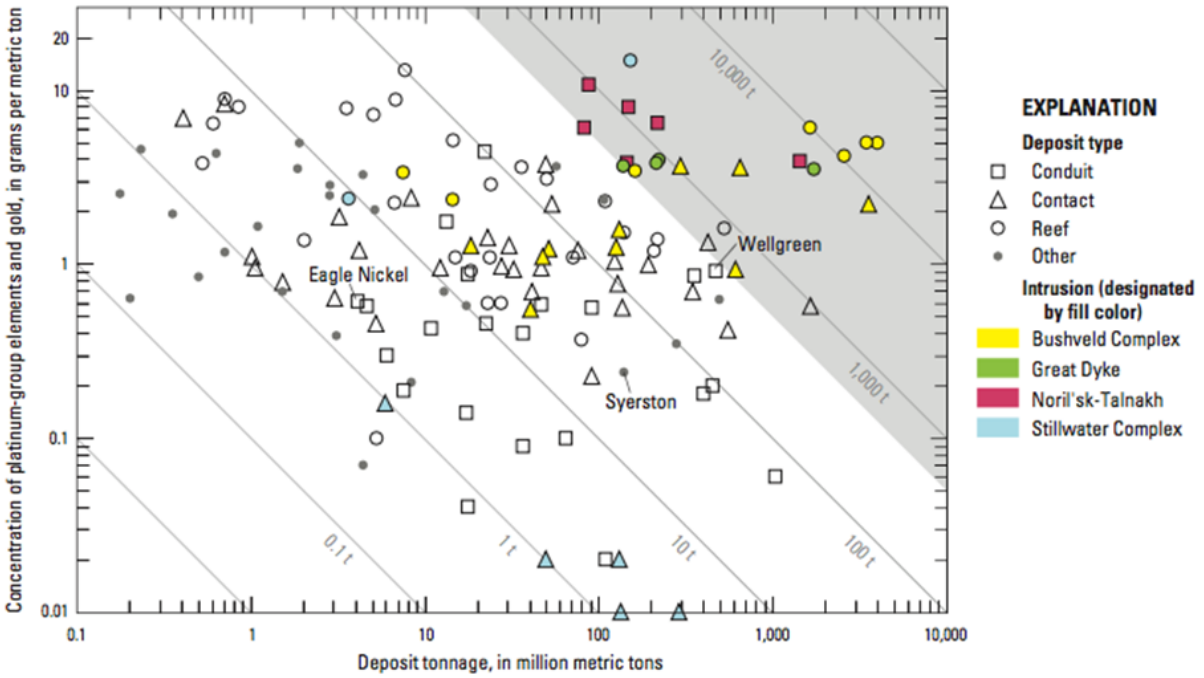

Figure 2. Plot showing the relationship between the tonnage and grades of PGE resources for different mineralization types. Diagonal lines are isolines that show amounts of contained PGEs and gold in the deposits, in metric tons (t). The shaded area highlights those deposits that are large enough to cover more than 1-years global PGE need. Figure used according to guidelines of USGS (Zientek et al. 2017).

since the resources are concentrated to a limited number of localities, production is susceptible to interferences (Zientek et al. 2017).

2.2 PGE mineralization in layered intrusions

Many PGE deposits are associated with ultramafic-mafic igneous rocks situated in the central areas of cratons and most economic deposits are found in thin stratiform reefs in the lower and central parts of layered intrusions (Wager & Brown 1967; Maier 2005; Maier & Groves 2011). They are predominantly Archean to Paleoproterozoic in age and have magnesian basaltic (picritic) parental magmas There is a correlation between the size of mineralization and the size of larger intrusions, with the largest PGE horizons extending laterally for more than 100 km. Conversely, the mineralization of smaller layered intrusions is often less continuous, with variable lower grades (Maier & Groves 2011; Maier 2015). Many of the Fennoscandian layered intrusions fit into this category (Alapieti et al. 1990; Alapieti & Lahtinen 2002; Iljina & Hanski 2005; Iljina et al. 2015). The thickness of PGE reefs varies greatly, from a few centimeters to several tens of meters, and may occasionally be thicker in the central parts of the intrusions (Maier & Groves 2011).

PGE mineralizations have been classified in various ways throughout the years. Naldrett (2004) based his classification on the parental magma composition, while Maier (2005) used a classification based on the stratigraphy and associated rock types (Fig. 3). The latter is the following (types 1 and 4 will be discussed in more detail in *Section 2.3*):

1. Contact reefs at the base and sidewall of intrusions
2. PGE reefs in the peridotitic and pyroxenitic lower portions of layered intrusions
3. PGE enriched chromitite layers
4. Silicate-hosted PGE reefs in interlayered mafic–ultramafic rocks, commonly within the central portions of layered intrusions
5. PGE reefs in the magnetite-enriched upper portions of layered intrusions
6. PGE-mineralized transgressive Fe-rich ultramafic pipes
7. Vein-hosted PGE deposits in the roof (and floor) of the intrusions

Some generalizations can be made based on the stratigraphy and rock types. Regarding PGE reefs, the stratigraphy varies greatly, although most economical reefs tend to be located in transitional zones of the layered subzones (Maier et al. 2013; Maier 2015). Most PGE reefs are medium-grained cumulate rocks, but pegmatoidal textures commonly exist locally (Schouwstra et al. 2000). The country rock varies greatly from intrusion to intrusion, and many of the Fennoscandian intrusions have granitic country rocks

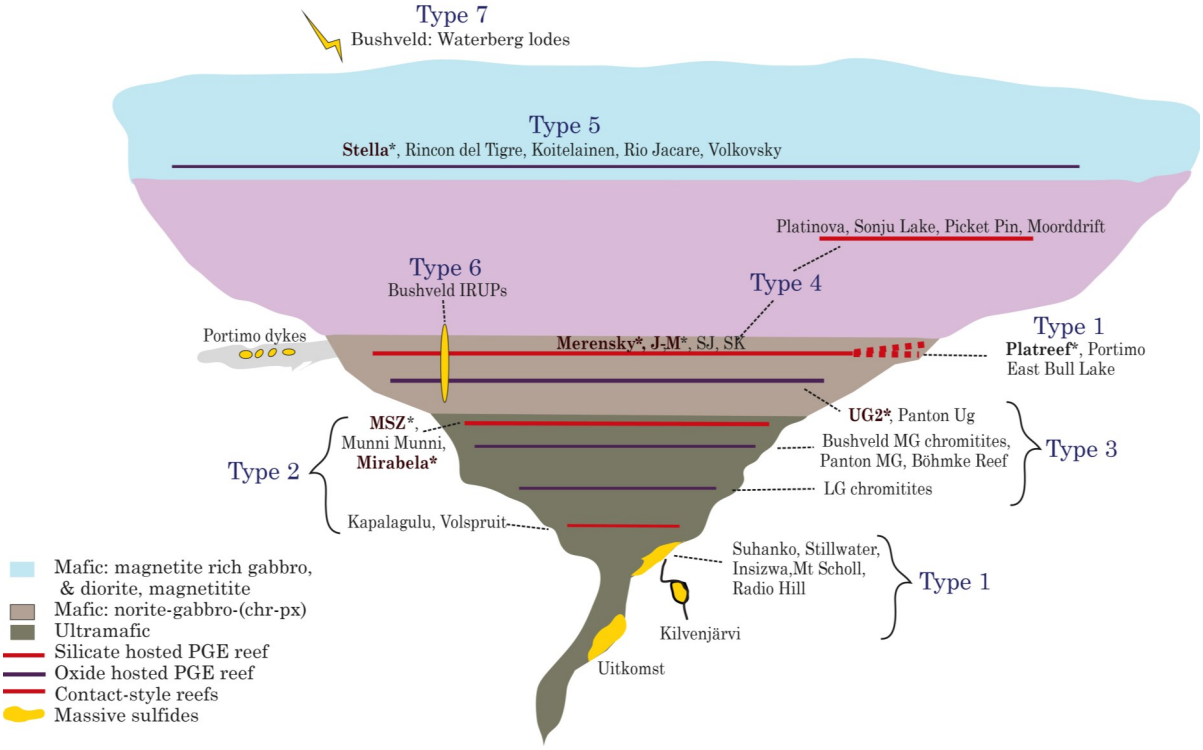

Figure 3. Illustration of the PGE deposit types in layered intrusions and their feeder conduits, as originally presented by Maier et al. (2005). Reef names written in bold with an "*" indicates that the reef is economical. Abbreviations: JM = J-M Reef of the Stillwater Complex, SJ = Sompujärvi Reef of the Penikat intrusion, SK = Siika-Kämä Reef of the Portimo intrusion, LG-MG-UG = lower-middle-upper group chromitites of the Bushveld Complex, MSZ = Main sulfide zone of the Great Dyke. Modified after Maier et al. (2005; 2013).

(Alapieti et al. 1990; Iljina & Hanski 2005), but other rock types are known to occur (Maier & Groves 2011). PGE reefs are often heterogeneous, and the mineralization is typically hosted by BMS and PGM (Cawthorn et al. 2005).

2.2.1 Location of PGE-bearing intrusions

While most Ni-Cu deposits are located along the margins of cratons, economical PGE deposits occur within stabilized cratons and often in the inner portions (Fig. 4)(Groves et al. 1987). This is evident, for example, in the case of the Bushveld Complex in the Kaapvaal craton and the Great Dyke Complex in the Zimbabwe craton (Groves et al. 1987; Maier & Groves 2011). Some cratons are PGE enriched (e.g., Karelia, Kaapvaal and Zimbabwe), while some are ostensibly PGE deprived (e.g., Yilgarn). All major deposits are thought to be associated with tectonic events, such as translithospheric faults, major shear zones or rift zones, where primitive magma ascend (Begg et al. 2010a). Certain intrusions are situated adjacent to probable intracratonic rifts, as is the case with the Karelian craton. It has been suggested that these may be reactivated Archean suture zones that originally nucleated the craton, through which PGE-rich magma rose as magma conduits (Maier & Groves 2011; Mitrofanov et al. 2012). Silver et al. (2004) argued that the Bushveld Complex was emplaced through a suture zone, known as the Thabazimbi-Murchison Lineament. Peculiarly, there have been no signs of flood basalts or remarkable extensions in association with layered intrusions. According to Maier et al. (2013), there is no convincing evidence for major rifting in relation to any of the significant deposits, stating that this may instead indicate a failed rift environment. They argue that this may create a suitable environment for major layered intrusions due to repeated "ponding" of magma into the crust, rather than surficial eruptions.

2.2.2 Time distribution of PGE deposits

All large PGE deposits are older than 1.8 Ga (Godel 2015), excluding the younger Skaergaard intrusion in Greenland (55 - 60 Ma; Brooks & Gleadow (1977)). The oldest known deposit is the 3.1 Ga Baula deposit in India (Augé et al. 2003). Ni-Cu deposits, on the other hand, were formed during a much broader time span up until recent times, and older Archean and Proterozoic deposits are generally more komatiitic and Ni-rich, while younger deposits tend to be more rich in sulfur (Naldrett 2010). There is a correlation between the formation of PGE and Ni-Cu deposits and the presence of supercontinents, and periods with high rates of juvenile crust formation, thought to be due to the amalgamation and breakup of supercontinents (Groves et al. 2005). However, to what extent supercontinents acted in terms of amalgamation and breakup, is still somewhat debated (Li et al. 2008b). In the Fennoscandian Shield, the many PGE and Ni-Cu deposits were formed at various times. The oldest deposits (komatiites) are 2.7 – 2.8 Ga in age (Huhma et al. 2012; Konnunaho et al. 2015), the 2.44 Ga layered intrusions of the Tornio-Näränkävaara Belt (incl. Koillismaa intrusion) (Huhma et al. 2011), the 2.05 Ga Kevitsa and Otanmäki intrusions (Mutanen & Huhma 2001; Kuivasaari et al. 2012), the 1.98 Ga Pechenga Nickel Belt (Hanski et al. 1990), and the 1.88 Ga

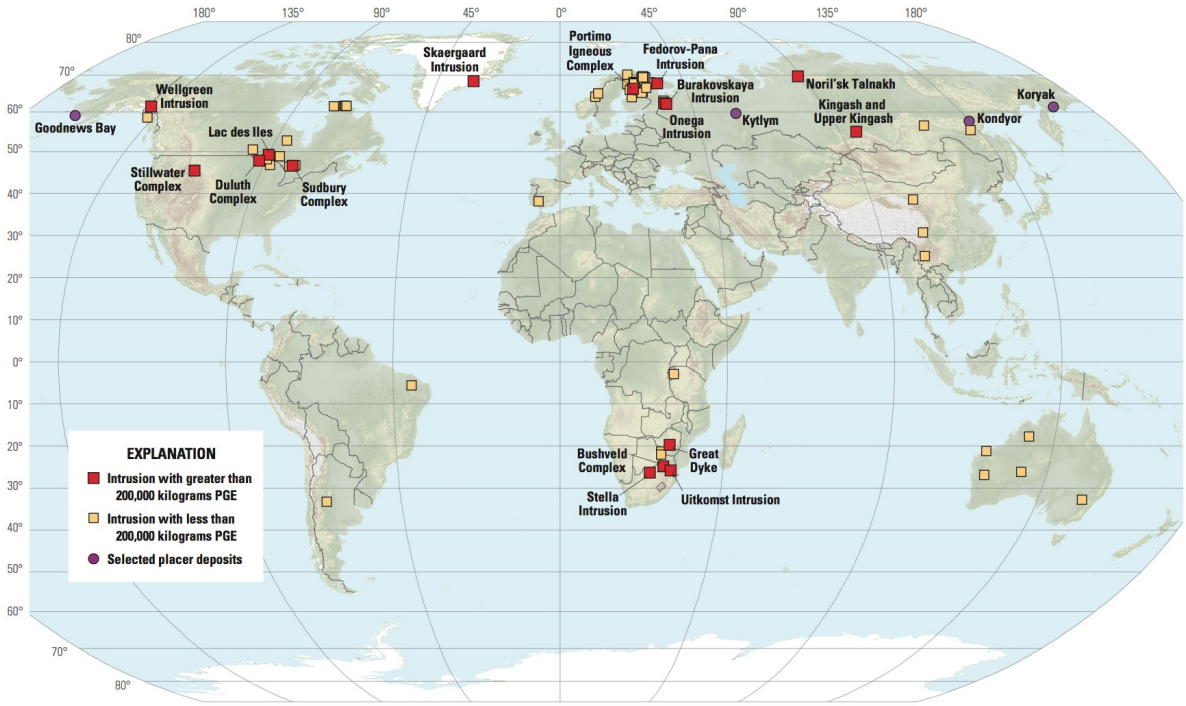

Figure 4. Global map displaying locations of notable platinum-group-element deposits. Red square indicates deposits greater than 200 tonnes, yellow square indicates deposits below 200 tonnes and purple dots illustrate placer deposits. Figure used according to guidelines of USGS (Zientek et al. 2017)

Svecofennian deposits (Hanski 2015).

2.3 Characteristics of different PGE deposit types

The PGE mineralization in the 2.45 Ga layered intrusions of Finland can broadly be categorized into two main groups: reef-type and contact-type deposits. Both types have been observed in several intrusions in Finland (Alapieti et al. 1990; Iljina & Hanski 2005). Here follows a brief review of typical characteristics of these deposit types.

2.3.1 Contact-type PGE mineralization

As the name implies, contact-type (or marginal series) PGE mineralization is situated at the base or sidewall contacts of layered intrusions. Examples of this deposit type include the Platreef and Sheba's Ridge of the Bushveld Complex (Sharpe et al. 2002; Holwell & McDonald 2007), the Portimo Complex in Finland (Iljina 1994), and the Federova-Pansky intrusion in Russia (Schissel et al. 2002). The Platreef on the Sandsloot farm is considered the type locality. Mineralization may also occur in the footwall of a layered intrusion and is then classified as an offset-type PGE mineralization. It is commonly considered a subcategory; hence, the mineralization is often thought to have formed of a redistributed contact-type mineralization, where sulfides and PGE have been remobilized due to deformation (Alapieti et al. 1990; Iljina & Lee 2005). However, offset-type PGE mineralization may also originate from injection in a primary magmatic stage.

Contact-type mineralization is usually of a scale of tens of meters, often occurring erratically, and may vary along strike. The host rock is commonly pyroxenite and gabbronorite, but occasionally anorthosite or peridotite is present. The deposits are characterized by disseminated to massive sulfides, and the sulfide content is typically higher than in reef-type deposits (<1% to 5% of S) but mineralization has lower PGE tenors (Godel 2015). Contact-type mineralization is, despite this, often economic due to its larger volumes. The host rock and their textures vary; they are often heterogeneous mafic rocks, but ultramafic hosts do occur (e.g., Platreef). Xenoliths from country rock are commonly observed in places. According to Iljina & Lee (2005), the contact-type mineralization associated with the Portimo Complex is thought to represent the edge of the internal reefs in contact with the marginal series of the intrusion. This feature is seen in the case of the Platreef as well (Holwell et al. 2007; Penniston-Dorland et al. 2008).

Contact-type deposits are often characterized by extensive interaction of mafic magma with the surrounding host rock, which generates a thick marginal series, commonly with a composition reversal. The Platreef (Holwell et al. 2008) and the Portimo Complex (Iljina 1994) contact-type deposits are particularly well mineralized, with high PGE tenors compared to many other contact-type deposits. It has been suggested that several magma pulses/fluxes favor higher grades of PGE (Iljina & Lee 2005).

2.3.2 Silicate-hosted internal reef-type PGE mineralization

Reef-type deposits are zones consisting of lateral PGE mineralization in a layered series. Reefs may occasionally be thicker in the central parts of the intrusions (Maier & Groves 2011). For example, the Bushveld Complex shows an increase in the thickness of reefs towards the center of the intrusion (Maier et al. 2013). There are both oxide-hosted reefs and silicate-hosted reefs. The former, e.g., UG2 of the Bushveld Complex (Osbahr 2012) and the Stella layered intrusion (Maier et al. 2003) will not be discussed here, as they are not found in the Koillismaa intrusion. The silicate-hosted reef-type deposits have numerous subclasses (Maier 2005), but can be simplified into deposits occurring at two different positions: either at the border between two megacyclic units or magma pulses, or as stratiform zones within a megacyclic unit.

Here, I will discuss reefs located in the lower and middle part of the layered intrusion, though upper reefs occur as well (e.g., the Stella layered intrusion (Maier et al. 2003)). PGE reefs within a megacyclic unit are usually hosted by anorthosite and gabbronorite cumulates, whereas reefs between two units are less correlated with a rock type (Cawthorn et al. 2005; Maier & Groves 2011). Reefs between zones are often several meters thick whereas reefs within a megacyclic unit are normally thinner. Reefs in the lower part of the layered series are characterized by disseminated BMS of 10s of meters (Barnes et al. 2011)). They usually have relatively low PGE-tenors with a sulfide content below five volume percent. The host rocks are normally peridotites and pyroxenites and are typically hosted within a megacyclic unit. Reefs occurring in the middle part, are characterized by disseminated BMS, with a comparatively high PGE tenor and sulfide content. These reefs are often found between two units, where interlayering have occurred. Examples are the Merensky Reef of the Bushveld Complex, the SJ- and PV Reefs of the Penikat intrusion, the SK Reef of the Portimo Complex, as well as the Rometölväs Reef of the Koillismaa Complex.

2.4 Host minerals of platinum-group elements

PGE mineralization of economic interest is mainly associated with internal PGE reefs and is associated with disseminated sulfides, oxides or silicates. Different hosts minerals of PGE are reviewed below.

2.4.1 Base-metal sulfides

Among the three dominant BMS minerals, pyrrhotite ($Fe_{(1-x)}S$), pentlandite ($(Fe,Ni)_9S$) and chalcopyrite ($CuFeS_2$), only pyrrhotite and pentlandite are significant carriers of PGE in solid solution, whereas chal-

copyrite is nearly barren (<10%) (Godel et al. 2008; Godel 2015). In some deposits, such as the Bushveld Complex (Merensky Reef (Godel et al. 2007; Osbahr et al. 2013), Platreef and UG2 (Osbahr 2012)) and the Stillwater Complex (JM-reef, (Godel & Barnes 2008)), pentlandite is the main carrier of PGE, followed by pyrrhotite. By contrast, in the Great Dyke and the Penikat intrusion, pyrrhotite and pentlandite are equally enriched in PGE. The mantle-normalized metal abundance patterns are in general similar for all major deposits in regards to pyrrhotite and pentlandite (Godel et al. 2008; Godel 2015). Godel (2015) stated that the similar PGE pattern for the major deposits suggests a similar formation process in concentrating the elements into BMS. Moreover, it may also indicate lack of post-magmatic influences, such as alteration or metamorphism.

Palladium is the most abundant PGE in BMS, and may constitute several weight percent of the whole-rock budget (Cabri 1992; Godel & Barnes 2008; and references therein). In the Merensky Reef (Godel et al. 2007; Osbahr et al. 2013), pentlandite constitutes up to 75% of the total whole-rock Pd budget. Platinum concentrations are low in both pentlandite and pyrrhotite, less than 5% of the total Pt. Although the sulfur content in the rock and the whole-rock PGE content are largely correlated, BMS host slightly less than half of PGE, except Pt which is mainly hosted in PGM or alloy (Godel et al. 2008; Godel 2015).

2.4.2 Platinum-group minerals

Platinum-group minerals are the predominant source of PGE in many PGE ores (Godel et al. 2007; Osbahr et al. 2013; Godel 2015). In contrast to BMS, PGM are much more variable in terms of their composition and less comparable between deposits. According to O'Driscoll & González-Jiménez (2016), there are 135 distinct PGM phases approved by the International Mineralogical Association. Besides native metals, known elements in PGM include transition metals such as Ni, Cu, Ag, post-transition metals such as Bi, Pb, Tn, metalloids such as Te, As, Sb, as well as non-metals like Se and S (Cabri 2002; Zientek et al. 2017). High-temperature PGM that originally forms part of the magmatic paragenesis may be modified in several ways at lower temperatures, due to metasomatic, hydrothermal, metamorphic and supracrustal processes (Hanley 2005). Hence, a delicate superimposition of low-temperature processes may be needed to understand the primary formation of PGM. The platinum-group mineral assemblages and textural relationships will be discussed in-depth in *Section 2.7*.

2.4.3 Oxides

There is a connection between the occurrence of chromitites and PGE mineralization in layered intrusions, as observed in reefs of the Bushveld Complex and the Great Dyke. The PGE grades are often higher in chromite-rich rocks compared to the adjacent silicate rocks. However, there is no clear consensus on why PGE are associated with chromitites. In the Bushveld Complex, all chromitite layers are enriched in PGE, though only the UG2 is currently economic.

Three proposed models have been given for why the chromitites are enriched in PGE: 1) PGE-rich sulfides and chromite crystalized together due to fractionation, where some sulfide liquid was trapped within the chromite lattices. Subsequent dissolution of sulfides by late magmatic fluids, and/or reaction with chromite, cause the sulfides carrying PGE to be expelled. In this model, sulfur loss caused partial dissolution of sulfides, forming monosulfide solid solutions, Pt-alloys and a Cu-Pd-rich liquid. The Pd and Cu were incorporated into the liquid, whereas IPGE and Pt remained behind in MSS and PGM. (Naldrett & Lehmann 1988; Peregoedova et al. 2004). 2) When chromite crystallized, a local reduced zone was formed adjacent to the chromites, allowing PGE to form as alloys around the chromite grains (Finnigan et al. 2008). 3) Crystallization of chromite accompanied the sulfide liquid, helping concentrate the PGE. In essence, the PGE crystallized as PGM (laurite and Pt-alloys) before the formation of immiscible sulfide liquid, the PGM were then collected and incorporated by crystallizing chromite. Subsequently, sulfide liquid collected the remaining PGE (Barnes & Maier 2002b; Godel et al. 2007). 4) The fourth option is a combination of the processes mentioned above.

It has been experimentally demonstrated that during the crystallization of chromite, Os, Ir and Ru can partition into the chromite lattice (Capobianco & Drake 1990; Brenan & Andrews 2001), which is also seen in komatiites (Locmelis et al. 2010; Pagé et al. 2012). However, in layered intrusions, oxide minerals, such as chromite, magnetite or other spinel minerals, are not thought to be significant carriers of PGE (Godel et al. 2008; Godel 2015). Studies of the Merensky Reef and J-M Reef have shown that there is no significant incorporation of PGE in chromite or magnetite (Ballhaus & Sylvester 2000; Godel et al. 2008; Osbahr et al. 2013).

2.5 Petrogenesis of PGE deposits

The contents of Ni, Cu and PGE in the mantle and crust are relatively low compared to the bulk composition of the Earth (McDonough & Sun 1995; Barnes & Maier 1999). The reason for this is the siderophile nature of these elements, which caused them to be concentrated in the Earth's core upon its formation. In order to form an economic PGE deposit, the PGE need to be concentrated by 10^3 - 10^4 times relative to the primitive mantle composition. The parental magmas of layered intrusions are considered to become relatively enriched in PGE during their formation by a high degree of partial melting. However, an enrichment by 10^2-10^3 relative to the parental magma, is thought to be necessary in order to form a PGE ore (Barnes & Light-

foot 2005; Godel 2015). As will be discussed later, there are many factors that affect the PGE content of a potential deposit. To determine the relative importance of each factor for the petrogenesis of mineralization is often difficult to estimate (Godel 2015).

2.5.1 Mantle source

The primary mantle is thought to contain up to 7 ppb of PGE (McDonough & Sun 1995), primarily in solution with micron-scale BMS (Barnes & Maier 1999; Alard et al. 2000; Lorand & Alard 2001; Lorand et al. 2008a; Lorand et al. 2008b). Lorand & Alard (2001) showed (from peridotite xenoliths) that two types of sulfides are present in the mantle:

1) Fe-Ni monosulfides in solid solution, termed MSS, within olivine or as grains or inclusions in oxides and silicates,
2) Fe-Ni sulfides and Cu-Fe sulfides as an intermediate solid solution (ISS) located at olivine contact boundaries.

The MSS is enriched in IPGE, i.e. Os, Ir, Ru, and Rh, whereas the ISS is enriched in Pd and to a minor degree in Pt, although most of the Pt content is thought to occur as Fe-Pt alloys under these conditions. It is generally believed that PGE-rich magma related to layered intrusions is derived from the asthenospheric mantle (Maier et al. 2013), although some argue for a subcontinental lithospheric mantle (SCLM) source (Harmer & Sharpe 1985; Hamlyn & Keays 1986). The arguments against this are that the SCLM is cold, therefore unfavorable in generating high degrees of melt (however, a mantle plume reaching the lithosphere may potentially generate such high degrees of melt). Furthermore, Pearson et al. (2004) showed that the SCLM is relatively poor in PGE. In order to facilitate high sulfur solubility, a high degree of melting is required, and therefore, the asthenospheric mantle or a plume-derived mantle is a more prospective source. Maier & Groves (2011) argued that regardless of whether the SCLM is a component of the source or not, its contribution of PGE is believed to be minor.

2.5.2 Partial melting of the mantle

During partial melting of the mantle, the partition coefficient of PGE between a sulfide melt and a silicate melt is in the order of at least 10^4 - 10^5 (Barnes & Lightfoot 2005; Fonseca et al. 2009). Consequently, the behavior of PGE is greatly controlled by the mass balance of the two coexisting liquids during melting. Magmas fertile in PGE are formed during sulfur undersaturated conditions. According to Crocket (2002), the PGE content in mantle-derived magmas varies between 0.2 to 40 ppb, predominantly due to the behavior of BMS and sulfur saturation in the magma during partial melting (Barnes et al. 1985; Godel 2015). Sulfur solubility is the key to a PGE-rich magma. Low-degree partial melts of primary mantle will contain only 200 - 250 ppm of sulfur (Barnes et al. 1985; Hamlyn & Keays 1986). In this situation, some of the PGE will be left behind in the mantle, mainly as MSS (Bockrath et al. 2004). Because of this, a high degree of melting of more than 20% is thought necessary in order to dissolve all sulfur into the silicate melt (Barnes & Lightfoot 2005; Fonseca et al. 2009).

For a fertile magma to become potentially mineralized, the magma needs to ascend to the surface with as much sulfur as possible without reaching sulfur saturation. Sulfur solubility, also known as the sulfur content at saturation (SCSS), is controlled by several factors, but the key components are pressure and temperature (Wendlandt 1982; Mavrogenes & O'Neill 1999; Mungall 2013). When temperature decreases, SCSS also decreases, whereas when pressure decreases, the sulfur solubility increases. During ascent of magma, the pressure influence of the sulfur saturation is more dominant than the decrease in temperature. Hence, sulfur saturation will increase as the magma rises towards the surface. Additionally, the chemical composition of the magma also controls SCSS of the magma. A high oxygen fugacity, i.e. a decrease in the Fe^{2+}-Fe^{3+} ratio, will decrease the sulfur solubility. Contamination from an external source will also affect SCSS, as siliceous contamination will decrease the sulfur solubility. The sulfur solubility in a typical basaltic melt varies greatly between 500 and 1000 ppm, and at 1400 °C and at a depth of 120 km, the sulfur solubility is ca. 800 ppm (Wendlandt 1982; Mavrogenes & O'Neill 1999; Mungall 2013).

2.5.3 PGE interaction with sulfide liquid

After a fertile magma has formed, it will ascend towards the crust due to buoyancy. During cooling and crystallization of the magma, sulfur is incompatible and will remain in the magma while the silicates crystallize. As fractional crystallization continues, the sulfur concentration in the magma will increase until the point where it reaches SCSS and will then form an immiscible sulfide liquid. Immiscibility depends on many factors, mainly related to the sulfur solubility, generally associated with the final crystallization of olivine, i.e. removal of the Ni-component (Jenner et al. 2010; Ripley & Li 2013). Some of the PGE are more incompatible during crystallization; thus Pt, Pd and also Cu will remain in the magma to a greater extent than some of the IPGE (Wohlgemuth-Ueberwasser et al. 2013). The immiscible sulfide liquid will eventually form growing droplets due to diffusion. When sulfide droplets surpass a certain size limit, they will sink to the bottom of the magma chamber. The first droplets to form are those with the highest PGE content. However, the PGE ratios in the sulfide droplets are governed by many processes, such as degree of supersaturation, diffusion rate and internal partition coefficient of different PGE species (Mungall 2002; Mungall 2014).

There are many models on the formation of a

PGE reef. The most favored one is where PGE are collected by an immiscible sulfide liquid that resulted from magma recharge and sulfur saturation by magma mixing (Irvine 1976; Campbell & Naldrett 1979; Hiemstra 1979; Campbell et al. 1983; Naldrett et al. 1986; Naldrett & von Gruenewaldt 1989; Maier & Barnes 1999). In order for PGE-rich sulfides to form, the sulfide liquid has to interact with a very large volume of silicate magma to scavenge PGE; in other words, it requires a high R factor of >10,000. The term R factor represents the volume of silicate magma that a segregated sulfide melt has equilibrated with, i.e. the silicate magma/sulfide liquid mass ratio. For example, if we have a sulfide liquid of one kg and an R factor of 10,000, that means that the sulfide liquid equilibrated with 10,000 kg of silicate magma. The higher the R factor, the more silicate magma the sulfide liquid can equilibrate with.

When a silicate magma reaches sulfur saturation, immiscible sulfide droplets form, and as they increase in size they will settle to the bottom of the cumulate pile. The PGE and base metal contents of the sulfide liquid can be calculated using the equation of Campbell & Naldrett (1979), the partition coefficients of metals between the silicate and sulfide melt (in a closed system), and the initial bulk metal content as follows:

$$C_{sul} = C_L D^{sul/sil} \frac{R + 1}{R + D^{sul/sil}} \quad (1)$$

In the formula, C_{sul}, is the metal tenor of the sulfide liquid, which is dependent on the silicate concentration of metal content, C_L, in the silicate magma. $D_{sul/sil}$, is the partition coefficient of an element between the sulfide liquid and the silicate magma. The formula reveals that a high R factor (high amount of silicate interaction with the sulfide liquid) will produce high PGE and other chalcophile element tenors. The opposite is true for a low R factor, where a larger number of sulfides relative to the silicate melt are formed and equilibrated. The PGE and metal concentrations will then be much lower, as the available amount of PGE carrying silicate magma available to equilibrate is less and will not form reef deposits. Key points include: 1) If the R factor is too low, the Ni and Cu contents of the sulfides are low, even from a metal-rich silicate magma; and 2) since the PGEs have a low abundance in the silicate magma, a high degree of PGE enrichment requires very high R factors (>10,000). The equation of Campbell & Naldrett (1979) assumes that the PGE in BMS and PGM were all previously accommodated in the sulfide liquid. One of the concerns with the equation is that it fails to account for the occurrence of PGE in chromite reefs, and in some layered intrusions, such as the Bushveld. The high R values that would be required to form the PGE reefs are considered too extreme to be realistic (Fonseca et al. 2009; Maier & Groves 2011; Godel 2015). Models trying to explain PGE in chromite reefs are discussed in *Section 2.6*.

2.5.4 Cooling of sulfide liquid

When immiscible sulfide liquid first starts to form as small droplets, it will collect PGE and other chalcophile elements from the silicate melt (Fig. 5a). During cooling (~900° C), the sulfide liquid will fractionate into an Fe-rich monosulfide solid solution (MSS) and a Cu-rich sulfide liquid (Fig. 5b) (Kullerud 1969; Ebel & Naldrett 1996; Naldrett 2004; Barnes et al. 2006). After further cooling (Fig. 5c), the Cu-rich liquid will form an intermediate solid solution (ISS). During fractionation, the least chalcophile elements (Os, Ir, Ru and Rh) will partition into the MSS, whereas the elements still residing in the sulfide liquid (As, Sb, Te, Pd, Pt, Au etc.) will ultimately crystallize into ISS. Occasionally, sulfosalts (semi-metal-bearing phases and sulfarsenides) may form at this stage.

At subsolidus temperatures (~600° C), MSS and ISS are no longer stable and will exsolve into BMS (Fig. 5d). The MSS will form pentlandite and pyrrhotite (± pyrite), and pentlandite may additionally form as exsolution flames in pyrrhotite. The Cu-rich ISS will form chalcopyrite (± pyrite, ± cubanite). Sulfosalts may exsolve and migrate toward the grain boundaries to crystallize as PGM, as they are not compatible with the newly formed sulfide lattices. Consequently, the commonly observed assemblage of magmatic sulfides are predominantly pyrrhotite, pentlandite and chalcopyrite (± pyrite, ± cubanite) together with various PGM minerals (Barnes & Lightfoot 2005; Barnes et al. 2006; Godel et al. 2007; Godel et al. 2008).

2.6 Orthomagmatic and metasomatic reef -forming models

The processes involved in the formation of a PGE deposit are complex, still poorly understood and controversial, and it is obvious no single model can explain all the different features of the PGE reefs (Cawthorn et al. 2005; Maier et al. 2013). In general, the sulfide content in the reefs are supercotectic by ~0.6 %, which means that some enrichment process is required to form the reefs (Barnes et al. 2009). The PGEs are chalcophile under these conditions and will therefore preferentially partition into a sulfide liquid, if present (Barnes & Lightfoot 2005). Two opposing sides have debated about the mineralization processes involved for more than 30 years (cf. (Mungall & Naldrett 2008; Maier et al. 2013; Godel 2015). The proposed models focus either on a purely orthomagmatic origin or that of metasomatism, i.e. deuteric fluids. In general, both models require the transportation of PGE to the site of accumulation, either downwards by a sulfide liquid or upwards by an aqueous fluid.

2.6.1 Orthomagmatic models

One of the main arguments for the magmatic models is the fact that, in most cases, PGE reefs are laterally very extensive homogenous horizons with similar grades, regardless of the thickness of the underlying floor

rocks and magmatic unconformities (Barnes & Maier 2002a; Barnes & Maier 2002b). The "classic" orthomagmatic models (Irvine 1976; Campbell & Naldrett 1979; Hiemstra 1979; Campbell et al. 1983; Naldrett et al. 1986; Naldrett & von Gruenewaldt 1989; Maier & Barnes 1999) focus on gravitational settling of sulfide liquid droplets in combination with replenishment and turbulent mixing of magmas, either from magmas of the same lineage (pulse) or a different lineage. Some involve contamination of the roof rocks, due to the heating from the intrusion (e.g., Irvine (1976)). Hiemstra (1979) proposed a purely magmatic model, where the PGE crystallize as PGM that accumulate on a crystal pile. In some circumstances, sulfides may instead form interstitial networks that percolate down through a crystallizing cumulate pile and settle (Godel et al. 2006). Some models involve the PGE being collected in chromitites as PGM (Scoon & Teigler 1994; Kruger et al. 2002).

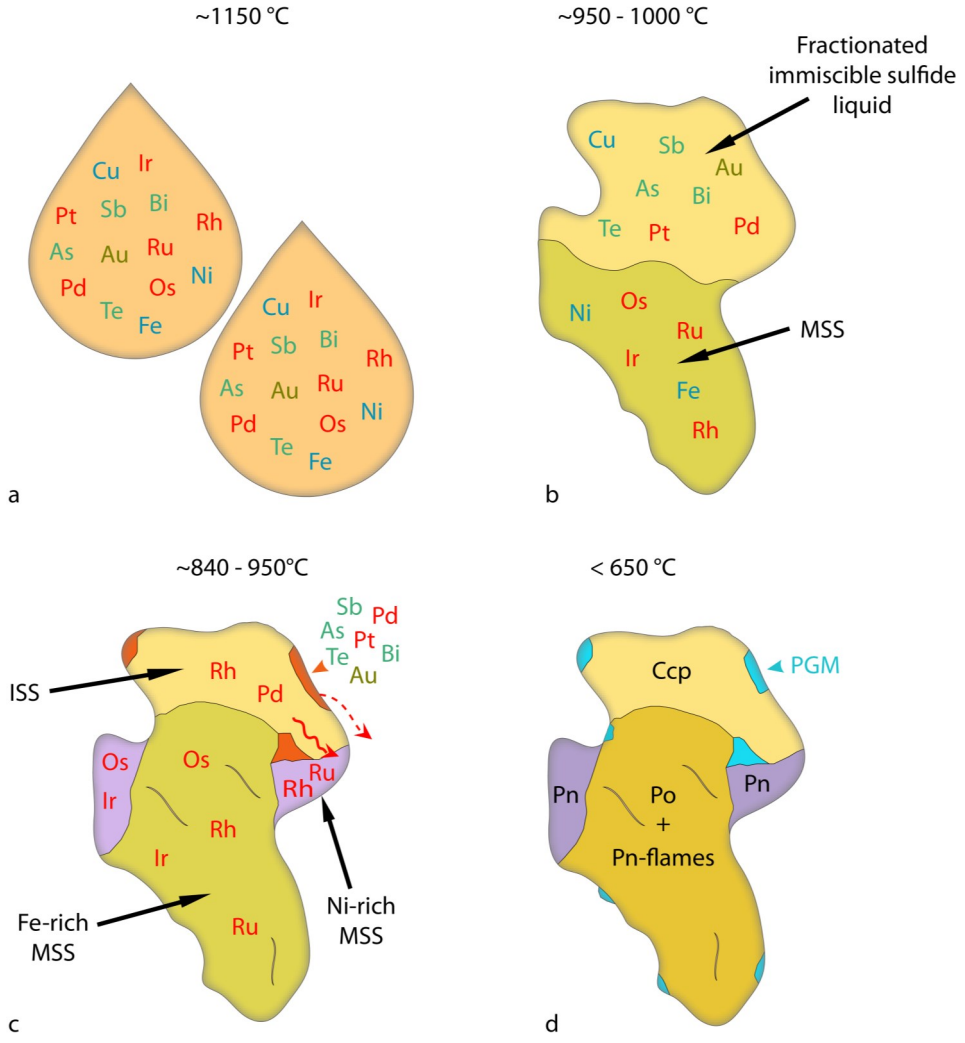

Figure 5. Illustration of the behavior of immiscible sulfide droplets during cooling, and the partitioning of PGE, base metals and chalcophile elements present. A. The sulfide droplets form and will scavenge PGE and chalcophile elements from the silicate magma. B. Upon cooling (~900° C), the sulfide liquid will fractionate into an Fe-rich monosulfide solid solution (MSS) and a Cu-rich sulfide liquid. The Cu-rich melt after further cooling, will form an intermediate solid solution (ISS). C. After further cooling, the Cu-rich melt, will form an intermediate solid solution (ISS) and Ni-rich MSS. During fractionation crystallization, the least chalcophile elements (Os, Ir, Ru and Rh) will partition into the MSS, whereas the elements still residing in the Cu-rich sulfide liquid (As, Sb, Te, Pd, Pt and Au), will ultimately crystallize into the ISS. At this point, sulfosalts may form as exsolutions and migrate towards the boundaries. D. At subsolidus temperatures (~600° C), MSS and ISS are no longer stable and will exsolve into BMS. The MSS will form pentlandite and pyrrhotite (± pyrite), whereas ISS will form chalcopyrite (±pyrite, ±cubanite). The sulfosalts (semi-metals and sulfarsenides) will exsolve and migrate toward the grain boundaries to crystallize as PGM, as they are not compatible with the newly formed sulfide lattices. Abbreviations: pyrrhotite - Po, pentlandite – Pn, chalcopyrite – Ccp. Modified after (Barnes et al. 2006; Godel 2015)

The replenishment model works best when there is a large density contrast between the different magmas, giving way of a possible magma fountain, which would help explain the very high R values necessary to generate the high metal tenors of the sulfide liquid. It endorses the common observation of reefs being situated at transition zones between different magma compositions. Furthermore, the interlayering of ultramafic and mafic cumulates observed in intervals favors this model.

Criticism has been presented against many of the models discussed above. First of all, the simple model of preferential settling of sulfides through a quiescent magma is considered unlikely, as most reefs are relatively narrowly confined, and it does not explain the knife-sharp contacts between the reefs and the adjacent rocks, as observed in the Bushveld Complex (Maier et al. 2013). Furthermore, the observed fine-scale rhythmic banding in the Bushveld is a perplexing feature. Boudreau (1994) suggested that the fine-scale rhythmic banding could be the result of mineral segregation during ”crystal ageing”. Additionally, supersaturation of sulfide in the magma due to mixing has been shown impossible when accounting for the observed magma compositions in the Bushveld, for example. The idea of mixing a primitive magma with an evolved residual magma, in order to produce a hybrid liquid compositionally close enough to sulfur saturation, does only work if both the magmas are already close to being saturated (Cawthorn et al. 2002; Li & Ripley 2005). In the case of the Bushveld Complex, the replenishing magma is highly sulfur undersaturated. If the ultramafic rocks formed through magma mixing, they should presumably still be sulfide poor, which clearly is not the case. The trouble explaining how a flat magmatic body could produce a continuous reef of more than 400 km in length, as argued by Maier et al. (2013), is enigmatic as the mixing magnitudes would be expected to vary along strike.

In order to address the many problems of the above-mentioned models, Naldrett et al. (2009) proposed a model involving an emplacement of an already PGE-rich magma. The magma was undersaturated and contained 100s of ppb of PGE. This model does not require a thick magma column of several hundreds of meters (as the other models do) to form a reef, instead only a few tens of meters would be necessary. The model involves a later magma pulse or pulses cannibalizing previously settled PGE-rich sulfides caught in feeder conduits or a staging chamber, to form an upgraded PGE-rich magma. Currently, there is no evidence for a PGE-rich magma to verify this, and the surrounding sills show no PGE enrichments (Maier et al. 2013).

A model somewhat similar to that of Naldrett et al. (2009) was previously proposed by Kerr & Leitch (2005), which invokes multi-stage upgrading processes where an early-formed sulfide liquid reacts with multiple batches of silicate magma. The model has been criticized by the fact that the many circumstances required are highly improbable (Cawthorn et al. 2005). Instead, Cawthorn et al. (2005) proposed a model involving a pressure change triggering sulfide saturation of the magma to form PGE reefs. It would presumably affect the entire intrusion at the same time and would explain the lateral homogeneity of the reef. However, whether such large changes are realistic is unknown, and still the initial problem, as with the other sulfide settling models, is how the sulfide liquid would settle through the cumulate pile and form continuous reefs efficiently, as argued by Maier et al. (2013).

Maier et al. (2013); (2016) proposed a model of downward percolation of sulfides in crystal mushes as a response to the subsidence of the central parts of the intrusion, due to crustal loading. This would lead to density and hydrodynamic sorting and kinetic sieving of crystal slurries and result in the formation of sulfide-chromite-magnetite-pyroxene-olivine-rich slurries. According to Maier et al. (2016), this would explain the observation of sharp contacts of the layers and the presence of injected sills. The model assumes that the emplacement depth is relatively shallow, as the crust needs to be ductile in order to collapse. Maier et al. (2013) further argued that in smaller intrusions, such as those in Finland, the subsidence would be smaller and the cooling faster, which could explain the more homogenous nature of PGE mineralization. The problem with this model is whether small sulfide droplets actually can be separated from a cumulate slurry.

2.6.2 Metasomatic models

There are several features associated with PGE reefs that have led researchers to suggest fluid-induced models, as some reefs cannot be explained by orthomagmatic processes (Barnes & Liu 2012; Maier et al. 2013; Godel 2015; O’Driscoll & González-Jiménez 2016). The main arguments for this include: 1) The presence of fluid- and hydrous melt inclusions in both silicates and oxides. 2) Pegmatoidal textures are associated with hydrosilicates, graphite and chlorapatite. 3) High Cl/F values in apatites underneath reefs. 4) Where potholes are present (e.g., Bushveld), desulfidization is often observed. 4) Plagioclase halos around chromitite rafts and xenoliths, that could be signs of fluid-related recrystallization (Maier & Barnes 2003; Godel 2015). The generalized metasomatic model (von Gruenewaldt 1979; Ballhaus & Stumpfl 1986; Boudreau & McCallum 1986; Boudreau & McCallum 1992; Willmore et al. 2000a; Willmore et al. 2000b; Boudreau 2008) involving percolation of Cl-rich fluids transporting and redepositing PGE is here briefly summarized. While the underlying cumulate pile is consolidating and compressing, deuteric interstitial fluids are exsolved from the silicate magma, as the intercumulus liquid is progressively becoming saturated in Cl-rich fluids. These high-temperature fluids percolate upward through semi-consolidating cumulates, dissolving sulfides, PGE and soluble metals from the magma. The Cl-rich fluid will transport

the PGE and metals in solution until it reaches the limit where it is no longer saturated, dissolving in the overlying undersaturated melt. As the underlying cumulate pile is consolidating, the front of saturation will progressively migrate upwards, thereby, progressively creating a PGE enriched horizon (Godel et al. 2007; Godel et al. 2008). Another aspect of this model is that the percolating fluids may also stop migrating if they encounter an impervious layer in the intrusion. Such a layer could be a buoyant plagioclase cumulate layer that had previously crystallized on top of the denser melt and were solid enough to prevent further transportation of the PGE fluids (Vermaak 1976; von Gruenewaldt 1979).

While the model discussed above may help to explain some of the observed features, it remains controversial. The arguments against this model, is that if deuteric fluids percolated upwards through the cumulate pile, thus, collecting PGE and metals by stripping out PGE-enriched sulfides, the following points and concerns have to be accounted for: 1) There should be an observed depletion in PGE and metal tenors in the rocks underlying the reef, which is not observed in the Bushveld Complex, for instance (Naldrett et al. 2009). 2) Some of the PGE, especially Ir, Ru and Rh, are thought to be insoluble (Hanley 2005). According to Cawthorn et al. (2002), there should be an enrichment in Os, Ir, and Ru compared to Rh, Pt and Pd in the primary PGM assemblages, but this is not observed in the Merensky Reef (Cawthorn et al. 2002). 3) How can a reef be homogenously consistent laterally when situated in close proximity to the floor rocks at the edges of the intrusions (especially if they are fairly flat as is the case with many layered intrusions), meaning that there is less of a magma column to derive metals from, compared to the central parts of the intrusions, which have hundreds of meters of underlying potential source rock (Maier et al. 2013). For more in-depth reviews, see (Barnes & Liu 2012; Maier et al. 2013; Godel 2015; O'Driscoll & González-Jiménez 2016).

2.7 Characteristics of platinum-group minerals

2.7.1 Magmatic and hydrothermal PGM assemblages and textures

When discussing magmatic and hydrothermal signatures, one would be advised to do so very carefully, as not much is known about the mineralization processes during the formation of PGM. There are many observations that lead to vagueness in even the most studied layered intrusions. One example is the Merensky Reef of the Bushveld Complex, where the difference in PGM assemblages varies greatly without any clear elucidation (Naldrett et al. 1986; Godel et al. 2007). One of the most critical concerns to bear in mind is the fact that while PGM may form at high magmatic temperatures of 900 – 1200° C, as the intrusion cools, the PGM may alter and change, even at much lower temperatures, approximately down to 300° C (O'Driscoll & González-Jiménez 2016). For the presence of PGE-bearing tellurides, there is no systematic distinction between telluride-bearing sulfide mineralization that are labeled as either orthomagmatic or hydrothermal in genesis (Helmy et al. 2007). Rather, the textural context of PGM is considered more reliable in determining the origin of mineralization. Nonetheless, some general observations seem to be indicative of their different formation processes.

2.7.1.1 Magmatic PGM

Regarding PGM assemblages inferred to be of magmatic origin, moncheite and merenskyite are often observed as inclusions in BMS or in close contact with BMS. The predominance of Pt and Bi over Pd and Te, respectively, are suggested to be indications of high-temperature crystallization (Garuti & Rinaldi (1986); Helmy (2005)). Helmy (2007) argued that temperature estimates from textures and phase relations were not useful, as there is no way to determine the actual difference in origin. Furthermore, Helmy (2007) stated that all varieties of sulfide-telluride mineralization reported in the literature are reset at temperatures below 320° C and they do not necessarily relate to the PGE forming event. Nevertheless, certain textures are thought to be indicative of a magmatic origin, e.g., PGM occurring as inclusions in BMS or at their contact. Telluride inclusions in high-temperature silicates or oxides would be strong indications of a magmatic origin (Helmy 2007).

2.7.1.2 Hydrothermal PGM

Tellurides are often observed at sulfide-silicate boundaries or hosted by remobilized BMS (e.g., ccp and viol) or hydrosilicates (Piispanen & Tarkian 1984; Rowell & Edgar 1986; Gervilla & Kojonen 2002). Hydrothermal PGM assemblages in layered intrusions, such as in the Platreef of the Bushveld Complex, are thought to be characterized by more alloy-dominated, sulfide-poor PGM. According to Holwell & McDonald (2006), hydrous or altered silicate-hosted PGM suggest the presence of fluids, or regression of the BMS boundary, causing the observation of satellite PGM grains. Furthermore, Holwell et al (2006) suggested that antimonides may be indicative of PGE transportation. It should be noted that Pt-Fe alloys are not necessarily fluid related, as they are also found in orthomagmatic assemblages (e.g., the Merensky Reef (Godel et al. 2008)). Palladium is more mobile than Pt in hydrothermal fluids, thus, a low Pt-Pd ratio of PGM would be an expected characteristic of a fluid-influenced system (Wood 2002).

The Platreef of the Bushveld Complex is particularly interesting as it displays both magmatic and hydrothermal features in different areas throughout the reef. The difference in PGM assemblages is correlated with the changes of host-rock in the footwall (Holwell & McDonald 2006; Holwell et al. 2006; Holwell & McDonald 2007). The footwall changes from dolomi-

tic in the south and central parts of Zwartfontein to Archean granitoids in the northern part. Where the country rock is BIF or shale as at Tweefontein, PGM sulfides are present. According to Holwell & McDonald (2006), the absence of PGM sulfides could possibly relate to low fS_2, when the Platreef magma interacted with the dolomitic footwall. Elsewhere in the Bushveld Complex, potholes in the Merensky Reef and platiniferous dunite pipes are low in PGM sulfides, being dominated by alloys, tellurides and sperrylites (Schouwstra et al. 2000; Cawthorn et al. 2002). It is thought that volatiles affected the Platreef when it intruded the dolomitic footwall, due to fluid activity related to metamorphism, assimilation and subsequent serpentinization (Holwell et al. 2006), which would cause decoupling of PGE from BMS, triggering redistribution of PGM into the footwall by fluids. In contrast, at Overysel, the Archean granitoid gneiss basement is anhydrous, and a more magmatic signature is observed as a more felsic partial melt with very low contents of volatiles was produced (Holwell et al 2006). A further observation thought to be related to hydrous fluids at Overysel is the replacement of BMS by hydrosilicates. This is interpreted to be a result of fluids reacting with BMS to form sulfuric acid, which dissolved the BMS around its margins, and thus, hydrosilicates could grow in the voids around the regressive margins.

In conclusion, the Overysel area is interpreted to be orthomagmatic, but the Sandsloot hydrothermal (Holwell et al. 2006). Holwell et al. (2006) proposed that the Overysel mineralization is due fluid fluxing at or close to the time of crystallization, and not due to later hydrothermal redistribution.

2.7.2 Characteristics of contact-type and reef-type mineralization

In general, there is a difference in the PGE mineralogy between typical contact- and reef-type mineralization. Their general mineralogical features are described below.

2.7.2.1 Reef-type PGE mineralization

The silicate-hosted reef-type PGE deposits are generally rich in Fe-alloys and Pt-Pd sulfides, along with arsenides and palladobismuthotellurides, which are also common in contact-style mineralization. This is seen, for example, in the mineralogy of the Merensky Reef and UG2 of the Bushveld Complex (Schouwstra et al. 2000; Cawthorn et al. 2002) and the J-M Reef of Stillwater Complex (Godel & Barnes 2008). The Merensky Reef exhibits a great variation in PGM assemblages in different places along the reef. Cawthorn et al. (2002) pointed out that there is a trend to higher proportions of PGM alloys in the northern part of Bushveld, while the southern and eastern parts contain more tellurides and PGM sulfides. For example, at the Union Mine, 82.8 vol.% of the PGM are Pt-Fe alloys, whereas the Impala Mine in the south only has 2 vol.% Pt-Fe alloys, being dominated by 56 vol.% Pt-Pd sulfides (contrasting the 2.3 vol.% at Union Mine). In the J-M Reef of the Stillwater Complex, there is a large heterogeneity in PGM assemblages. Nevertheless, approximately 44% of the PGM are Pd-Pt sulfides and 31% Pt-Fe alloys (Godel et al. 2008). The major difference compared to the Merensky Reef is that that most PGM of the J-M reef are associated with either magnetite or sulfides (Godel et al. 2008).

It may be difficult to determine the primary host assemblage of the PGM, as late-stage metamorphism, hydrothermal processes or surficial weathering may have remobilized the PGM to an unknown extent (common in the Fennoscandia-Kola region; Yakovlev et al. (1991); Alapieti & Lahtinen (2002)) and therefore, the observed mineral hosting PGM may not represent the primary magmatic host. However, in the Merensky Reef (Schouwstra et al. 2000; Cawthorn et al. 2002) and J-M Reef (Godel & Barnes 2008), most of the observed PGM are hosted in BMS or occur at contacts between BMS and silicates or oxides. Here 33 and 24 vol.% of the PGM are hosted in BMS, respectively, and 45 and 43 vol.% are observed at the BMS-silicate contacts. Textural observations alike and experimental studies (e.g., Helmy et al. (2007)) suggest that the PGE, Bi and Te possibly exsolved during the cooling of the sulfide liquid, in which they were hosted (Godel et al. 2007).

2.7.2.2 Contact-type PGE mineralization

In contact-type mineralization, the dominant PGM assemblage is often composed of low-temperature minerals, such as Pd-(Sb) tellurides, palladobismuthotellurides, and Pt-arsenides. PGM sulfides and Fe-alloys are comparatively rare (Iljina & Lee 2005; O'Driscoll & González-Jiménez 2016). This contrasts with the reef-type mineralogy discussed above. An example of this is the Overysel locality of the Platreef in the Bushveld Complex, where the majority of PGM are tellurides of Pd and Pt, comprising 46% of the observed PGM. Sperrylite and Pt-sulfides are frequent, as well as Pd-Pt bismuthotellurides (Holwell & McDonald 2006). As will be discussed later, the Platreef is very heterogeneous and its PGM assemblages vary greatly throughout the reef, depending on locality (Armitage et al. 2002; Holwell et al. 2006)). For instance, the Sandsloot occurrence lacks PGM sulfides, whereas at Drenthe and Overysel, PGM sulfides comprise more than 50% of the observed PGM assemblages. The Sandsloot locality also hosts more alloy-rich assemblages, in contrast to the other previously mentioned localities (Holwell et al. 2006).

Contact-type mineralization is often related to prolonged interaction of mafic magma with the surrounding country rock. It is plausible, that the marginal series would tend to have less PGM hosted in BMS and more satellite-grains in silicates, due to their environment of formation. However, I have not come across any empirical data to either prove or disprove this.

3 Review of sulfur isotopes

3.1 Principles

Sulfur isotopes are an important appliance for determining the source of sulfur and potential sulfur contamination of magma by country rock, provided the country rock exhibits a different isotopic composition from that of mantle-derived sulfur (e.g., evaporites and black shales). Most sulfur-poor PGE deposits, such as the J-M Reef of the Stillwater Complex (Ripley et al. 2017) or the Merensky Reef of the Bushveld Complex (Penniston-Dorland et al. 2012), exhibit an isotopic signature suggesting negligible contamination of crustally derived sulfur (Ripley & Li 2003). However, many sulfur-rich Cu-Ni deposits, including Noril´sk (Grinenko 1985), the Duluth Complex (Ripley 1981), the Uitkomst Complex (Li et al. 2002b) and Voisey's Bay (Ripley et al. 2002), show clear isotopic evidence that external sulfur was involved in ore formation (Li et al. 2002b; Ripley & Li 2003; Seal 2006).

The servicability of sulfur isotopes became evident in 1965, when Hulston & Thode (1965a,b) described the principles of mass-dependent sulfur isotope fractionation. There are five isotopes of sulfur ^{32}S, ^{33}S, ^{34}S, ^{35}S, and ^{36}S, of which ^{35}S is radiogenic and is produced by the breakdown of ^{40}Ar by cosmic rays in the atmosphere. The four stable isotopes and their ratios are expressed in relation to a global reference standard, a troilite in the Vienna Canyon Diablo Meteorite (V-CDT), which is thought to represent the bulk composition of the Earth (Macnamara & Thode 1950). The abundances of each isotope in V-CDT are the following: ^{32}S 95.02% , ^{33}S 0.75 %, ^{34}S 4.21%, and ^{35}S 0.02% (Ding et al. 2001; Rollinson 2014). The isotopic compositions of samples are expressed as delta values, which are per mill deviations from the standard composition. For example, for the $^{34}S/^{32}S$ ratio, $\delta^{34}S$ is defined as follows:

$$\delta^{34}S = \left(\frac{(^{34}S/^{32}S)_{sample} - (^{34}S/^{32}S)_{reference}}{(^{34}S/^{32}S)_{reference}} \right) \times 1000 \quad (2)$$

For stable isotope systems, the interest is in the relative partitioning of the isotopes, i.e. the changing ratios of isotopes. The partitioning of the isotopes (fractionation) is driven by kinetics and equilibria. For sulfur, the most common ratio of interest is the $^{34}S/^{32}S$ ratio. There are many reasons for this. Firstly, they are the two most abundant sulfur isotopes and thus easiest to analyze. Secondly, in thermodynamic equilibrium, the distribution of sulfur isotopes is determined by the relative difference of their masses (Urey 1947). This gives theoretical sulfur isotope variations of $\delta^{33}S \sim 0.5 \times \delta^{34}S$ and $\delta^{36}S \sim 2 \times \delta^{34}S$ (Hulston & Thode 1965a). This kind of behavior of sulfur isotopes is generally true for many non-equilibrium processes as well. However, it has recently been observed that mass-independent processes also affect the fractionation of sulfur isotopes in nature. Unforeseen values have been measured for many rocks that deviate from the theoretical mass fractionation laws (Farquhar & Wing 2003; Ripley & Li 2003; Penniston-Dorland et al. 2008). This concerns especially sulfur in ancient sedimentary rocks and has been explained by sulfur isotope fractionation in the atmosphere due to cosmic radiation, in times when the oxygen level in the atmosphere was very low (Farquhar et al., 2000). Therefore, the coupled $^{33}S/^{32}S$ and $^{36}S/^{32}S$ systems have gathered much interest recently.

Most magmatic processes related to degassing or crystallization of mafic magma are relatively insignificant in modifying the sulfur isotope ratios that are formed when sulfide melt crystallize. $\delta^{34}S$ signatures are therefore principally dependent on the isotopic composition of the magma source. To estimate the amount of crustal sulfur assimilation in a mafic magma, a simple two-component mixing model (Lambert et al. 1998; Ripley et al. 1999; Ripley & Li 2003) can be applied to estimate the amount of sulfur contamination;

$$\delta^{34}S(sulfide\ mixture) = \frac{\delta^{34}S_c f_c C_c^{\ s} + \delta^{34}S_m f_m C_m^{\ s}}{f_c C^s{}_c + f_m C_m^{\ s}} \quad (3)$$

Equation 3 (Ripley & Li 2003) involves two sulfur sources with differing $\delta^{34}S$ signatures interacting with each other, for example, a sedimentary country rock, with large non-zero $\delta^{34}S$ values, and a mafic magma with mantle-derived sulfur values close to zero. In the equation, f_m represents the mass proportion of the magma and f_c that of the contaminant (country rock) and C_s is the sulfur concentration in each component..

3.2 Reference reservoirs

Sulfur isotope ratios are interpreted in relation to empirically determined reservoirs. One of them is the mantle, whose sulfur isotope composition has been equated with that of V-CDT ($\delta^{34}S = 0$), and the other is modern seawater with heavy sulfur ($\delta^{34}S \sim 20$) (Allègre 2008). MORBs are very close in their sulfur isotope ratios to meteorites, demonstrating the theorem of a near-zero $\delta^{34}S$ value for mantle-derived magmas.

There is a general increase in the range of variation of $\delta^{34}S$ in sedimentary rocks with time, where the record of $\delta^{34}S$ exhibits a progression from relatively small fractionation in older rocks to much larger fractionation in younger rocks (Canfield 2001). The increase in fractionation of $\delta^{34}S$ is commonly attributed to the change of biological cycling of sulfur throughout time, mainly due to microbial sulfate reduction, but other factors also play a role, such as disproportionation and reduction of sulfur intermediates, as well as oxidation of different compounds (c.f. Canfield (2001)). Simplified, most reductive processes will decrease the $\delta^{34}S$ values, whereas oxidative process will increase the $\delta^{34}S$ values. The most effective process, as mentioned, is biogenic sulfate reduction driven by anoxic sulfate reducing bacteria, predominantly in marine sediments. The metabolism of the bacteria can be described by the following simplified

equation (Seal 2006):

$$2CH_2O + SO_4^{2-} \rightarrow H_2S + 2HCO_3 \quad (4)$$

The degree of fractionation by bacteria is dependent on the concentration of dissolved sulfate and other sulfur-carrying substrates needed for metabolism in their environment (Seal 2006). In marine near-surface settings, i.e. oxic settings, the process is dictated by the abundance of available organic matter. The bacteria preferably metabolize lighter ^{32}S over ^{34}S, and therefore, the residual sulfate becomes enriched in ^{34}S. Goldhaber & Kaplan (1975) showed that the degree of fractionation is partly governed by sedimentation rates, where a fast sedimentation rate will correspond to a small degree of fractionation and slow sedimentation will produce a higher degree of fractionation. There are, however, additional factors that contribute to the variation of S isotope fractionation. The isotopic composition of sulfur related to bacterial reduction is further controlled by the openness of the system. In a closed system, the amount of source of sulfate is finite, whereas in an open system, there may be an unlimited supply of sulfate, though the material needs to be efficiently transported into the anoxic environment. Furthermore, in a closed system, diagenetic cementation may isolate the sediments from the sulfate-reducing bacteria (Goldhaber & Kaplan 1975; Seal 2006).

A compilation of $\delta^{34}S$ data from different Ni-Cu (PGE) deposits is shown in Figure 6. For layered intrusions, the $\delta^{34}S$ signature of 0 ± 2‰ is commonly considered a pristine signature, uncontaminated from country rock (Ripley & Li 2003; Holwell et al. 2008). As is illustrated in Figure 6, many deposits have a $\delta^{34}S$ value near 0 ± 2‰, suggesting the dominance of mantle-derived sulfur, whereas in others, $\delta^{34}S$ deviates from the near-zero value, indicating assimilation of country sulfur with a different isotope signature. However, in some cases, such as in the Sudbury Complex, the Archean metasedimentary country rocks exhibit a $\delta^{34}S$ value very close to that of the mantle (Thode et al. 1962: Schwarcz 1973). Diagnosis of sulfur contamination using solely the $^{34}S/^{32}S$ system is thus problematic for older rocks due to lesser $\delta^{34}S$ fractionation in sedimentary rocks. However, this can be solved using multiple sulfur isotopes, as will be discussed below.

Studies of $\delta^{34}S$ systematics are normally straightforward and, in many cases, show a high contrast between the country rock and mantle-derived $\delta^{34}S$ values. Country rock can exhibit variations of more than one order of magnitude in relation to a non-zero value (Seal 2006). The $\delta^{34}S$ system is imperfect in some ways. Firstly, as already mentioned, the source rock may exhibit a near-zero $\delta^{34}S$ value, which is the case with many older Proterozoic and Archean sediments (Ripley & Li (2003)). Secondly, the $^{34}S/^{32}S$ ratios are susceptible to alteration in some magmatic and hydrothermal settings (Ripley & Li 2003; Pennistion-Dorland et al. 2008). These recent discoveries highlight the uncertainties in the behavior of sulfur in many geological systems. Thus, a $\delta^{34}S$ signature of a near-zero value, may not necessarily be mantle derived.

3.3 The $\delta^{33}S$ system

Due to the fact that the $\delta^{34}S$ system is occasionally very equivocal, the application of multiple sulfur isotopes, particularly ^{33}S coupled with $\delta^{34}S$, is becoming more and more common for rocks with an age of >2 Ga. The $\delta^{33}S$ system is unique in that even when the $\delta^{34}S$ system displays values close to zero, and therefore overlap magmatic signatures, $\delta^{33}S$ may still be useful. As discussed earlier, mass-dependent fractionation gives a $\delta^{34}S/\delta^{32}S$ ratio of ~0.515 and a $\delta^{36}S/\delta^{32}S$ ratio of ~1.91 (Hulston & Thode 1965a). For the $\delta^{33}S$ system, we study the deviation of a measured quantity of $\delta^{33}S$ and/or $\delta^{36}S$ relative to the predicted mass-dependent fractionation values previously established for $\delta^{34}S/\delta^{32}S$ and $\delta^{36}S/\delta^{32}S$. The equations are defined as:

$$\Delta^{33}S = \delta^{33}S - 1000((1+ \delta^{34}S/ 1000)0.515 -1))$$

$$\Delta^{36}S = \delta^{36}S - 1000((1+ \delta^{34}S/ 1000)1.91 -1))$$

When plotting $\Delta^{33}S$ as a function of sample age, there is a drastic change in $\Delta^{33}S$ at ca. 2.4 Ga (Farquhar et al. 2000; Johnston 2011), where the variation of $\Delta^{33}S$ in older rocks is vast (Fig. 7). The $\Delta^{33}S$ values cannot be explained by mass-dependent fractionation, but instead, the change in $\Delta^{33}S$ is thought to be due to mass-independent processes (Farquhar & Wing 2003; Johnston 2011). These processes produce non-zero values for $\Delta^{33}S$ and $\Delta^{36}S$. Using multiple sulfur isotopes can therefore provide a definite tool for tracing crustal sulfur contributions, even when $\delta^{34}S$ display mantle values (Farquhar & Wing 2003). Important key points regarding $\Delta^{33}S$ are:

1. Mass-dependent processes produce only small variations in $\Delta^{33}S$ ($\Delta^{36}S$), whereas they create significant fractionation of $\delta^{34}S$.
2. Mass-independent processes create greater variations in $\Delta^{33}S$ ($\Delta^{36}S$), whereas $\delta^{34}S$ may or may not display a deviation.

The mass-independent fractionation of sulfur isotopes is suggested to be due to an unoxygenated atmosphere, which allowed for nucleosynthetic and photochemical processes and other unknown processes to take place in the atmosphere (Farquhar et al. 2000; Farquhar & Wing 2003; Johnston 2011). The $\Delta^{33}S$ record of sedimentary rocks can be divided into three stages throughout geological time (Fig. 7). Stage 1, from ca. < 3.8 Ga until 2.45 Ga, is characterized by highly variable non-zero $\Delta^{33}S$ values, both negative and positive. This is suggested to be due to SO_2 and SO photolysis caused by deep ultraviolet radiation in the primitive

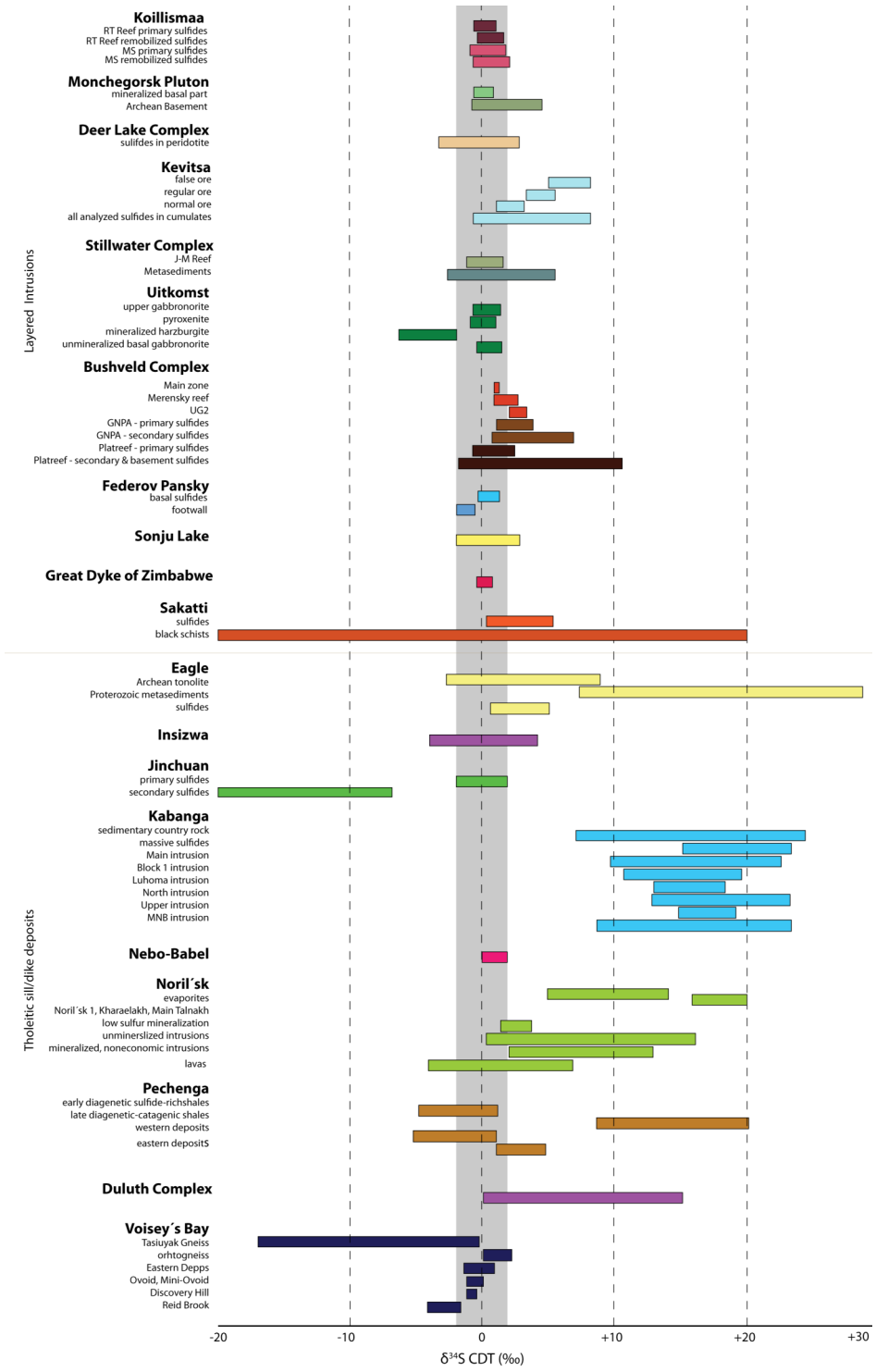

Figure 6. Comparison of $\delta^{34}S$ V-CDT values from various Ni-Cu-PGE deposits, including both layered intrusion-related PGE deposits and magmatic Ni-Cu sulfide deposits in tholeiitic and picritic sills/dikes. Shaded area indicates $\delta^{34}S$ of 0 ± 2, generally representing the mantle-derived isotope composition. Figure modified after (Schulz et al. 2010). Sources of data: Eagle (Ding et al. 2009); Insizwa (Lightfoot et al. 1984); Jinchuan (Ripley et al. 2005); Kabanga (Maier et al. 2010); Nebo-Babel (Seat et al. 2009); Noril´sk (Grinenko 1985; Li et al. 2003; Ripley et al. 2003); Pechenga (Abzalov & Both 1997; Barnes et al. 2001); Uitkomst - (Li et al. 2002a); Voisey's Bay (Ripley et al. 1999; Ripley et al. 2002). Added data for this figure; Bushveld Complex, Main Zone, Merensky Reef and UG2 (Penniston-Dorland et al. 2012); Stillwater Complex, J-M Reef (Ripley et al. 2017); Sakatti (Brownscombe et al. 2013); Great Dyke of Zimbabwe (Li et al. 2008a; Maier et al. 2015); Sonju Lake (Park et al. 2004); Federov Pansky (Schissel et al. 2002); Bushveld Complex, GNPA (Smith et al. 2016); Bushveld Complex, Platreef (Holwell et al. 2007); Duluth Complex (Ripley 1981); Kevitsa (Luolavirta et al. 2018); Deer Lake Complex (Ripley 1983) and Monchegorsk (Bekker et al. 2016); Koillismaa, this study. During assembly of this figure, it was noted that the data of Jinchuan and Nebo-Babel were missplotted in the cited sources. This has now been corrected.

Archean atmosphere without an ozone shield, as suggested by Farquhar & Wing (2003). Stage 2, from ca. 2.45 Ga to 2.0 Ga, has a much smaller range in $\Delta^{33}S$ (-0.1 to +0.5 ‰). This has been suggested to be due to the appearance of an oxygenated atmosphere. The prevalence of oxygen allowed for the advance of an ozone layer, which protected the atmosphere from ultraviolet radiation, unlike in the Archean when the lack of ozone caused the photochemical reactions (Farquhar et al. 2000; Farquhar & Wing 2003; Bekker et al. 2004). Lastly, stage 3 from ca. 2.0 Ga until present shows a near-zero $\Delta^{33}S$ value of ±0.2 ‰ (Farquhar & Wing 2003). In conclusion, a non-zero value of $\Delta^{33}S$ is indicative of the presence of sulfur that at some stage was exposed to cosmic radiation in the Archean atmosphere. Because the $\Delta^{33}S$ fractionation is formed by atmospheric processes, subsequent processes, such as high-temperatures, metamorphism and hydrothermal alteration, cannot alter the original $\Delta^{33}S$ signature, except by dilution of the original signature by mixing of sulfur from different sources (Farquhar et al. 2000; Farquhar & Wing 2003; Bekker et al. 2004; Johnston 2011).

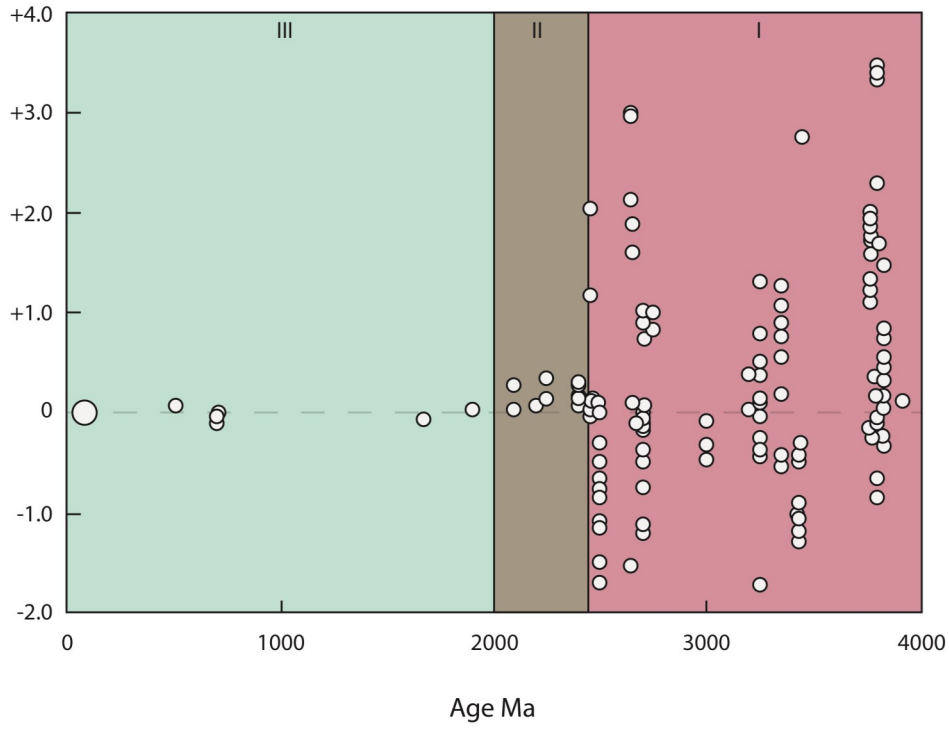

Figure 7. Plot illustrating the variation in $\Delta^{33}S$ through time. Stage I spans from >3.8 to 2.45 Ga and is distinguished based on highly varying $\Delta^{33}S$ values, which is suggested to be due to SO_2 and SO photolysis caused by deep ultraviolet radiation in the primitive Archean atmosphere without an ozone shield. Stage II, spanning from 2.45 to 2 Ga, is characterized by lesser variability and absence of negative $\Delta^{33}S$ values, suggested to be due to the onset of an oxygenated atmosphere, causing oxidative weathering. Finally, stage III, spanning from 2.0 Ga until present time, displays a very small deviation from $\Delta^{33}S$ of 0 ±0.2 ‰. Modified after Farquhar & Wing (2003).

4 Geological background

4.1 Exploration history of the Koillismaa intrusion

The mining company Outukumpu Oy launched a Ni-Cu exploration project in the Koillismaa area in 1962, where they observed disseminated sulfides in the basal parts of the Koillismaa intrusion. Inferred to be of economic value, a pilot plant was setup. However, the grades proved inadequate and the project was terminated in 1968. Otanmäki Oy continued exploration in the area and subsequently found vanadiferous magnetite-gabbro, which lead to the opening of the Mustavaara mine in 1976. At this time, between 1971 – 1976, a project termed the Koillismaa Research Project was carried out by the University of Oulu. It included re-mapping of the Koillismaa Complex and nearby bedrock (Piirainen et al. 1978)*. Until then, the general opinion was that the blocks of the Koillismaa intrusion represented smaller separate intrusions (Enkovaara et al. 1953)*, but now it was concluded that they were all part of one big layered intrusion which had been repeatedly sheared, causing segregation of the original intrusion into the separate blocks observed (Piirainen et al. 1978). Moreover, based on gravimetric data, it was suggested that the Koillismaa and Näränkävaara intrusions were interrelated by a hidden connecting dyke.

Alapieti (1982) thoroughly described the Koillismaa intrusion in terms of its structure, stratigraphy, mineralogy and geochemistry. The rocks overlaying the intrusion had previously been considered to be felsic lavas (Piirainen et al. 1974; Alapieti et al. 1979), until Alapieti (1982) suggested that they were granophyres. It has later been proposed that the granophyre represents pre-intrusion volcanic rocks (Lauri 2004).

Associated with the PGE mineralization in the layered series are meter-sized noncumulus gabbronoritic bodies, also called micro-gabbronorites (Alapieti & Piirainen 1984), hosted by sulfide-bearing pegmatitic and mottled gabbronorites (Alapieti 1982; Karinen 2010). These noncumulus bodies have been interpreted as dykes (e.g., Piispanen & Tarkian (1984)) or as xenoliths (e.g., Iljina et al. (2001)).

4.2 Geological setting of the Koillismaa intrusion

The beginning of the Proterozoic eon was concomitant with global igneous activity, involving many coeval layered intrusions and dyke swarms located in cratons worldwide (e.g., East Bull Lake Suite of the Superior craton (Peck et al. 2001) and the Jimberlana intrusion of the Yilgarn craton (McClay & Campbell 2009)). More than 20 early Paleoproterozoic layered intrusions were emplaced in the Fennoscandian Shield during this period, many of which are mineralized in PGE and Ni-Cu (Alapieti et al. 1990; Alapieti & Lahtinen 2002). Two age groups are recognized, one at ca. 2.44 Ga and the other at ca. 2.5 Ga (Amelin & Semenov 1996). It has been proposed that the igneous activity was caused by prolonged plume magmatism, associated with a super-continental breakup where Fennoscandia, Superior and Wyoming were the nearest neighbors (Bayanova et al. 2009; Davey et al. 2018). The Fennoscandian Paleoproterozoic layered intrusions have all been affected by several stages of post-magmatic deformation and metamorphism, particularly subsequent deformation and metamorphism are thought to have occurred during the Svecofennian orogeny at 1.9 – 1.8 Ga.

The Koillismaa-Näränkävaara Complex (Fig. 8) is part of the Tornio-Näränkävaara belt, an E-W-trending, 300-km-long, discontinuous zone, making up approximately half of the 2.4 - 2.5 Ga layered intrusions in the Fennoscandian Shield (Iljina & Hanski 2005). The Tornio-Näränkävaara belt extends from the Tornio intrusion in Sweden, to the eastern border of Finland, continuing further east as the Oulanka Complex in Russia (Alapieti 1982; Alapieti et al. 1990). The belt consists of the following layered intrusions: The Tornio, Kemi and Penikat intrusions in the west, the centrally located Portimo Complex, the Koillismaa-Näränkävaara Complex in the east (plus the Oulanka Complex in Russia). The Tornio-Näränkävaara belt varies in composition, with the Tornio- and Näränkävaara intrusions being ultramafic and the Koillismaa intrusion mainly consisting of mafic cumulates (Alapieti 1982; Karinen 2010; Iljina et al. 2015).

Apart from the Näränkävaara intrusion, the layered intrusions have Archean granite-gneiss basement rocks to the south and supracrustal volcano-sedimentary formations on their northern sides. Overlying the Koillismaa intrusion is a thick section of granophyric rocks, and above them, occasionally supracrustal rocks of the Kuusamo schist belt (Alapieti 1982; Karinen 1998; Karinen 2010). The magmatic layering of the intrusion dips between 10° and 50°, towards the supracrustal overlying rocks (Karinen 2010).

The intrusions have an age of ca. 2.44 Ga (Huhma et al. 1990; Huhma et al. 2011) and were formed during bimodal igneous activity, with large volumes of mafic and minor A-type granitic intrusions, generating both intrusive and extrusive formations. This igneous activity has been suggested to be related to failed cratonic rifting related to a mantle plume (Amelin & Semenov 1996; Hanski et al. 2001).

Using the U-Pb zircon method, the Koillismaa-Näränkävaara Complex has been dated at 2436 ±5 Ma (Alapieti 1982). The complex includes the Koillismaa intrusion in the west and the Näränkävaara intrusion in the east (Fig. 9). They are connected by a strong gravity-anomaly zone (Alapieti 1982) that has been interpreted as a hidden feeder zone and may itself be a layered intrusion (Alapieti 1982; Iljina 2004; Iljina & Hanski 2005). According to Karinen (2010), the connecting zone is associated with currently undescribed

* See *Appendix I*, regarding nomenclature

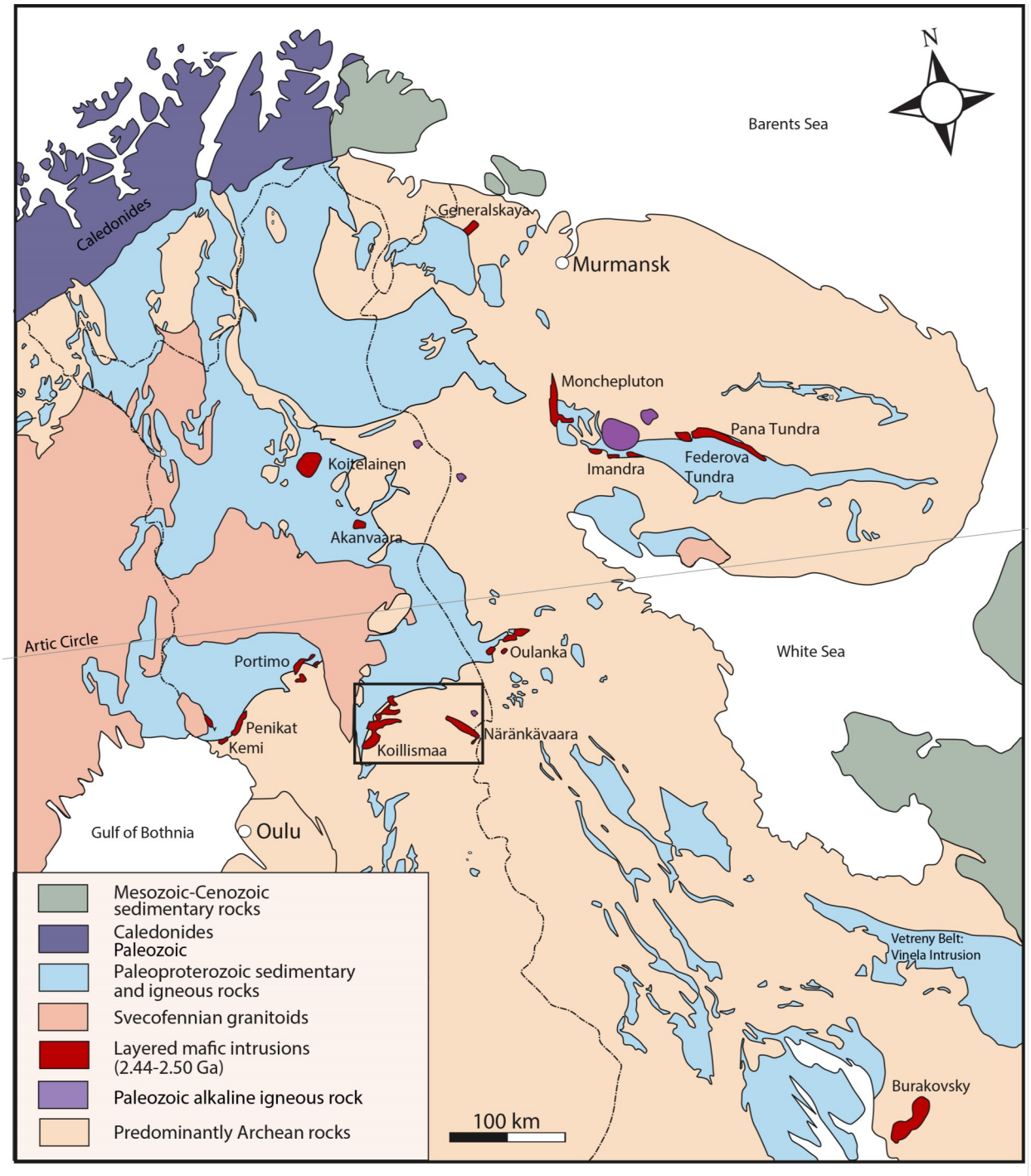

Figure 8. Generalized geological map of the northeastern Fennoscandian Shield, with Paleoproterozoic layered intrusions shown in red . The black square outlines the area of the Koillismaa Complex, as shown in detail in Fig. 10. Modified after Alapieti (1990), Alapieti & Lahtinen (2002), Karinen (2010) and Yang et al. (2016).

breccias. Alapieti (1982) inferred the geophysical data to suggest that its upper surface is 1.4 km below current erosion level and approximately 3 km wide and vertically oriented. The Näränkävaara intrusion is ultramafic, consisting of pyroxenitic and peridotitic rocks (Alapieti 1982; Telenvuo 2016). It has been suggested that the two intrusions and the feeder zone were derived from three separate magmas with one large magma source below Näränkävaara (Alapieti & Lahtinen 2002)

4.3 Structure of the Koillismaa intrusion

The Koillismaa intrusion consists of several severed blocks (Fig. 10), displaying a synformal structure with a W-E-oriented axis. From north to south, they are labeled as: Murtolampi, Kaukua, Lipeävaara, Tilsa, Kuusijärvi, Porttivaara, Syöte, Pirivaara, and Pintamo. The Porttivaara, Kuusijärvi and Lipeävaara blocks are

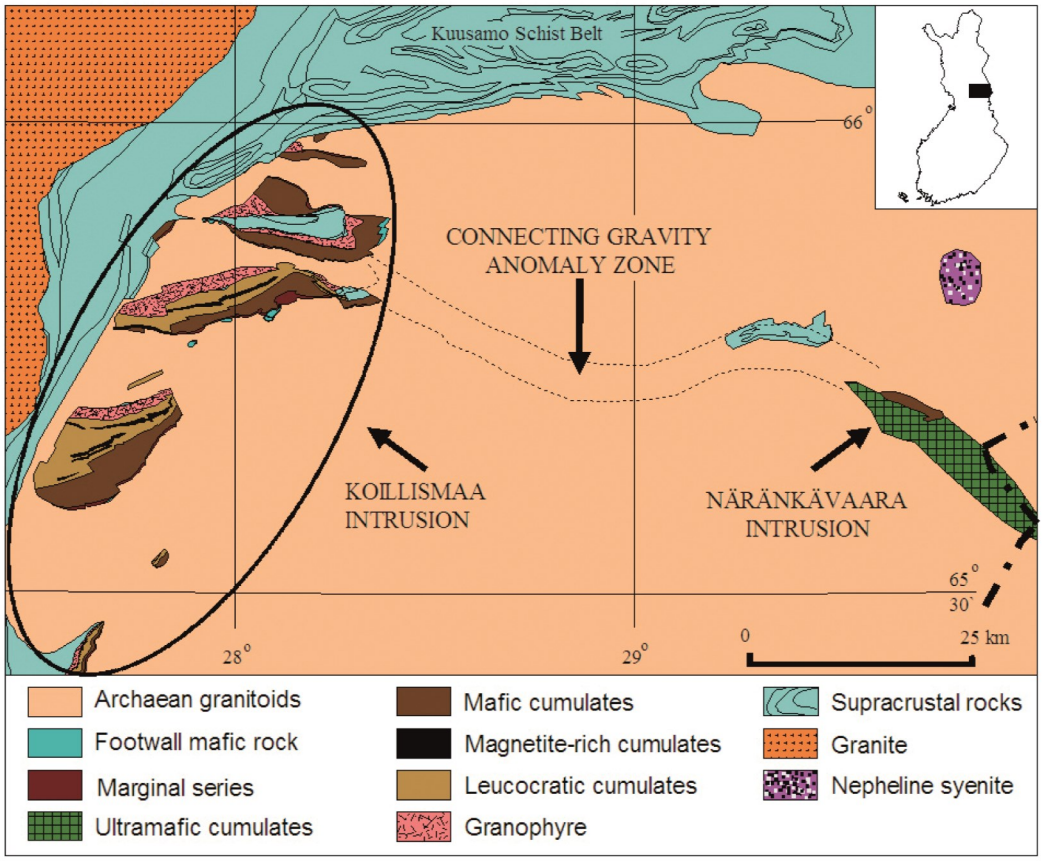

Figure 9. Generalized geological map of the Koillismaa-Näränkävaara Complex. Reprinted with kind permission from Karinen (2010).

estimated to be 2000 – 2500 m thick, whereas the southern Pirivaara and Syöte blocks are estimated to be 1100 m thick, based on gravimetry. The northern blocks Lipeävaara, Kaukua and Murtolampi dip S-SW and the southern blocks Pintamo, Pirivaara, Syöte, Porttivaara, Tilsa and Kuusijärvi dip N-NW. The dip is greater in the central blocks around Portivaara, 35 - 50°, whereas the exterior blocks gradually dip less, ca 10 - 30°. All of the blocks are partially displaced and faulted, and in some parts (e.g., the Syöte block), the stratigraphy is repeated because of the faults (Alapieti 1982). Alapieti (1982) proposed that the original pretectonic Koillismaa intrusion was a flat and sheet-like body, 1 - 3 km in thickness (Fig. 12). It has been proposed that the disjointing of the intrusion was produced in a N-S compressional setting (Karinen & Iljina 2009).

The Näränkävaara intrusion is thought to have preserved its original elongated shape and remains as a single intact layered intrusion, thought to be about 6 km deep, based on gravimetric data (Alapieti 1982; Alapieti & Lahtinen 2002). The Koillismaa intrusion is divided into two series, the Layered Series and the Marginal Series, where there is an observed angular discordance in between (Fig. 11-12).

4.3 Igneous lithostratigraphy and petrography of the layered suite

The Koillismaa intrusion is approximately 2500 m thick and its general lithostratigraphy (Fig. 13) is predominantly based upon the Portivaara block, where the lithostratigraphic units are thought to be most complete. The lithostratigraphy is based on the presence of major cumulate minerals and the grain size of plagioclase (Alapieti 1982; Karinen 2010). All the rocks of the marginal- and layered series are altered, but primary magmatic textures are commonly preserved. The Marginal Series is divided into two zones and the layered series is divided into three zones, with each zone being further divided into subzones. The lithostratigraphy, as presented by Karinen (2010), is the following:

- Roof rocks
- Granophyre
- Upper chilled margin
- Layered Series (LS)
- Upper Zone (UZ)
  - Upper Zone c (UZc)
  - Upper Zone b (UZb)
  - Upper Zone a (UZa)
- Middle Zone (MZ)
  - Middle Zone c (MZc)
  - Middle Zone b (MZb)

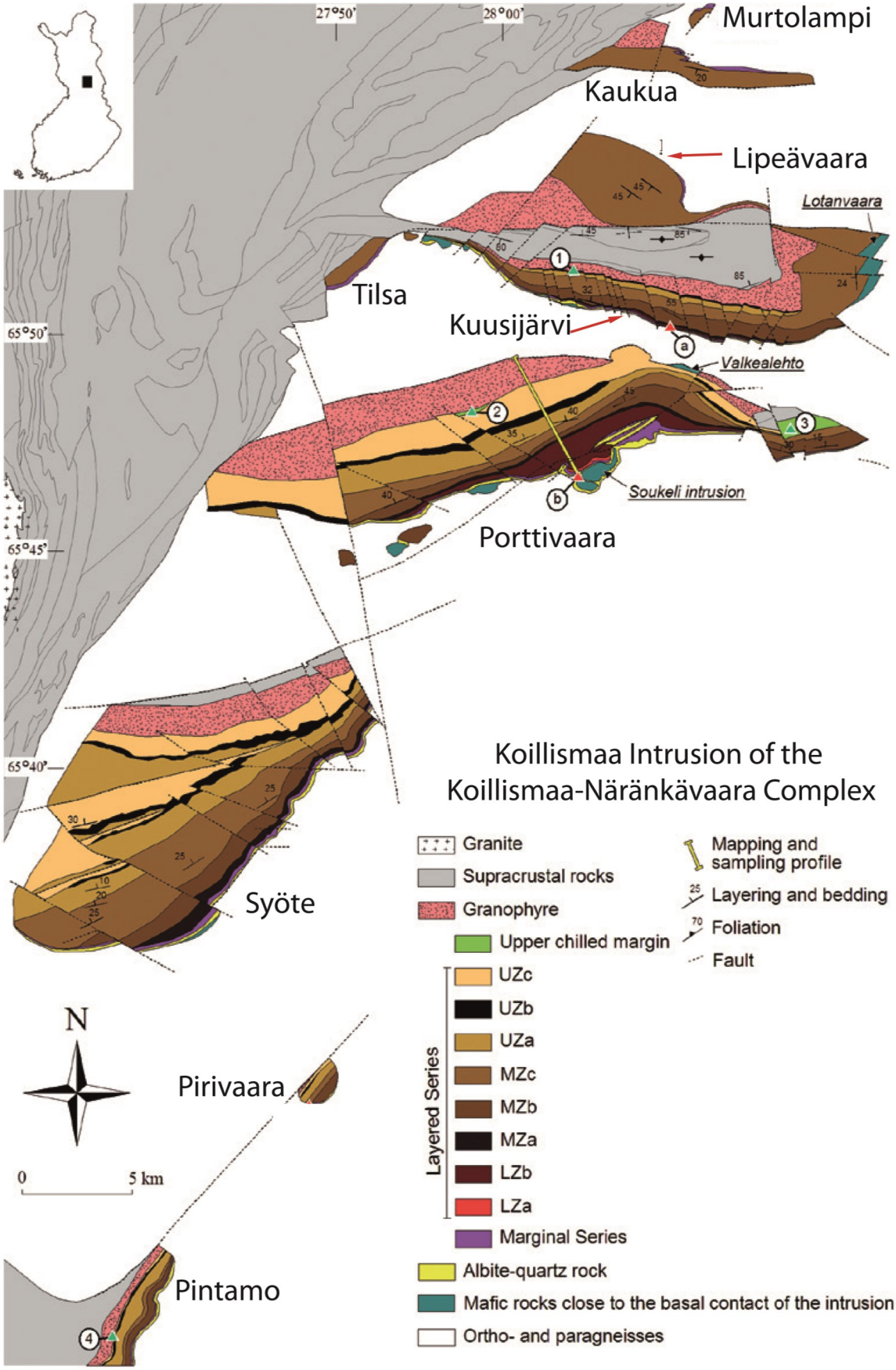

Figure 10. Geological map of the Koillismaa intrusion. Abbreviations: UZ = Upper Zone, MZ = Middle Zone, LZ = Lower Zone. Reprinted with kind permission from Karinen (2010).

Middle Zone a (MZa)

- Lower zone (LZ)
  - Lower Zone b (LZb)
  - Lower Zone a (LZa)
    - Olivine gabbronorite unit II
    - Gabbronorite unit
    - Olivine gabbronorite unit I
- Marginal Series (MS)
  - Upper Zone of the MS (UZMS)
    - Upper Zone b of the Marginal Series (UZMSb)
    - Upper Zone a of the Marginal Series (UZMSa)
  - Lower Zone of the MS (LZMS)
    - Lower Zone b of the Marginal Series (LZMSb)
    - Lower Zone a of the Marginal Series (LZMSa)
- Lower chilled margin
- Archean basement

4.3.1 Chilled margins

Observations of chilled margins are scarce and when observed, they are highly altered (Karinen 2010). Alapieti (2002) suggested that the scarcity is a consequence of continuous magma injection, assimilating the margins. The chilled margins are fine-grained gabbronoritic rocks of boninitic composition. The lower chilled margin is less evolved than the upper chilled margin, but both are less evolved than the average rocks composition of the actual intrusion (Karinen 2010). Above the upper chilled margin is a 1000-m-thick sequence of granophyre (Lauri 2004).

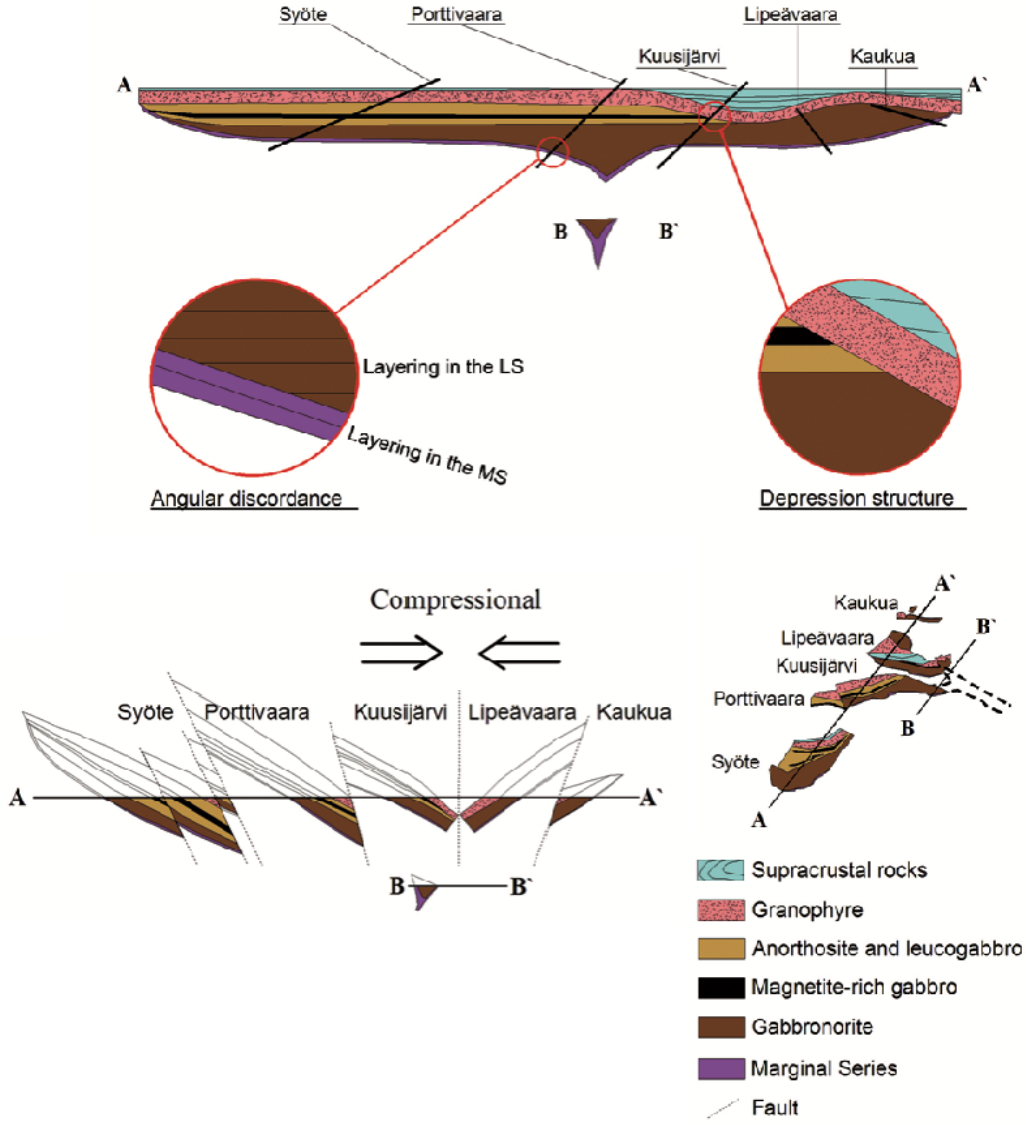

Figure 11. Cross section of the suggested originally flat stratified Koillismaa intrusion with current erosion levels of the blocks and possible compressional setting, explaining the present structural setting of the intrusion. Used with kind permission from Karinen (2010). Modified after Alapieti & Lahtinen (2002); Karinen (2010).

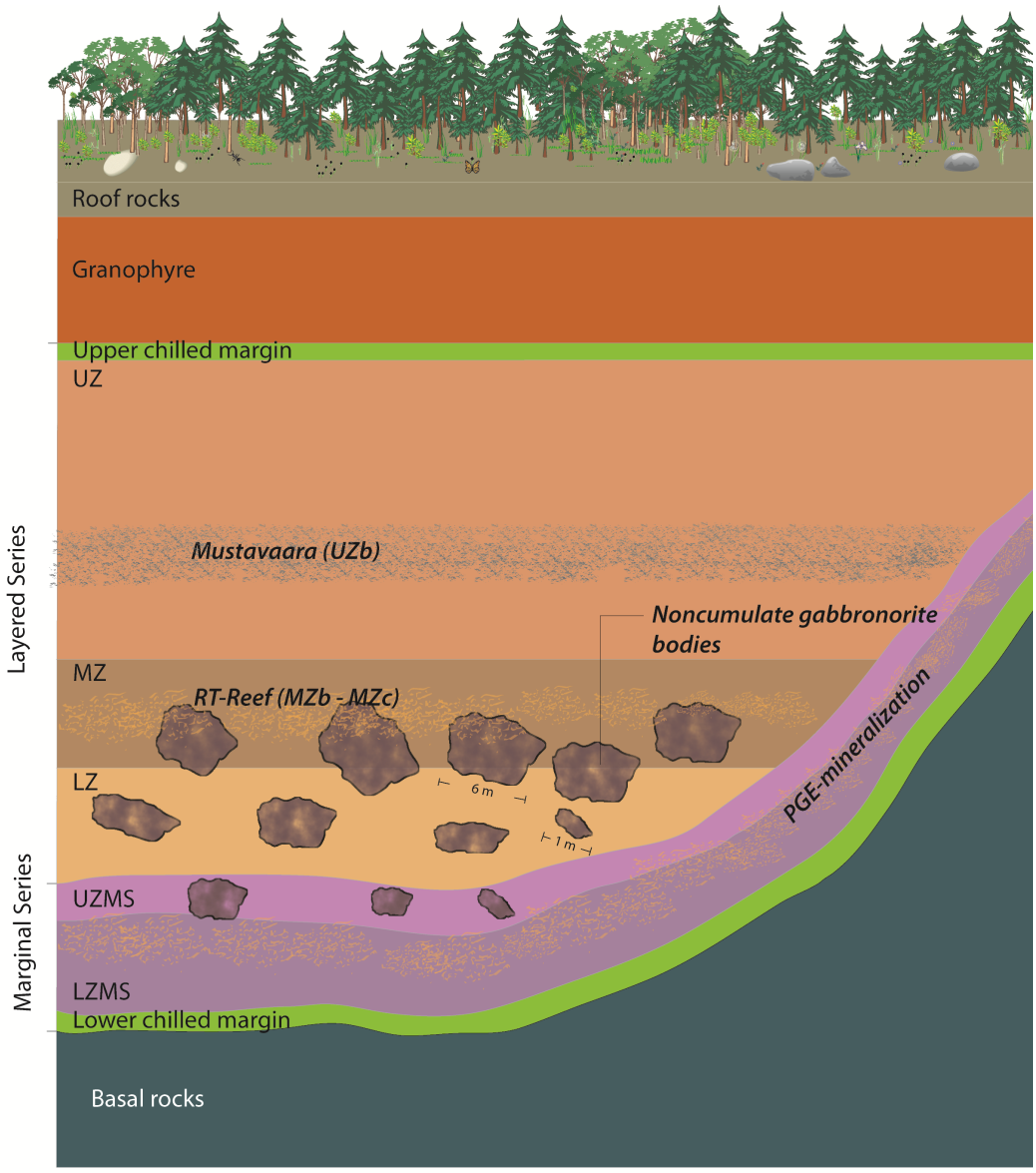

Figure 12. Illustration showing a simplified conceptual layered stratigraphy for the Koillismaa intrusion before segregation (not to scale). The heterogenous marginal series and its relation to the chilled margin is not depicted in this figure.

4.3.2 Marginal Series

The Marginal Series varies from 50 to 200 m in thickness (Alapieti 1982) and in the stratigraphic section of the Portivaara block, it is estimated to be 60 m thick (Karinen 2010). The Marginal Series is oriented parallel with the basal margin of the intrusion and is discordant with respect to the overlying layered series. It exhibits a reversal fractionation trend, grading upwards from mafic gabbronorite into ultramafic pyroxenite and peridotite. The modal abundance of plagioclase gradually decreases as the modal abundance of mafic minerals increases upwards, and the mafic minerals become more magnesian and plagioclase more calcic upwards (Alapieti 1982).

The Marginal Series consists of two zones, the gabbronoritic Lower Zone (LZMS) and the more ultramafic Upper Zone (UZMS). The Lower Zone is heterogeneous, containing albite-quartz veinlets and inclusions of partially melted basement rocks in its lowermost subzone, which gradually becomes more homogenous upwards. Xenoliths from the basement frequently have gneissic structures preserved and the abundance of fragments diminish as the rock becomes more homogenous (Alapieti 1982). The lowermost zone (LZMS) comprises plagioclase-orthopyroxene cumulates with intercumulus clinopyroxene, whereas the UZMS consists of orthopyroxene cumulates grading into peridotitic poikilitic olivine orthocumulates (Karinen 2010). The basal contact is associated with albite-quartz rocks, which have been suggested to be signs of partial melting and hydrothermal alteration (Alapieti 1982; Karinen 2010). The Marginal Series is associated with a contact-type PGE sulfide mineraliza-

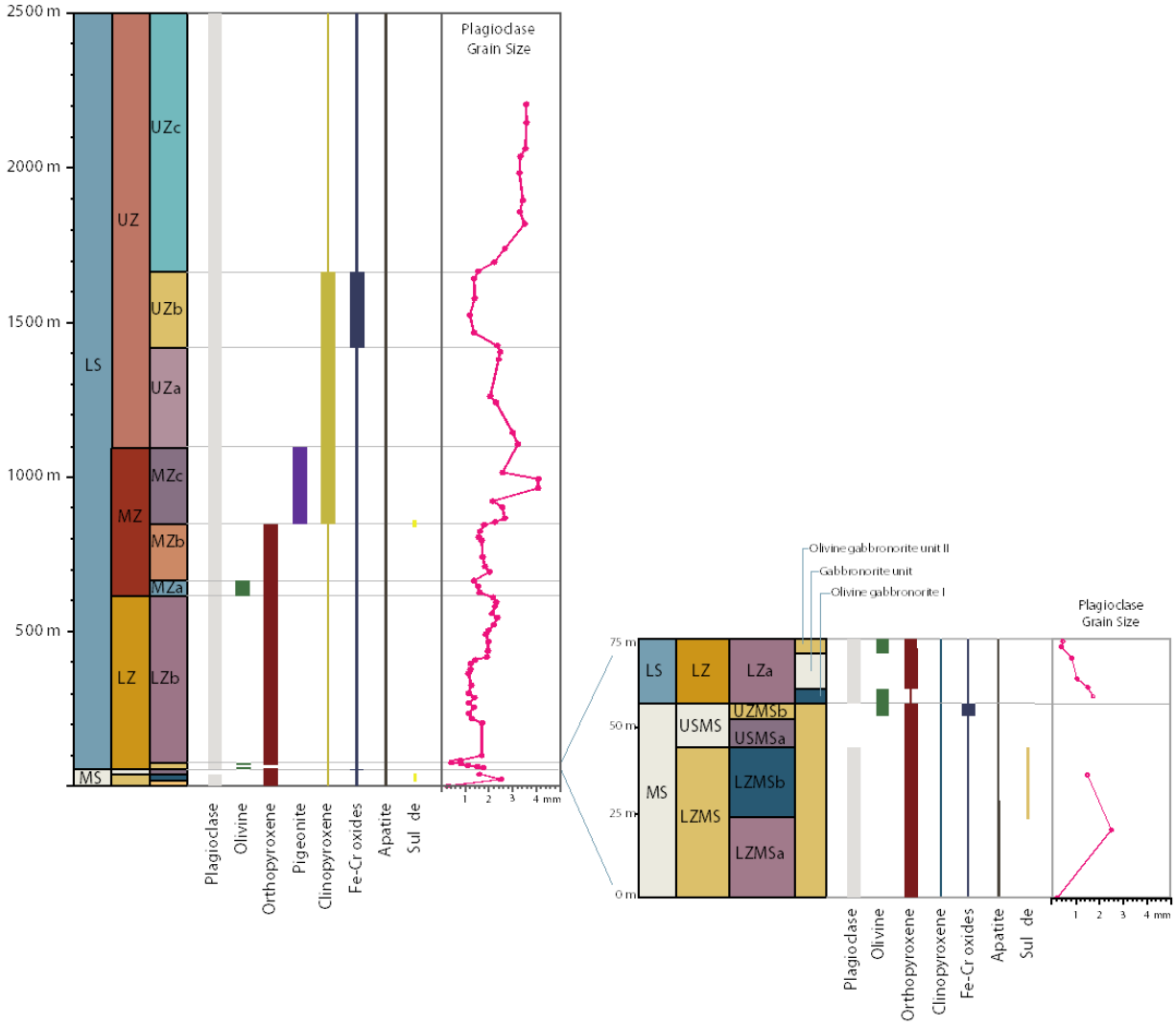

Figure 13. Stratigraphic section of a profile of the Portivaara block, illustrating the grain size of plagioclase and the presence of cumulus minerals throughout the section. Thick lines indicate the present cumulus minerals and thin lines the presence of intercumulus minerals. Modified after Karinen (2010).

tion (Alapieti 1982; Karinen 2010).

4.3.3 Layered Series

The layered series consists of three mineralogically distinct zones. They are further divided into eight subzones, which can be mineralogically correlated throughout the dislocated blocks in the area (Alapieti 1982; Karinen 2010). The 620-m-thick Lower Zone (LZ) consists of olivine gabbronorites in its lower part (LZa), whereas the upper part (LZb) comprises gabbronorites. The 450-m-thick Middle Zone (MZ) is characterized by the absence of olivine and the presence of augite as a cumulate mineral. The exception is the thin MZa unit, which consists of a thin layer of cumulate olivine gabbronorite. The central part of the Middle Zone is characterized by the first appearance of cumulus augite and inverted cumulus pigeonite, which is the distinguishing boundary between the subzones MZb and MZc. This boundary contains the Rometölväs Reef PGE mineralization. The reef is laterally heterogeneous and is observed to be <20 m thick in places. The 1250-m-thick Upper Zone (UZ) is characterized by plagioclase-rich cumulates of leucogabbro (UZa) and anorthosites (UZc). The Upper Zone b (UZb) is composed of an Fe-Ti-V mineralized plagioclase-clinopyroxene-magnetite adcumulate, the host of the Mustavaara deposit (Alapieti 1982; Karinen 2010).

In contrast to the Marginal Series, the Layered Series generally shows a normal differentiation trend, where most of the Mg and Cr content decline upwards in the stratigraphy. However, there are observed reversal trends in the upper LZb and the lower MZ. The most An-rich plagioclase occurs in the UZc, being notably more juvenile than in the underlying layers. Furthermore, the underlying UZb contains the most albite-rich plagioclase, thus being the most evolved. The Rometölväs Reef located between the MZb and

MZc marks a boundary of rocks with contrasting rock chemistry (Karinen 2010). The underlying part of the intrusion is characterized by Cr- and Mg-rich cumulates, which are enriched in nickel and chlorine in comparison with the overlying cumulates. Karinen (2010) observed that samples from the reef show contrasting chemical trends and suggest that the reef contains components from both the overlying and underlying rocks, at the same time noting that at a local level, the chalcophile element content is dictated by the rock texture where the most mottled rocks display the best ore-grades.

4.3.4 Noncumulus-textured gabbronorites

The Koillismaa intrusion contains lenticular noncumulus-textured gabbronorite bodies (Karinen 2010), also called microgabbronorites (Alapieti 1982), which are conformable with the igneous layering. These bodies occur in both the Marginal Series and Layered Series, though are sparser in the Marginal Series. They progressively increase in size and abundance upwards in the stratigraphy until the MZb-MZc boundary (Alapieti 1982; Karinen 2010). According to Karinen (2010), the largest observed body is approximately six meters in thickness. However, Alapieti (1982) described them as "veinlets" or inclusions ranging between <1 m up to 30 m in diameter.

The Rometölväs Reef is the uppermost level where the noncumulus-textured gabbronorites bodies have been observed and is the only place where sulfide mineralization occurs in association with gabbronorite bodies (Alapieti 1982; Karinen 2010). The bodies have been inferred as xenoliths from earlier magma pulses, as interrupted dykes or to have formed due to decompression effects (Iljina et al. 2001; Alapieti & Lahtinen 2002; Karinen & Iljina 2009). The bodies display a sharp contact with the surrounding cumulate rocks of the intrusion. However, no definite chilled margins are observed. They are often situated near altered, mottled and mineralized zones of the intrusions. Certain bodies associated with the reef are mineralized in their upper portions, but none of the stratigraphically lower bodies are mineralized. The mineralization consists of pyrrhotite, chalcopyrite and pentlandite in relatively coarser-grained centimeter-sized pockets (Alapieti 1982; Iljina et al. 2001; Karinen 2010). Additionally, the bodies at Portivaara and Kuusijärvi are more magnesian than in the more southern Pirivaara block (Karinen 2010).

4.4 Mineralization

4.4.1 Contact-type PGE mineralization

Contact-type PGE sulfide mineralization occurs in the Marginal Series and is estimated to extend laterally for 100 km, being predominantly hosted in the middle part of the Marginal Series (Alapieti 1982; Iljina et al. 2005; Karinen 2010). The zone of mineralization is 15 - 40 m in thickness and has a sulfide content of 1 - 5 vol.%. The sulfides are represented by pyrrhotite, chalcopyrite and pentlandite, with sporadic pyrite. Chalcopyrite is often finely disseminated in silicates, whereas pyrrhotite and pentlandite tend to cluster in blebs up to 2 cm in size (Alapieti 1982; Karinen 2010). Accessory sulfides are pyrite, bornite, sphalerite, galena-clausthalite, violarite (alteration of pentlandite), cobaltite, and covellite (Iljina et al. 2001; Karinen 2010; Iljina et al. 2012). Most of the PGM and Au- and Ag-bearing minerals are tellurides (Fig. 14a) with an average grain size of 3.2 μm^2 (Karinen 2010). According to Kojonen and Iljina (2001), the grain size of PGM are generally less than 40 μm and most grains are 5 - 10 μm in diameter, in the Marginal Series at Haukiaho. In the contact-type mineralization of the Kaukua and Kuusijärvi blocks, the average grades are 0.2 - 0.4 wt.% for Cu and 0.2 - 0.3 wt.% for Ni (Iljina et al. 2015). The more central areas, such as Kuusijärvi, Lavotta and Rusamo, have higher sulfide contents, whereas the northern Kaukua and Murtolampi blocks have relatively higher PGE grades (Iljina 2004; Iljina et al. 2005; Iljina et al. 2012). In the study by Karinen (2010), the cumulate rocks in the Portivaara Marginal Series were found to contain up to 3.9 wt.% S, 0.9 wt.% Cu, 1.1 wt.% Ni, 2650 ppb Pd, 846 ppb Pt, and 790 ppb Au. The content of precious metals often correlates with the modal abundance of sulfides. The principal Pt mineral is sperrylite ($PtAs_2$), whereas Pd is associated with tellurides, bismuthides, and antimonides (Alapieti 1982; Karinen 2010; Iljina et al. 2015)

Karinen (2010) examined the PGE mineralogy of Portivaara block, finding out that the PGM assemblages consist of 93% Pt-Pd tellurides and 7% Pt arsenides. Studies undertaken in the Haukiaho area of the Kuusijärvi block by Kojonen & Iljina (2001) revealed 93.6% Pd-Pt tellurides, 6% sperrylite, and minor amounts of PGE-cobaltite as inclusions in BMS. The predominant tellurides are merenskyite ($PdTe_2$) (62%) and Pd-rich melonite ($NiTe_2$) (25.3%). Further north in the Kaukua block, the PGM assemblage is reported to be fairly similar, where the majority of the PGM are found in silicates and only 10% are hosted by BMS (Iljina et al. 2005; Iljina et al. 2012). In conclusion, the Marginal Series seems to be dominated by Pd-Pt bismuthotellurides and Pt-arsenides (chiefly sperrylite). PGE-sulfides and alloys are very rare, with those identified by Iljina et al. (2012) belonging to the vysotskite–braggite series, (Pt,Pd,Ni)S - (Pd,Ni)S.

In the study of Karinen (2010), the minerals in the Rometölväs Reef and Marginal Series PGM assemblages (including Au and Ag-bearing minerals) were divided into different groups based on their composition (Fig. 14b). In the Marginal Series, the groups are in the order of decreasing abundance: 1. kotulskite-sobolevskite-sudburyite (PdTe-PdBi-PdSb), 2. merenskyite-melonite-moncheite ($PdTe_2$-$PtTe_2$-$NiTe_2$), 3. Au- Ag alloys, 4. sperrylite, 5. michenerite (PdBiTe), and 6. hessite (Ag_2Te). The minerals occur predominantly in silicates (83%) or at the contact boundary of

BMS (8%) or as inclusions in BMS (10%).

4.4.2 Reef-type PGE mineralization

The Rometölväs Reef Cu-Ni-PGE mineralization of the Layered Series is laterally heterogeneous and is observed to be < 20 m thick in places. It displays a close association with the noncumulus-gabbronorite bodies in the MZb - MZc boundary zone (Piispanen & Tarkian 1984; Iljina et al. 2001; Karinen 2010). The rock displays variable mottled textures, where mottles have replaced the intercumulus phases of the cumulate rocks. The sulfide mineralization correlates with higher degrees of mottling, where mottles occur in voids of the intercumulus phases of the cumulate rock. The mottles contain up to 2.2 wt.% S, 0.9 wt.% Cu, 0.3 wt.% Ni, 241 ppb Pd, 263 ppb Pt and 103ppb Au. Karinen (2010) pointed out that the most sulfide- and mottle-rich rocks are orthocumulates, while the less mottled rocks are adcumulates and mesocumulates. Some of the noncumulus-textured gabbronorites associated with the reef are also mineralized. Pyrrhotite, pentlandite, and chalcopyrite often occur as clusters in centimeter-sized mottles in association with low-temperature minerals (and accessory sulfides much like the contact-type assemblage). Most of the PGM and Au, Ag minerals are tellurides (Fig. 14c) with an average grain size of 16.2 μm^2 (Karinen 2010). The central areas of the mottles mainly consist of scapolite, pyrrhotite, and pentlandite, whereas such minerals as chalcopyrite and clinozoisite-epidote are observed along the margins of mottles. Notably, the reef does not show a great contrast in silicates, though the apatites in the stratigraphy above the reef exhibits a lower chlorine content (Karinen 2010).

According to Karinen (2010), who based his study on the localities in the two blocks, Portivaara and Syöte (in the areas of Rometölväs, Baabelinälkky, Lanttioja, Välivaara & Mustavaara), the PGM assemblages are 88% Pt-Pd tellurides and 12% Pt-arsenides. The observed assemblages of precious minerals are: 1. merenskyite-moncheite-melonite, 2. hessite, 3. sperrylite, 4. volynskite ($AgBiTe_2$), 5. michenerite, and 6. Au-Ag alloys (Fig. 14d). Much like in the Marginal Series, the PGM of the Rometölväs Reef are mainly hosted by silicates (62%) or occur at the silicate-sulfides boundaries (15%). An estimate of 38% of the minerals are hosted by sulfides, as determined by Karinen (2010).

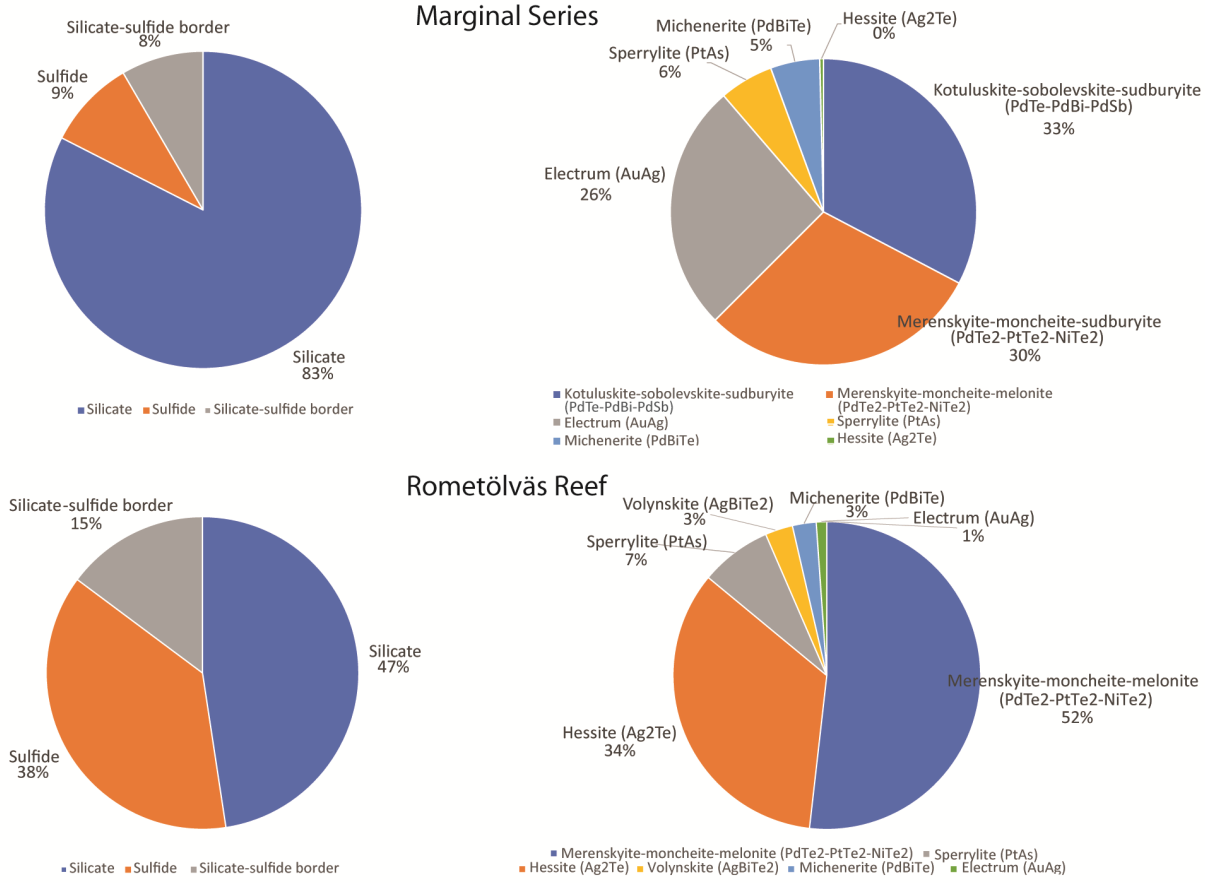

Figure 14. Relative proportions of PGM as categorized by mineralogy group and PGM host, based upon the data of Karinen (2010). A. PGM species identified in the Marginal Series. Relative proportions of different PGM hosts. B. PGM-hosts identified in the Marginal Series. C. PGM species identified in the Rometölväs Reef. D. PGM-hosts identified in the Rometölväs Reef.

5 Samples and methods

5.1 Samples and material

This study utilizes available sample material that was collected during fieldwork in 1999-2000 for the GTK project "Layered Igneous Complexes in Northern Finland" (Karinen 2010). Twenty-two hand samples that had previously been assayed for whole-rock compositions where chosen from both the Marginal Series and the Rometölväs Reef. Different localities of the two mineralized zones were taken into consideration when selecting the analytical material. Samples chosen from the Marginal Series were from the Soukeli area of the Portivaara block and samples from the Rometölväs Reef were from the Lanttioja and Mustavaara areas of the Portivaara block, as well as the Rometölväs area of the Syöte block. The selection of samples was based on two main criteria: high PGE values and a sulfur content above 0.5 wt.%. Already existing thin sections were used for petrographic studies and thicker (150 μm) thin sections were prepared from the selected hand samples to facilitate the use of in-situ laser ablation in the analysis of the sulfur isotope composition of sulfides. In Table 1, the samples used in this study are listed together with their stratigraphic unit, area, target, rock type and cumulate texture, as well as the analytical techniques used for each sample. The petrographic rock classification and cumulate terminology had already been described by Karinen (2010) for most of the material, and thus, these classifications were used when available. Photomicrographs of all thin sections can be found in *Appendix II*.

5.2 Microscopy

Studies of all 22 polished thin sections using transmitted and reflected microscopy were carried out at the Department of Geology at Lund University. Optical microscopy was used to study the mineralogy of the samples prior to selecting thin sections suitable for SEM-EDS analysis, as well as choosing representable base-metal sulfides for LA-ICP-MS work.

5.2.1 Transmitted light microscopy

Transmitted light microscopy were used to determine mineralogy and textures of the selected samples. Focus were principally on the primary magmatic characteristics of the host rock, but signs of alteration and metamorphism, especially in relation to sulfides were studied. Conventional optical methods of identification of the minerals were used.

Table 1. Information of the samples used for making thin sections of this study. The symbol "x" denotes the type of analysis the sample were used for. Additionally, the sample materials location in the Koillismaa intrusion, rock type and texture are described.

						LA-ICP-MS	SEM-EDS
Sample ID	Area	Target	Stratigraphy	Rock Type	Texture	S-isotopes	PGM
80-TTK-99	Porttivaara	Baabelinälkky	RT Reef (MZb/MZc)	Anorthosite (highly mottled)	pC	x	x
135.6-TTK-99	Porttivaara	Lanttioja	RT Reef (MZb/MZc)	Gabbronorite (highly mottled)	pahC	x	x
135.8A-TTK-99	Porttivaara	Lanttioja	RT Reef (MZb/MZc)	Gabbronorite (highly mottled)	phCa*		x
135.8B-TTK-99	Porttivaara	Lanttioja	RT Reef (MZb/MZc)	Gabbronorite (highly mottled)	phCa*	x	x
135.11-TTK-99	Porttivaara	Lanttioja	RT Reef (MZb/MZc)	Gabbro (highly mottled)	pCa*		x
137.1-TTK-99	Porttivaara	Välivaara	RT Reef (MZb/MZc)	Gabbronorite (highly mottled)	pahC		
4-TTK-00	Syöte	Pikku-Syöte	RT Reef (MZb/MZc)	Gabbro (highly mottled)	pCa*		
39.3-TTK-00	Porttivaara	Mustavaara	RT Reef (MZb/MZc)	Gabbronorite (highly mottled)	pahC		x
50-TTK-00	Syöte	Aurinkokallio	RT Reef (MZb/MZc)	Gabbro (highly mottled)	pCa*		
77.2-TTK-00	Syöte	Rometölväs	RT Reef (MZb/MZc)	Anorthosite (highly mottled)	pCa*		
82-TTK-00	Syöte	Rometölväs	RT Reef (MZb/MZc)	Anorthosite (highly mottled)	pCa*		x
83-TTK-00	Syöte	Rometölväs	Noncumulus-textured body	Noncumulus- gabbronorite			
257-TTK-00	Porttivaara	Soukeli area	LZMSa	Gabbronorite	pbCa	x	x
261-TTK-00	Porttivaara	Soukeli area	LZMSb	Gabbronorite	pbCa		x
264-TTK-00	Porttivaara	Soukeli area	UZMSa	Pyroxenite	bCa*		x
397-TTK-00	Porttivaara	Lavotta	UZMSa	Pyroxenite		x	
400-TTK-00	Porttivaara	Soukeli area	LZMSa	Gabbronorite	pbCa	x	x
401-TTK-00	Porttivaara	Soukeli area	LZMSb	Gabbronorite	pbCa	x	
402-TTK-00	Porttivaara	Soukeli area	LZMSb	Gabbronorite	pbCa		x
11-TTK-00	Porttivaara	Soukeli area	LZMSa	Gabbronorite	pbCa		x
53-TTK-00	Porttivaara	Soukeli area	LZMSb	Gabbronorite		x	
53-TTK-01	Porttivaara	Soukeli area	UZMSa	Pyroxenite			

5.2.2 Reflected light microscopy

Reflected light microscopy was used to study ore minerals, which are opaque in conventional transmitted light, and thus can only be studied using reflected light. Such ore minerals are for example native elements, alloys, oxides, sulfides and PGM. Special attention was paid to the sulfide assemblages and their textural relationships.

Much like a standard polarization microscope, the reflected light microscope is equipped with a pair of polarizing filters. The only difference from a traditional transmitted light microscope is that the source of light is from above, as opposed to the transmitted light source from below. Most new ore microscopes are so called modular microscopes, i.e. equipped for both transmitted and reflected light. For the reader unfamiliar with reflected light microscopy, minerals are mainly identified based upon reflectance and color, polishing hardness, bireflectance, as well as reflection pleochroism (Craig et al. 1981; Pracejus 2015). Crossed polarized light, anisotropism and internal reflections are further used to determine the identity of studied minerals. Some methods used in conventional transmitted light microscopy are also used, such as observation of crystal form, cleavage and twinning.

5.2.4 Scanning electron microscopy - SEM-EDS

As PGM are often very small (below 10 µm), and exhibit similar reflectance to sulfides, identifying them are exceptionally hard below 5 µm, not to mention time consuming, through optical microscopy, and therefore PGM studies are often complemented by SEM and also frequently additionally complemented with electron probe microanalysis (Osbahr et al. 2015). Moreover, the usage of a SEM-EDS allows for a much higher resolution, faster tracking and is more reliable in terms of mineral identification. Hence, the reason for choosing the SEM instrument for identification and documentation of PGM.

5.3 Chemical micro-analytical techniques

5.3.1 SEM-EDS

Twelve carbon-coated thin sections from the Rometölväs Reef and the Marginal Series were examined by semi-quantitative identification of PGM minerals using automated SEM-EDS. Analyses were carried out at the Geological Survey of Finland (GTK) in Espoo, Finland, using a JEOL JSM 7100F Schottky field emission scanning electron microscope (FE-SEM) attached to an Oxford Instruments energy dispersive spectrometer (EDS, X-max 20 mm^2)., Carbon-coating of the polished thin sections were done using a JEOL JEE-420 vacuum evaporator. The INCA software by Oxford Instruments was used to automatically identify mineral features. During EDS analysis, an accelerating voltage of 20 kV, probe current of 1.5 nA and working distance of 10 mm were employed. During the setup of INCA feature, the following parameters were used: magnification 160 x, smallest expected feature width, ECD, 1.5 µm, field of image 1024 x 768 and a BSE signal threshold of 103 - 255. The first pass image, i.e. the overall acquisition time of the general field of view used, was 4 ms. The second pass image, i.e. the detailed acquisition of already detected values above BSE, was 10 ms. Further SEM-EDS analyses were conducted at the Department of Geology at Lund University, to confirm the mineralogy of a few previously selected sulfides during reflected microscopy while preparing thin sections for laser ablation. A Tescan Mira3 Schottky Fe-SEM attached to an Oxford Instruments EDS X-MaxN 80 was used. During EDS analysis, an accelerating voltage of 20 kV, probe current of 1.2 nA and working distance of 12 mm were used together with the AZtec software by Oxford Instruments. The thin sections were carbon-coated using a Cressington 208HR high resolution sputter coater attached to a Cressington MTM-20 thickness monitor.

5.3.1.1 Automated feature identification

The semi-automated feature mode of the INCA software was used to identify PGM. The INCA feature mode operates on the principle of setting a desired grayscale detection range, in order to identify features of desired density. Denser minerals such as PGM are among the brightest features, so the detection limit is setup such that PGM and other heavier minerals are identified, but not unwanted, less dense minerals, such as silicates, oxides or sulfides. The software supplies information of each analyzed feature, such as size, shape, chemical composition and stage coordinates.

Here follows a brief explanation of the main steps of setup and operation: Each loaded thin section, prior to analysis, is manually assigned a virtual grid area of which to analyze. The detection limit is then set so that only features of interest are detected. Subsequently, the operating spatial resolution is selected, which is dictated by the allotted magnification used. The higher the magnification the better resolution and lower pixel size. High magnification, i.e. lower detection limits, are more time consuming and therefore a compromise has to be made, depending on the studied features of interest. For this study, the smallest detection limit was set to 1.5 µm, and the analysis of one thin section took between 2 - 4 hours, depending on the number of features detected for each thin section. The automated analyses were scheduled to operate during the night and results were subsequently examined during daytime. The initial results were displayed in a table (and saved as an excel file) with identified features, chemical composition, size variables and coordinates. Here, PGM were manually differentiated from non-wanted features (non-PGE bearing features) based on the elemental composition given by the software. Every identified PGM feature was then manually revisited, to precisely point analyze the features and surrounding minerals and textures of interest. Backscattered electron images were generated and saved in a word document, together with analyzed

points marked and the compositions given as weight percent for each point. Evaluation and classification of each PGM feature were subsequently done manually in excel, with the aid of available reference literature (Cabri 2002; O'Driscoll & González-Jiménez 2016).

5.3.2 In-situ sulfur isotopes

A representable set of eight thin sections from the Marginal Series (5) and the Rometölväs Reef (3) were chosen for sulfur isotope analysis using in-situ laser ablation. The sulfides were classified as either primary or secondary based on textural observations and mineralogical traits. Pyrrhotite, chalcopyrite, and pyrite grains which exhibit textural and compositional homogeneity in reflected-light were selected for analysis (a representative selection is found in *Appendix IV*). Sulfur isotope analysis was performed at the Geological Survey of Finland (GTK), Espoo, Finland, using a Nu Plasma HR multi-collector ICP-MS (Nu Instruments Ltd., Wrexham, UK) attached to a Photon Machine Analyte G2 laser microprobe (Photon Machines, San Diego, USA). The samples were ablated in He gas (gas flows = 0.4 and 0.1 l/min) within a HelEx ablation cell (Müller et al. 2009). Sulfur isotopes were analyzed at medium resolution, during the ablation, data were collected in static mode (^{32}S, ^{34}S). Chalcopyrite, pyrrhotite and pyrite grains were ablated at a spatial resolution of 40 µm using a pulse fluency of 3.5 J/cm^2 at a frequency of 3 Hz. The total sulfur signal was 1.5 - 5.0 V. Under these conditions, after a 20 second baseline, 50 - 60 seconds of ablation is needed to obtain an internal precision of $^{34}S/^{32}S \leq \pm 0.000005$ (1 SE). Two pyrite standards were used for external standard bracketing (PPP-1;(Gilbert et al. 2014)) and quality control (in-house standard Py2) of analyses. The in-house pyrite standard Py2 had previously been measured by gas mass spectrometry, obtaining a $\delta^{34}S$ V-CDT reference value of -0.4 ± 0.5‰ (1σ). We measured an average value of -0.27 ± 0.19‰ (2σ, n=14). Chalcopyrite samples were ablated using the same parameters. Two in-house chalcopyrite standards were used for external standard bracketing and quality control. These standards have been measured by gas mass spectrometry for a $\delta^{34}S$ V-CDT value of -0.7 ±0.5‰, while we obtained an average value of -0.70 ±0.47‰ (2σ, n=10).

6. Results

6.1 Petrography

Results of optical microscopy and SEM-based analyses of the Marginal Series and the Rometölväs Reef are presented in the following sections. First, general petrography is presented, where both primary mineralogy and cumulate textures, as well as secondary alteration mineralogy and textures are described. Thereafter, sulfide petrography and PGM petrography are reported.

6.1.1 General petrography

All rocks are pervasively metamorphosed, where retrograde minerals such as epidote, amphibole, quartz, alkali feldspar and chloritic alteration are commonly observed. Pyroxenes are often heavily uralitized, which makes it hard to classify them in more detail. The pyroxenes are mainly altered to light amphibole (tremolite-actinolite), additional minor alteration to serpentine, chlorite, biotite and talc is also observed. Furthermore, scapolite is occasionally seen as a replacement mineral along plagioclase boundaries and granophyric alteration occurs heterogeneously in the intercumulus phases. The Marginal Series is, in general, more altered than the Rometölväs Reef, and thus, primary textures are less preserved. Representable photographs of the thin sections are presented in Figures. 15-16.

6.1.1.1 Marginal series

The rocks from the Marginal Series of the Portivaara block consist of gabbronorites in the lower parts and pyroxenites in the upper parts. The gabbronorites are more plagioclase-rich than the pyroxenites and are also larger in terms of grain size, ca. 2mm, whereas the pyroxenites are on average 1 mm. The gabbronorites are plagioclase and orthopyroxene cumulates, with intercumulus clinopyroxene. Whereas the pyroxenites are poikilitic orthopyroxene orthocumulates with intercumulus clinopyroxene. Moreover, the pyroxenites are significantly more altered than the gabbronorites and the size of the cumulates are smaller, and large plagioclase are virtually absent. Cumulus plagioclase grains are the most well-preserved minerals and are relatively pristine and euhedral. Nonetheless, cracks are frequently observed, and in them sporadically minor saussuritization is observed. In one gabbronorite sample (261-TTK-00) the plagioclase grains are ophitic, with high degrees of alteration of the pyroxenes, now uralitized and epidotized. In the gabbronorites granophyric intergrowths are scarce but does occur interstitially to plagioclase grains locally. The pyroxenes are highly altered to light amphiboles and clinozoisite-epidote, chlorite, and minor amounts of mica, in both rock types. The alteration is especially widespread in the pyroxenite rocks, where hardly any cumulate pyroxenes remain, instead they are heavily uralitized into smaller grains of chlorite, epidote and amphibole.

6.1.1.2 Rometölväs Reef

The rocks from the Rometölväs Reef of the Portivaara and Syöte blocks are medium-grained (2–5 mm) anorthosite, gabbronorite and norite cumulate rocks, and are frequently poikilitic. The cumulus minerals of the gabbro and gabbronorites are plagioclase and orthopyroxene, with intercumulus clinopyroxene. Occasionally clinopyroxene occurs as a cumulus mineral, and in some samples, plagioclase is the only cumulus mineral, with intercumulus clinopyroxene. All studied anorthosites consist of cumulus plagioclase with inter-

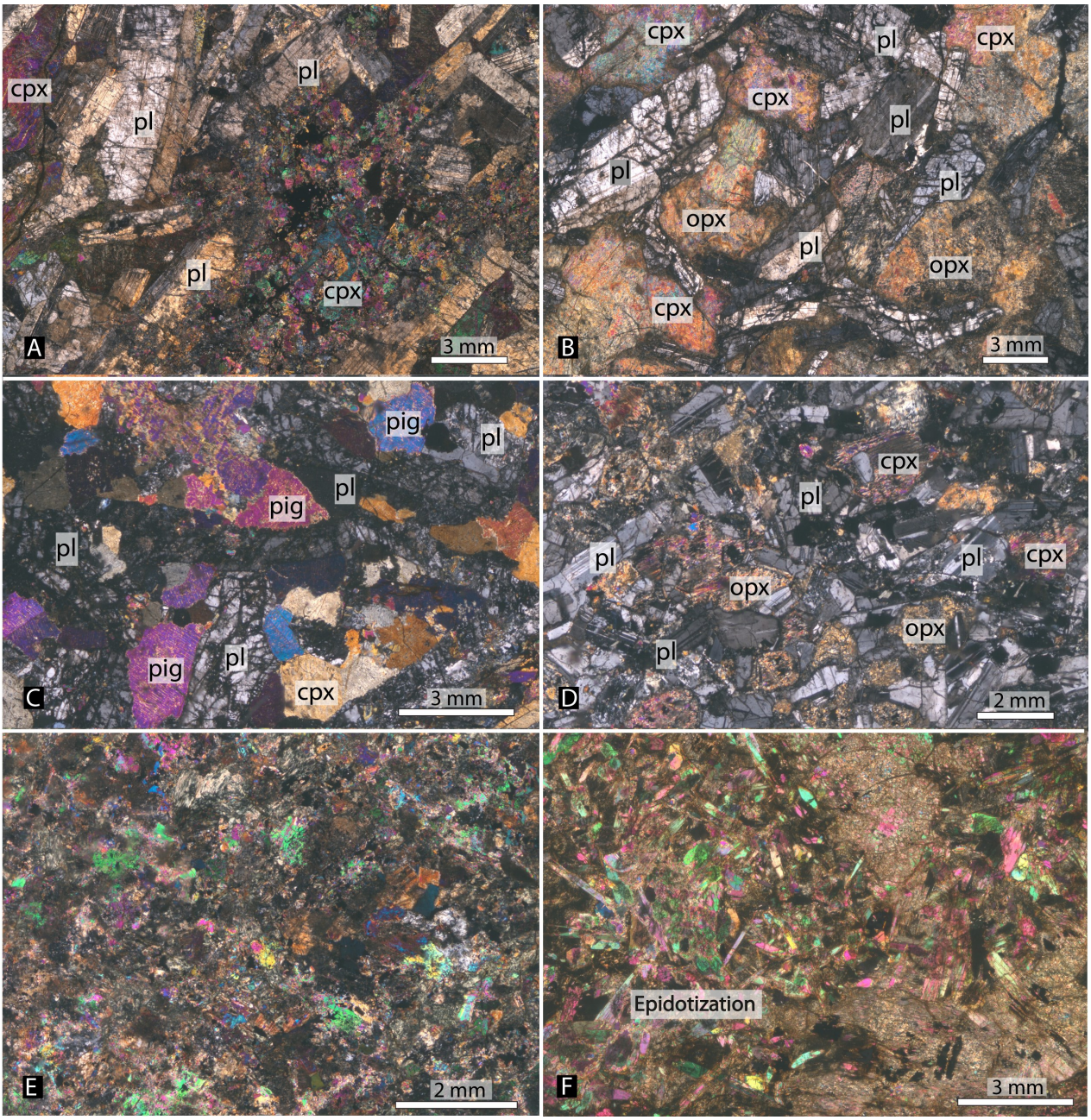

Figure 15. Photomicrographs taken in transmitted light with crossed polars, showing textures of representable thin sections from the Rometölväs Reef and Marginal Series. A. Anorthosite (pCa*) with cumulus plagioclase and oikocrystic clinopyroxene from the Rometölväs Reef (Syöte). In the center a typical "mottled texture" can be observed. Sample 82-TTK-99. B. Gabbronorite (phCa*) from the Rometölväs Reef (Porttivaara), containing cumulus Plag and Opx with oikocrystic Cpx. Plagioclase are weakly laminated. Sample 135.8A-TTK-99. C. Gabbronorite (pahC) with cumulus plagioclase, ortho- and clinopyroxene from the Rometölväs Reef (Portivaara). Note the presence of inverted pigeonite with fine exsolution lamellae. Sample 39.3-TTK-00. D. Gabbronorite (pbCa) with cumulus plagioclase and orthopyroxene and intercumulus clinopyroxene from the Marginal Series (Porttivaara). Sample 402-TTK-00. E. Gabbronorite from the Marginal Series (Porttivaara). Sample 53-TTK-00. F. Pyroxenite (bCa*) from the Marginal Series (Porttivaara), representing poikilitic orthopyroxene orthocumulate with a high degree of alteration of the primary minerals. Sample 397-TTK-00. Original cumulate classification of thin sections by Karinen (2010) and verified by the author, except for E and F which were classified by the author.

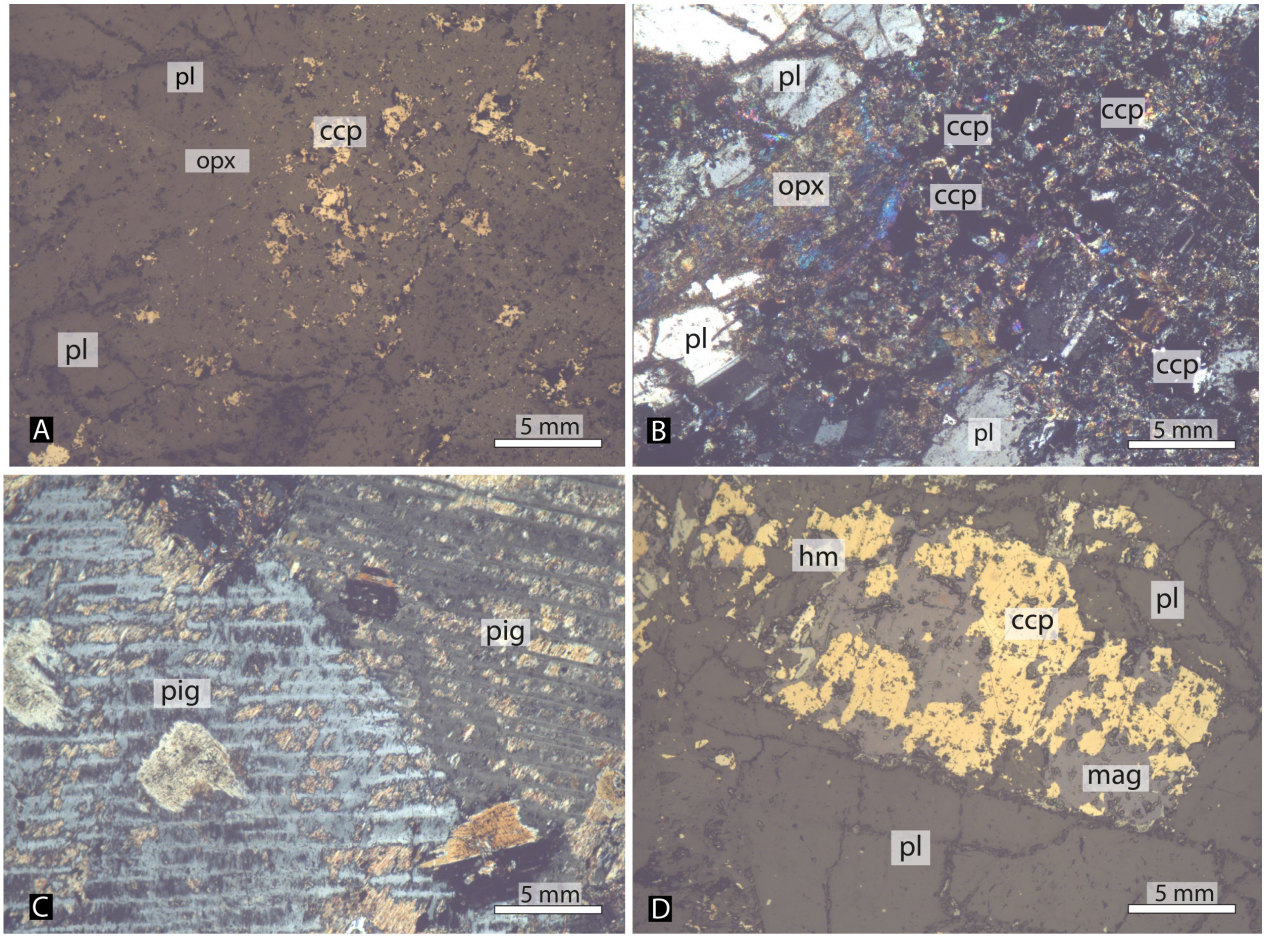

Figure 16. Photomicrographs of textures of representable thin section from the Rometölväs Reef and Marginal Series. A-B. Typical disseminated chalcopyrite in highly altered pyroxene from the Rometölväs Reef (Portivaara). Sample 135.8B-TTK-99; (reflected light and crossed nicols, respectively) C. Distinct Stillwater-type pigeonite from the Rometölväs Reef (Portivaara). Note the coarse exsolution lamellae of pigeonite. Sample 137.1-TTK-99; (crossed nicols) D. Chalcopyrite grain altered and partly replaced by magnetite in the Marginal Series (Portivaara). Small hematite specks associated with magnetite are thought to be due to recent oxidation. Sample 402-TTK-00; (reflected light).

cumulus clinopyroxene, that are frequently oikocrystic. The cumulus grains are significantly larger in the Rometölväs Reef, than in the contact-type mineralization of the Marginal Series. Here, the cumulus plagioclase crystals are approximately 2–3 mm.

The rocks from the lower part of the Rometölväs Reef (MZb) are medium-grained plagioclase-orthopyroxene mesocumulates, with intercumulus clinopyroxene. The upper parts of the Rometölväs Reef (MZc) are predominantly adcumulates of plagioclase, orthopyroxene and clinopyroxene. The upper parts (MZc) contains cumulus clinopyroxene, probably augite, and inverted pigeonite orthopyroxene, presumably in the form of enstatite. Here, two different types of orthopyroxene, with associated exsolution textures are observed; one in the form of coarse clinopyroxene exsolution lamellae along the 001-plane (primary orthopyroxene), and the second one with fine exsolution lamellae of orthopyroxene along the 100-plane in clinopyroxene (inverted pigeonite).

Cumulus plagioclase grains are the most well-preserved primary minerals, and are relatively pristine and euhedral, with no major saussuritization. Cracks are, however, frequently observed, and in them, minor saussuritization infrequently occurs. Furthermore, the rocks of the lower part of the Rometölväs Reef (MZb) all have low degrees of granophyric intergrowths interstitially. Some samples have relatively high degrees of apatite associated with intercumulus granophyric intergrowth.

All the studied rocks of the Rometölväs Reef are mottled to various degrees, meaning that clusters of hydrosilicates and other low-temperature minerals, together with sulfides, occur as the predominant intercumulus minerals. The mottles contain scapolite, amphibole, pentlandite and pyrrhotite in the central areas, with clinozoisite-epidote and chalcopyrite more generally located around the edges. Additionally, chlorite, calcite, quartz, biotite and apatite are sometimes associated with the mottles. Moreover, amphiboles are occasionally zoned, with darker brims and lighter centers. A trend between hydrosilicates and the abundance of sulfides is apparent. Additionally, minor amounts of oxides are present interstitially in the form ilmenite and magnetite in some samples.

6.1.2 Sulfide petrography

The sulfide assemblages of both the Marginal Series and the Rometölväs Reef consists of chalcopyrite, pyrrhotite, pentlandite, and minor additions of pyrite. Observed rare sulfides are sphalerite, galena and bornite. Pentlandite is frequently altered to violarite. The sulfide mineralization is solely disseminated in character, with no observations of sulfide veins or massive sulfides. In general, most sulfides are heavily altered and display a speckled porous appearance. Significant grain reduction and remobilization of sulfides are observed in all samples. Several sulfides are "dusty" in appearance, and infrequently contain late-stage oxides, replacing the outer parts of the sulfides.

6.1.2.1 Marginal Series

The sulfides of the Marginal Series are, in order of abundance, chalcopyrite, pyrrhotite, and pentlandite, with infrequent pyrite present in several samples. Chalcopyrite and pyrrhotite make up the dominating portion of the sulfides. The sulfides occur either as very small disseminated monograins or as larger polygrains in clusters. The most common observation is finely disseminated chalcopyrite grains in silicates, that have experienced hydrothermal alteration (Fig. 16a-b). Even smaller grains of sulfides, specifically chalcopyrite, is seen disseminated throughout the rock, but are particularly abundant next to adjacent primary sulfides. Evidence of grain reduction and remobilization of the sulfides are observed, with pseudocrystic sulfide remnants visible. Larger chalcopyrite grains (Fig. 16d) occur interstitially and occasionally shows signs of oxidation by the presence of late-stage oxides. Pentlandite and pyrrhotite are commonly observed together as clusters. Pentlandite is almost always associated with pyrrhotite, whereas pyrrhotite is also observed as disseminated smaller single grains. Small, often euhedral pyrite grains are observed as single grains in silicate cracks and sometimes in association with pyrrhotite.

Primary sulfides of pyrrhotite and chalcopyrite are often highly altered around the edges, where grain reduction is seen, and nearby remobilized very small disseminated satellite grains are commonly observed. Chalcopyrites are the most altered sulfides and also the most common remobilized sulfide, frequently scattered throughout the rock. Secondary remobilized sulfides are much more commonly observed in the Marginal Series, compared to the Rometölväs Reef.

All sulfides are significantly altered, and chalcopyrite seems to be the most altered and disintegrated of the BMS. Pentlandite mainly occurs in bigger pyrrhotite grains or as small flames, but is often altered to violarite. Pyrrhotite is the least altered of the BMS, but is also significantly altered, with grain reduction present and a "dusty" shine, as well as several small speckled porous holes.

6.1.2.2 Rometölväs Reef

The sulfides of the Rometölväs Reef are, in order of abundance, chalcopyrite, pyrrhotite and pentlandite, with infrequent pyrite present in some samples. Chalcopyrite and pyrrhotite are, by large, the most common sulfides. The sulfides occur either as very small disseminated grains or as larger grains in clusters of hydrosilicate mottles. Contrasting the Marginal Series, where scattered, disseminated, small chalcopyrite grains dominate the sulfide assemblage. The sulfides in the Rometölväs Reef are often much larger, and primary sulfides are more common. Primary sulfide clusters occur as single grains and as multigrain blobs in mottles, typically with pyrrhotite as the dominant component, pentlandite either as inclusions or at the edges of the pyrrhotite. Chalcopyrite occur both as inclusions in pyrrhotite and as separate grains, typically at the exterior margins of the sulfide blobs. The most common observation of sulfides is finely disseminated chalcopyrite grains in hydrosilicates. Smaller grains of sulfides, mainly chalcopyrite, is seen scattered throughout the rock but are especially prominent adjacent to primary sulfides. Clear evidence of grain reduction and remobilization of the sulfides are observed, with pseudocysts still visible. Larger chalcopyrite grains occur interstitially and occasionally with late-stage oxides at the margins. Pentlandite and pyrrhotite are commonly observed together as clusters, and pentlandite is almost always associated with pyrrhotite, whereas pyrrhotite is also observed as disseminated smaller grains. Euhedral to subhedral pyrite grains are observed as single grains in silicate cracks and frequently in association with pyrrhotite.

Primary pyrrhotite and chalcopyrite are often highly altered, where grain reduction and alteration of the grain margins are observed. Associated with the primary sulfides are very small disseminated satellite grains. Chalcopyrite is the least preserved sulfide and also the most remobilized sulfide, and is frequently scattered throughout the rock.

All sulfides are notably altered; however, chalcopyrite is the least well-preserved of the BMS. Pentlandite almost exclusively occurs in bigger pyrrhotite grains or as flames (but is frequently altered violarite) and no single-grains are observed. Pyrrhotite is the most well-preserved of the BMS, but is also significantly altered, displaying grain reduction and often have "dusty" shine, as well as several small holes.

6.1.2.3 Sulfide classification

Textural classification was carried out for the sulfides used in laser ablation analysis. The sulfides were classified as either primary or remobilized grains to assess any differences in the chemical composition between different assemblages, and to evaluate the contribution of secondary mobilized sulfides from late-stage alteration. In this way, a primary magmatic assemblage could be studied and a comparison with secondary sulfides could be made to see compositional differences and to consider any external sulfur influxes.

Even though all samples have experienced some degree of alteration, a distinction between primary BMS grains and remobilized ones could still be made, apart from three grains from the Marginal Series, which could not be confidently classified and are therefore omitted from the assessment. The classification was based on a few observation criteria. Primary sulfides were defined as those that display magmatic textures and contain BMS of pyrrhotite, pentlandite and chalcopyrite. For example, sulfide blebs of composite grains of pyrrhotite, pentlandite with chalcopyrite (generally on the margins) are considered to display primary textures. Flamed pyrrhotite (exsolution of chalcopyrite or pentlandite) was considered a primary feature. Furthermore, the occurrence of single grains as interstitial contacts with respect to cumulus minerals and with coarse grain size were also determined primary. Fine-grained, disseminated sulfides tend to be remobilized compared to coarser grains. Secondary sulfides were determined based mainly on their textural occurrence, i.e., whether they were situated in cracks or in secondary minerals. Chalcopyrite is more mobile; therefore, its grains easily become mobilized, occurring as fine disseminations in silicates. Furthermore, pyrite is considered a secondary sulfide in the studied assemblage.

6.1.3 PGM petrography

During SEM analyzes and data acquisition, attention was paid to the textural relationships of PGM (and selected gold and silver-bearing minerals). Figures 17-20 show a photo documentation of representative grains based on close-up morphology (Fig. 17-18), as well as their textural relationships (Fig. 19-20). A common mineral association with many of the identified PGM grains includes Ag tellurides (e.g., hessite (Ag_2Te)) and electrum (Au-Ag), with silver tellurides being the most commonly observed near-PGM precious mineral. They typically occur as very small (< 4mm), scattered grains, but occasionally are also observed as much bigger grains (Fig. 18). Large hessite grains, when observed, occasionally host inclusions or compounds of altaite (PbTe), electrum and clausthalite (PbSe). Hessite grains were observed as multiple small grains in a strange cluster in one location (Fig. 19c-d) and altaite was observed in relation to PGM (Fig. 20e). Clausthalite was observed as an inhomogeneity in hessite (Fig. 18), but this is not a common observation, though a good example of inclusions in some of the observed tellurides.

The majority of PGM occur as discrete grains within silicates and a minor part as intergrowths on the grain boundary of BMS or as inclusions. There is a positive correlation between the alteration of silicates and the presence of PGM. Where the PGM is associated with BMS, there is often a mottled texture due to the presence of intergrown hydrosilicates with sulfides. The identified hydrosilicates include chlorite, amphibole, scapolite, zoisite, epidote, and serpentinite. The occurrence of nearby oxides (Fig. 20d), where the PGM occur as satellite grains, were scarcely observed in the Marginal Series. The presence of magnetite occurring interstitially with pyrrhotite and pentlandite (Fig. 19e) was detected in the Rometölväs Reef. The mottles occasionally host low-temperature sulfides, such as galena-clausthalite, sphalerite, and altaite. The PGM grains are commonly anhedral in all hosts, with a minor portion being subhedral. Occasionally, grains occur interstitially, along silicate and sulfide boundaries (Figs. 19d, 20e).

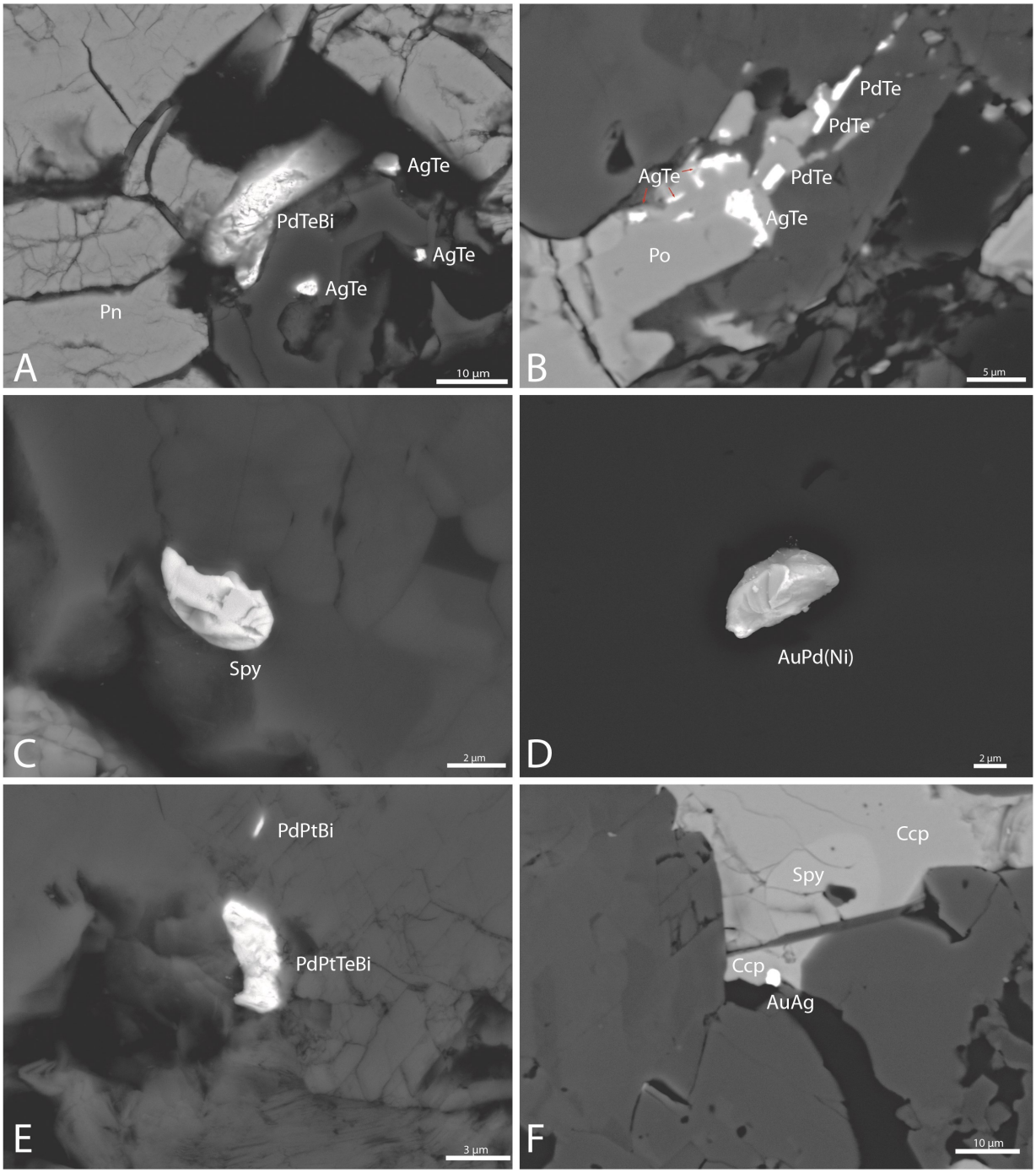

Figure 17. Back-scattered electron images (BSE) showing different PGM assemblages. A. PdTeBi grain in BMS-contact with Pn (Rometölväs Reef). Sample 80-TTK-99. B. PdTe's hosted by Po (Rometölväs Reef). Sample135.6-TTK-99. C. Sperrylite grain in silicate (Marginal Series). Sample 11-TTK-00. D. AuPd(Ni)-alloy in silicate (Marginal Series). Sample 11-TTK-00. E. PdPtTeBi and PdPtBi grains in silicate host (Marginal Series). Sample 257-TTK-00. F. Electrum grain in a Ccp grain. Note the presence of sphalerite. (Rometölväs Reef) Sample 135.6-TTK-99. Abbreviations: sphalerite (Sp), chalcopyrite (Ccp), pyrrhotite (Po) and pentlandite (Pn).

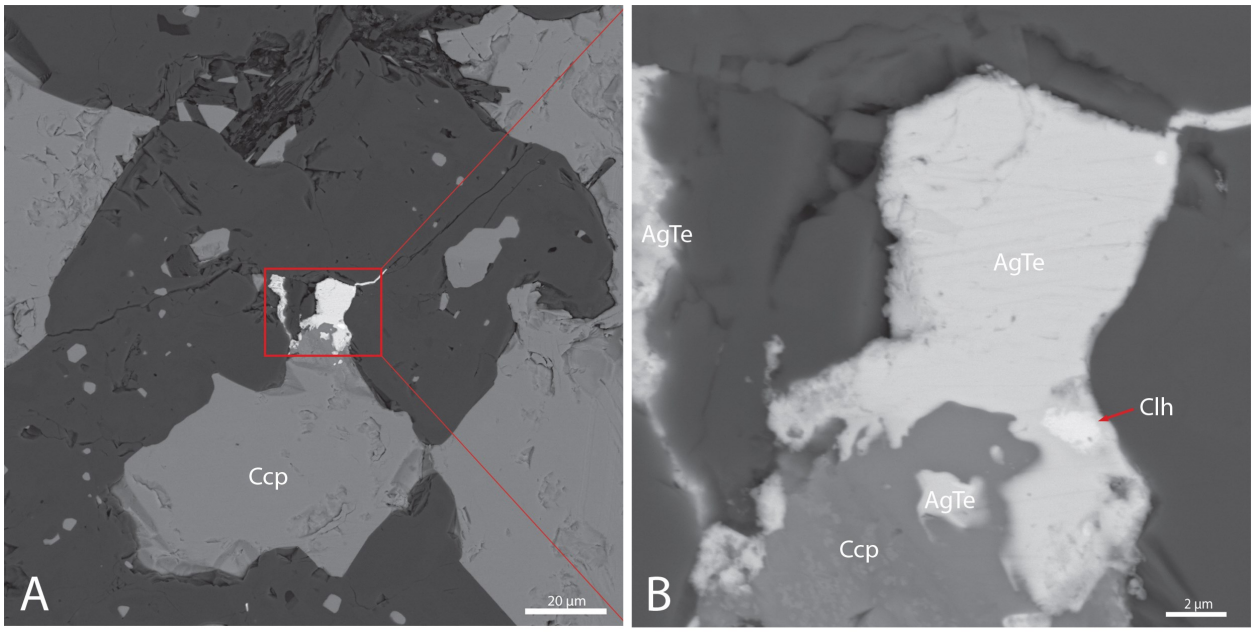

Figure 18. Back-scattered electron images showing a heterogeneous telluride grain from the Rometölväs Reef. Sample 80.3-TTK-99. A. Overview. B. Close-up view of a telluride grain with clausthalite. Abbreviations: chalcopyrite (Ccp), and clausthalite (Clh).

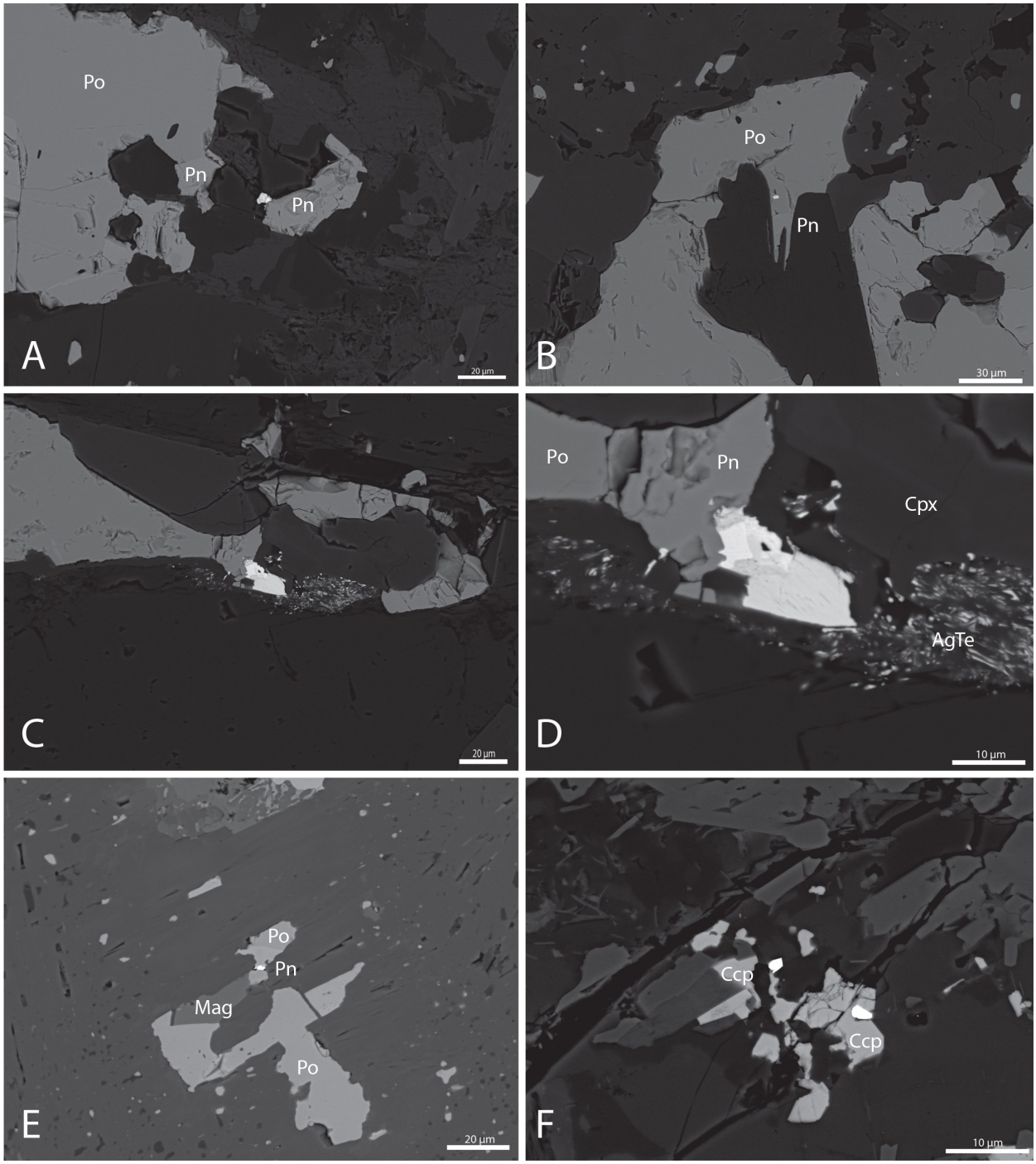

Figure 19. Back-scattered electron images showing different PGM assemblages and their textural relationships. A. Compound grain of PdTeBi-PdAgTeBi in contact with Pn (Marginal Series). Sample 402-TTK-00. B. PdTeBi-grain hosted by Po (Marginal Series). Sample 402-TTK-99. C. & D. Compound grain of PdTeBi in contact with Pn. The lighter grain exhibit much higher Bi-content. To the right several a grain swarm of mainly AgTe in a dark silicate matrix (Marginal Series). Sample 400-TTK-00. E. PdTe-grain hosted by Pn. Note the Mag in the BMS (Rometölväs Reef). Sample 135.6-TTK-99. F. PdTeBi and PdTe-grains hosted by Ccp (Rometölväs Reef). Sample 135.8B-TTK-99. Abbreviations: chalcopyrite (Ccp), pyrrhotite (Po), pentlandite (Pn), magnetite (Mag), and clinopyroxene (Cpx).

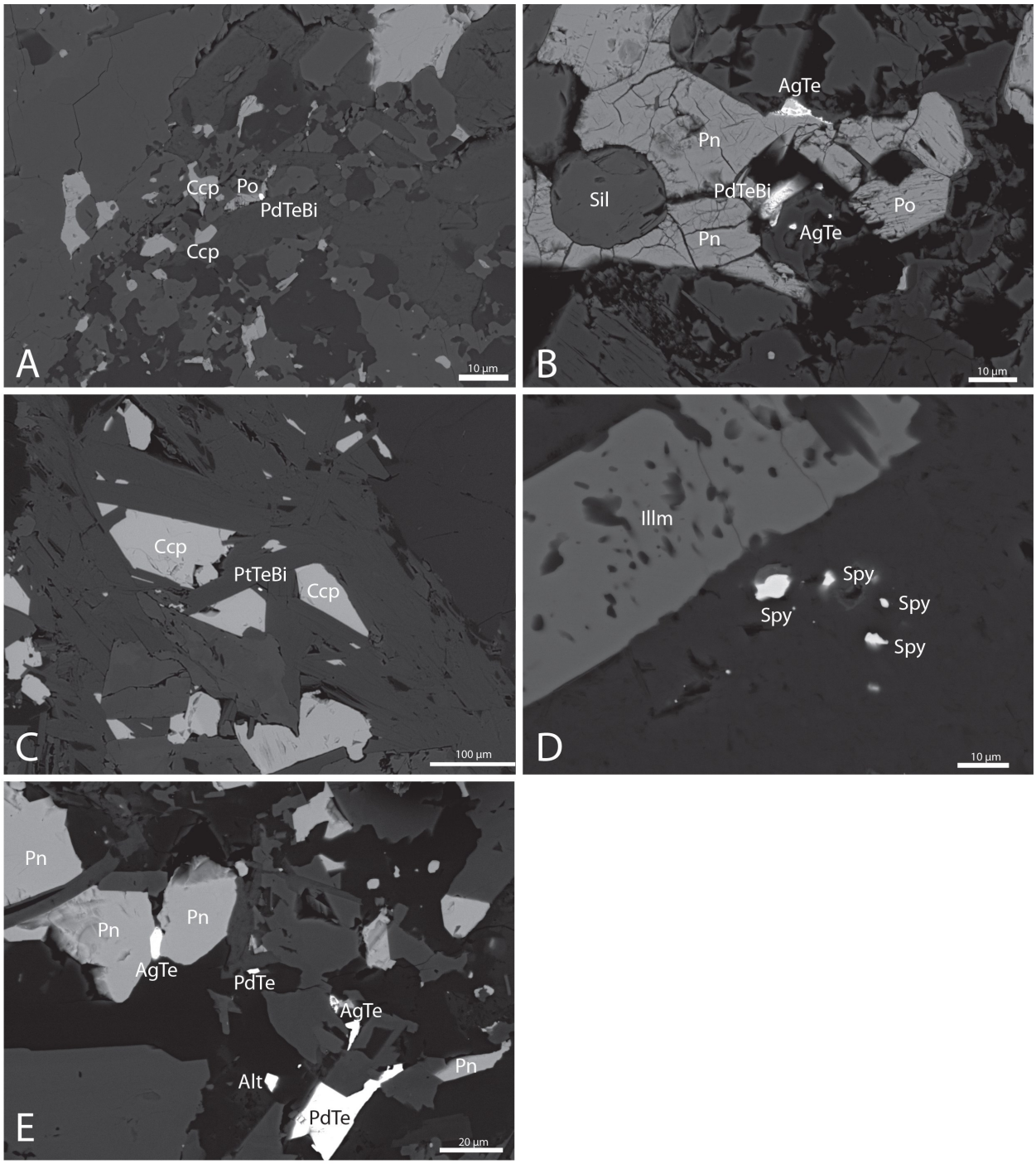

Figure 20. Back-scattered electron images showing different PGM assemblages and their textural relationships. A. PdTeBi in contact with Po (Marginal Series). Sample 257-TTK-00. B. Heterogeneous electrum grain and PdTeBi grain hosted by Pn (Rometölväs Reef). Sample 82-TTK-99. C. PdTeBi grain in silicate near Ccp (Rometölväs Reef). Sample 135.8A-TTK-99. D. Several sperrylite grains in close vicinity of an ilmenite grain (Marginal Series). Sample 264-TTK-00. E. Large PdTe grain in silicate in association with Alt, AgTe and remobilized Pn (Rometölväs Reef). Sample 135.8B-TTK-99. Abbreviations: chalcopyrite (Ccp), pyrrhotite (Po), pentlandite (Pn, silicate (Silc), altaite (Alt), ilmenite (Illm), and sperrylite (Spy)

6.1.3.1 Platinum-group mineral hosts

The PGM hosts were classified into three distinct groups: 1) silicates, 2) BMS, and 3) BMS-contact, as illustrated in Figure 21. A fourth and fifth category (oxides and oxide-contact) were intended, but not utilized due to their absence. To clarify, even if PGM occurred as satellite grains in the near vicinity of a BMS, they were categorized as silicate-hosted. No category of BMS satellite grains were made, as the categorization itself is hard to standardize. Grains observed as inclusions in BMS were classified as BMS-hosted and grains occurring at the sulfide-silicate boundaries as BMS-contact hosted.

The analyzed grains from the Marginal Series are mainly hosted by silicates (81%), with the remaining 19% being hosted either by BMS (14%) or occurring at BMS contacts (5%). All observed PGM hosted by BMS are part of the merenskyite-moncheite-

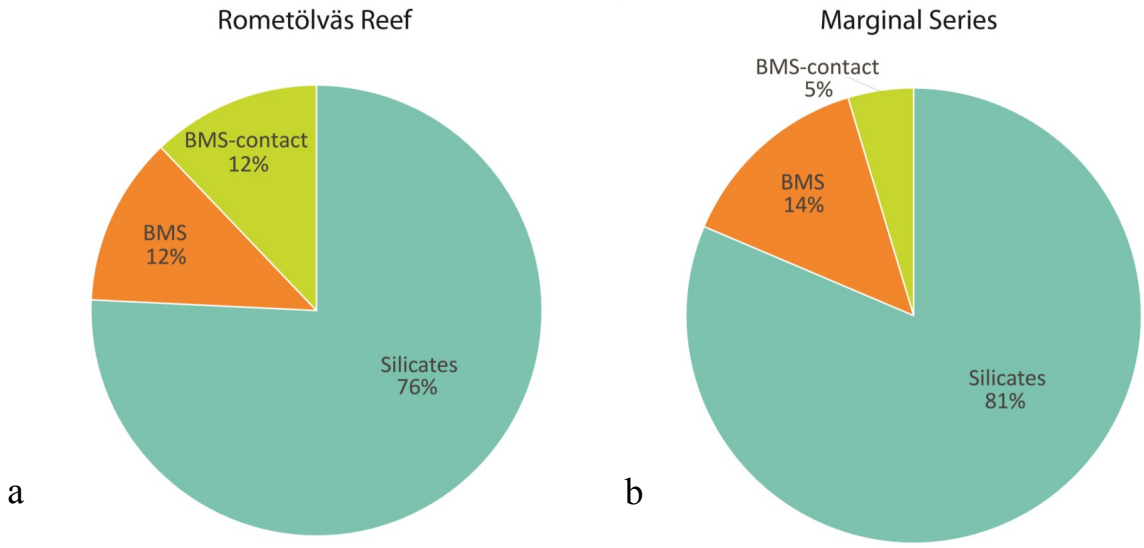

Figure 21. Relative proportions of different PGM hosts, based upon number of grains. A. PGM-hosts identified in the Rometölväs Reef (n = 35), and B. PGM-hosts identified in the Marginal Series (n = 43).

Table 2. Variety of sulfides containing identified platinum-group minerals, n = 18.

	Ccp	Po	Pn
Marginal Series	10% (1)	50% (5)	40% (4)
Rometölväs Reef	25% (2)	13% (1)	63% (5)
Total	17% (3)	33% (6)	50% (9)

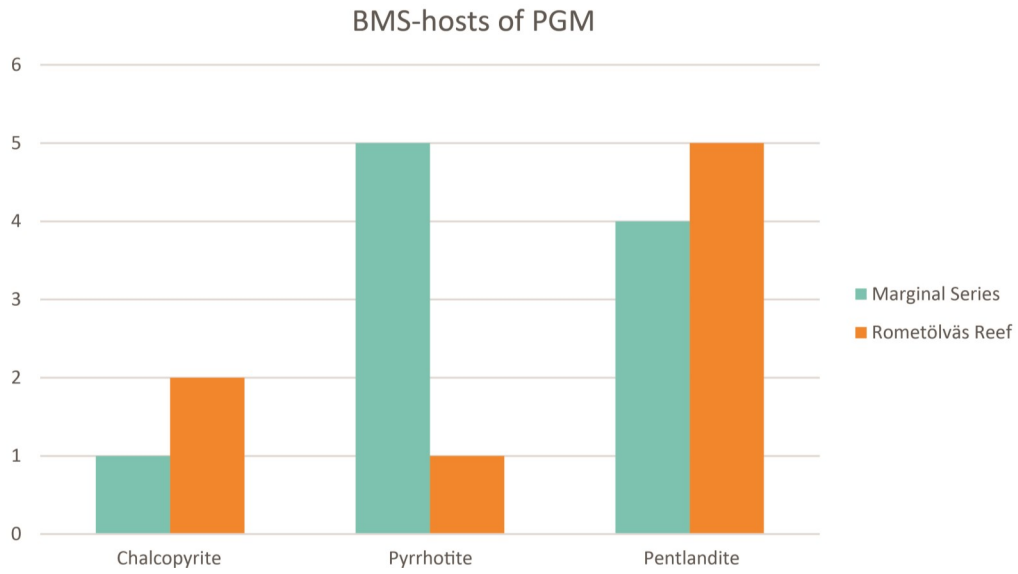

Figure 22. Histogram showing the BMS hosts of PGM for the Marginal Series (n = 10) and the Rometölväs Reef (n = 8).

melonite group ($PdTe_2$-$PtTe_2$-$NiTe_2$). Ten grains were documented in a BMS host (Table 2), with the hosts being, in order of abundance, pyrrhotite (5), pentlandite (4) and chalcopyrite (1).

In the Rometölväs Reef, 76% of the identified PGM grains hosted by silicates, 12% by BMS, and 2% are situated at BMS contacts. Eight grains, all belonging to the merenskyite-moncheite-melonite group, were identified in a BMS host (Table 2), with five occurring in pentlandite, two in chalcopyrite and one feature in pyrrhotite.

The two mineralization types are similar, in that the main hosts of PGM are silicates. The Marginal Series has a higher relative abundance of BMS, in contrast to BMS contact relationships, whereas the proportions PGM observed in BMS or at BMS contacts is equal in the Rometölväs Reef.

6.1.3.2 Grain size

A table showing all identified PGM grains and their grain sizes can be found in *Appendix III*. Histograms are plotted for both the Rometölväs Reef and the Marginal Series in Figure 23. Green blocks display the true grain size frequency for analyzed grains. The purple curve shows a calculated adaptive kernel density estimation.

The Rometölväs Reef displays an average grain size of 23 μm^2, and all grains except one PdBiTe (395 μm^2) are between 1.65 μm^2 and 85 μm^2 in size. The largest PGM feature greatly obscures the mean grain size, which is 13 μm^2 if it is excluded. The Marginal Series shows an average grain size of 16 μm^2. The grain size distribution is similar to that of the Rometölväs Reef, with the grain sizes ranging between 1.65 μm^2 and 72.45 μm^2 and averaging 11 μm^2, with the exclusion of one large, 191-μm^2-sized PdTe (>90% Te) grain (Fig. 20e.). The PGM grains are commonly observed as anhedral grains in all hosts, with a minor portion being subhedral. Occasionally, grains occur interstitially, along silicate and sulfide boundaries.

6.1.3.3 Composite grains

During assessment of PGM features, six composite grains were identified, five from the Marginal Series and one from the Rometölväs Reef. Common for all is that they consist of two or three distinct grains of PdBiTe phases, with varying high Bi proportions (Fig. 19d). With the exception of two features, a AuAg-PdTeBi composite grain and a composite grain comprised of PdTeBi-PdAgTeBi phases..

6.2 Analytical results

6.2.1 Platinum-group mineralogy

Twelve polished thin sections from the Rometölväs Reef and the Marginal Series were examined for platinum-group minerals using SEM-EDS analysis (Table 3). In total, 78 individual PGM grains were identified, 35 from the Rometölväs Reef and 43 from the Marginal Series. The identified PGM were grouped into the following classes: (1) merenskyite-moncheite-melonite ($PdTe_2$-$PtTe_2$-$NiTe_2$), (2) sperrylite ($PtAs_2$), (3) kotulskite-sobolevskite-sudburyite (PdTe-PdBi-PdSb), (4) keithconnite-telluropalladinite ($Pd_{3-x}Te$ - Pd_9Te_4), and (5) PGE-alloys. The chosen classification was used in order to later compare the PGM assemblages to the previous study by Karinen (2010). The identified PGM could also be grouped into (1) Pt-Pd tellurides, (2) Pt-arsenides, and (3) PGE-alloys. The identified PGM were additionally cataloged by grain size and textural association.

6.2.1.1 PGM assemblages

The PGM assemblage for both the Rometölväs Reef and the Marginal Series is shown in Fig. 24. A simplified categorization is that Pt-Pd tellurides (85%) are the dominating group, with Pt-arsenides making up the remaining 15% of the PGM assemblage. No Fe-alloys or Pt-Pd sulfides were observed.

PGM species in the Rometölväs Reef are, in order of abundance: 1. merenskyite-moncheite-melonite ($PdTe_2$-$PtTe_2$-$NiTe_2$), 2. sperrylite ($PtAS_2$), (3) kotulskite-sobolevskite-sudburyite (PdTe-PdBi-PdSb), and (4) keithconnite-telluropalladinite ($Pd_{3-x}Te$-Pd_9Te_4). The merenskyite-moncheite-melonite solid solution series is the most abundant group. Tellurides represent 85% of the PGM in the Rometölväs Reef. Sperrylite is the only arsenide present and constitutes 15% of the identified PGM. In tellurides, the average atomic percentages of Bi, Te, Pt and Pd are 6%, 67%, 24% and 23% respectively. The most common tellurides are composed of PdTe(Bi) and PdPtTe(Bi). Nearly 45% of the examined tellurides consist of Pd and Pt to some extent, whereas the remainder of the tellurides have Pd as their only PGE component. For the Pt-Pd-bearing tellurides, the Pt-Pd ratio is on average 1.12.

A simplified categorization of the Marginal Series is that Pt-Pd tellurides (70%) are the dominating group, occurring together with Pt-arsenides (28%) and PGE-alloys (2%). The Marginal Series PGM species are, in order of abundance: 1) merenskyite-moncheite-melonite, 2) sperrylite, (3) kotulskite-sobolevskite-sudburyite, and 4) PGE-alloy (Fig. 24). The telluride groups merenskyite-moncheite-melonite and kotulskite-sobolevskite-sudburyite make up 70% of the total PGM assemblage, and sperrylite 28%. On average, the tellurides contain 6% of Bi, 63% of Te, 9% of Pt and 28% of Pd. The most common tellurides are PdTe(Bi) followed by PdPtTe(Bi). Approximately 25% of the tellurides consist of Pd and Pt to some extent, whereas 75% of the tellurides have Pd as their only platinum group-element. For the Pt- and Pd-bearing tellurides, the Pt-Pd ratio is 0.77 on average.

The two studied zones exhibit relatively similar PGM assemblages. Sperrylite is more abundant in the Marginal Series. The higher-grade PGM-group keithconnite-telluropalladinite was found in the Rome-

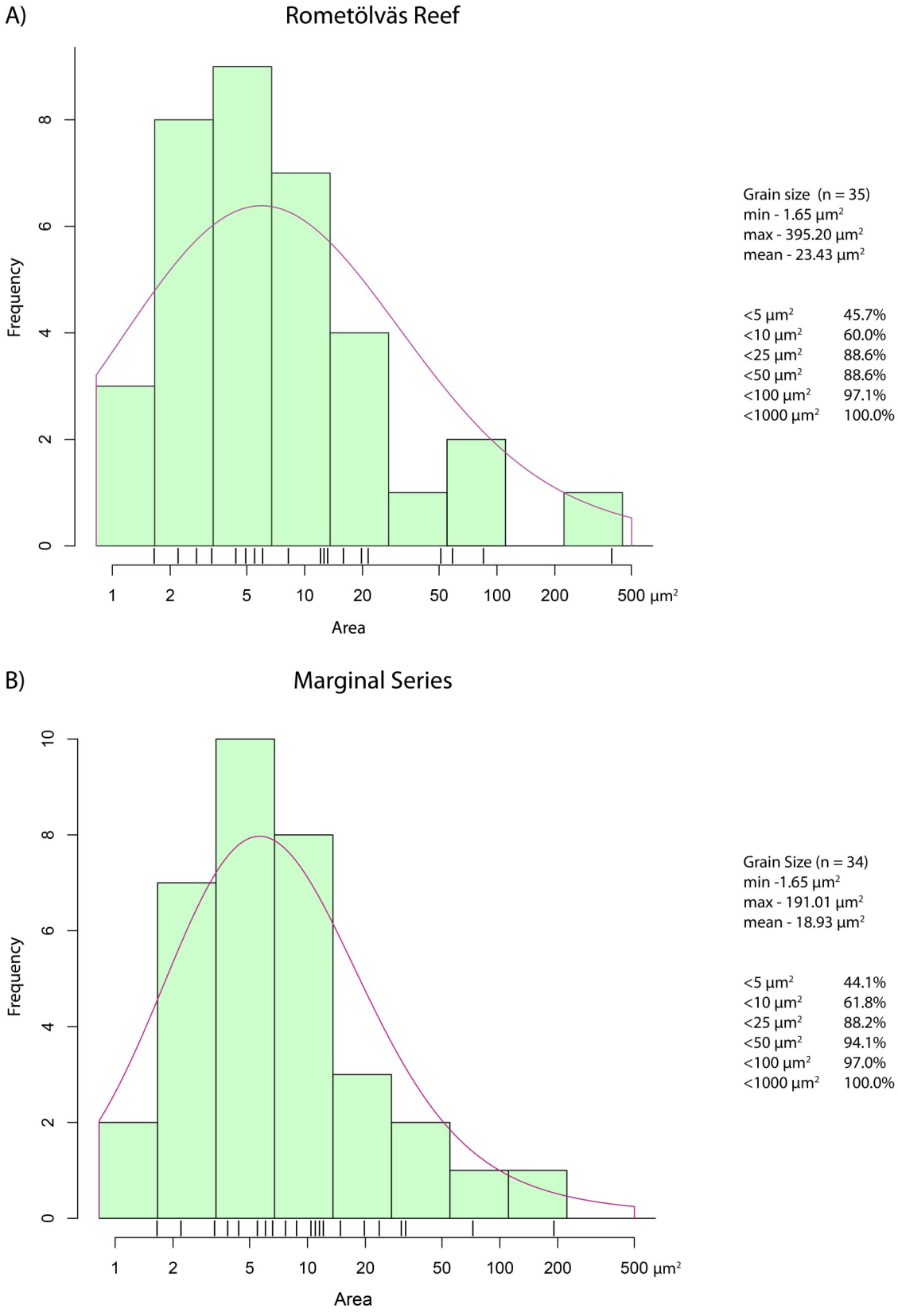

Figure 23. Histograms of the grain size distribution of the analyzed PGM grains in the Rometölväs Reef (A) and the Marginal Series (B). Grain sizes were obtained from SEM analyses using INCA software. Gold and silver-bearing grains are excluded. The purple curve shows adaptive kernel density estimation for data smoothing.

Table 3. Chemical composition of PGM (in atomic %) from the Marginal Series and the Rometölväs Reef, based upon SEM-EDS analysis. Feature ID marked "*" are composite grains.

Stratigraphy	Sample ID	Feature ID	Lithology	S	Fe	Ni	As	Pd	Ag	Au	Te	Pb	Pt	Bi	Total at. %	Classification	Host
Soukeli- MS	257-TTK-00	f30	Gabbronorite (pbCa)					13%			64%		19%	4%	100%	Merenskyite-moncheite-melonite	BMS-contact
"	"	f29	"					19%			67%		10%	3%	100%	Merenskyite-moncheite-melonite	silicate
"	"	f28	"					19%			62%		14%	4%	100%	Merenskyite-moncheite-melonite	silicate
"	"	f8	"					22%			66%		8%	4%	100%	Merenskyite-moncheite-melonite	silicate
"	"	f39	"					21%			65%		10%	4%	100%	Merenskyite-moncheite-melonite	silicate
"	"	f5	"					15%			78%		6%	2%	100%	Merenskyite-moncheite-melonite	silicate
"	"	f38	"					19%			65%		12%	4%	100%	Merenskyite-moncheite-melonite	silicate
"	"	f35	"					33%			63%			4%	100%	Merenskyite-moncheite-melonite	BMS
"	"	f6	"					31%			59%		3%	7%	100%	Merenskyite-moncheite-melonite	silicate
"	"	f40	"					32%			62%			6%	100%	Merenskyite-moncheite-melonite	silicate
"	"	f32	"					32%			63%			6%	100%	Merenskyite-moncheite-melonite	silicate
"	"	f26	"					31%			67%			2%	100%	Merenskyite-moncheite-melonite	silicate
"	"	f14	"					26%			74%				100%	Merenskyite-moncheite-melonite	BMS
Soukeli - MS	261-TTK-00	f30	Gabbronorite (pbCa)				67%						33%		100%	Sperrylite	silicate
Soukeli - MS	400-TTK-00	f21*	Gabbronorite (pbCa)					28%			63%			10%	100%	Merenskyite-moncheite-melonite	BMS
"	"	f18	"					27%			68%			5%	100%	Merenskyite-moncheite-melonite	silicate
"	"	f15	"					18%			78%			4%	100%	Merenskyite-moncheite-melonite	BMS
Soukeli - MS	402-TTK-00	f6	Gabbronorite (pbCa)					2%			83%		5%	10%	100%	Merenskyite-moncheite-melonite	silicate
"	"	f8*	"					20%	9%	21%	44%			5%	100%	erenskyite-moncheite-melonite (electru	silicate
"	"	f9*	"					32%			60%			8%	100%	Merenskyite-moncheite-melonite	BMS
"	"	f3*	"					31%			65%			4%	100%	Merenskyite-moncheite-melonite	BMS-contact
"	"	f20	"					17%			83%				100%	Merenskyite-moncheite-melonite	silicate
"	"	f19*	"					16%			81%			3%	100%	Merenskyite-moncheite-melonite	silicate
"	"	f30	"					22%			78%				100%	Merenskyite-moncheite-melonite	BMS
Soukeli - MS	264-TTK-00	f10a	Pyroxenite (bCa*)				67%						33%		100%	Sperrylite	silicate
"	"	f10b	"				67%						33%		100%	Sperrylite	silicate
"	"	f10c	"				67%						33%		100%	Sperrylite	silicate
"	"	f10d	"				62%	9%					29%		100%	Sperrylite	silicate
"	"	f15a	"				67%	2%					31%		100%	Sperrylite	silicate
"	"	f15b	"				67%						33%		100%	Sperrylite	silicate
"	"	f15c	"				68%						32%		100%	Sperrylite	silicate
"	"	f15d	"				67%						33%		100%	Sperrylite	silicate
"	"	f16	"					32%			58%			10%	100%	Merenskyite-moncheite-melonite	silicate
Soukeli - MS	11-TTK-00	f1a	Gabbronorite (pbCa)				58%	7%			8%		27%		100%	sperrylite	silicate
"	"	f1b	"					37%			55%			9%	100%	Merenskyite-moncheite-melonite	silicate
"	"	f1c	"					31%			60%		9%		100%	Merenskyite-moncheite-melonite	silicate
"	"	f15a	"				11%	29%			48%		3%	10%	100%	Merenskyite-moncheite-melonite	silicate
"	"	f15b	"				68%						32%		100%	Sperrylite	silicate
"	"	f14	"				67%						33%		100%	Sperrylite	silicate
"	"	f9	"					62%		38%					100%	PGE alloy	silicate
"	"	f13	"					49%			41%			10%	100%	Kotulskite-sobolevskite-sudburyite	silicate
"	"	f6	"					50%			40%			10%	100%	Kotulskite-sobolevskite-sudburyite	silicate
"	"	f4	"					49%			44%			7%	100%	Kotulskite-sobolevskite-sudburyite	silicate
Rometölväs - RT	82-TTK-00	f1	Anorthosite (pCa*)				67%						33%		100%	Sperrylite	silicate
"	"	f5	"					25%			73%			3%	100%	Merenskyite-moncheite-melonite	silicate
"	"	f73a	"					25%			70%			5%	100%	Merenskyite-moncheite-melonite	silicate
"	"	f73b	"					24%			70%		2%	4%	100%	Merenskyite-moncheite-melonite	silicate
"	"	f4	"					18%			78%			4%	100%	Merenskyite-moncheite-melonite	silicate
"	"	f57	"					10%			86%			3%	100%	Merenskyite-moncheite-melonite	BMS-contact
"	"	f47	"					10%			87%			3%	100%	Merenskyite-moncheite-melonite	BMS
"	"	f72	"					12%			85%			3%	100%	Merenskyite-moncheite-melonite	BMS-contact
"	"	f50	"					12%			88%				100%	Merenskyite-moncheite-melonite	silicate
Mustavaara - RT	39,3-TTK-00	f12	Gabbronorite (pahC)				67%						33%		100%	Sperrylite	silicate
"	"	f10	"				65%						35%		100%	Sperrylite	silicate
"	"	f4	"					32%			14%		43%	11%	100%	Kotulskite-sobolevskite-sudburyite	silicate
"	"	f3	"					32%			17%		51%		100%	Kotulskite-sobolevskite-sudburyite	silicate
"	"	f11	"				66%						34%		100%	Sperrylite	silicate
"	"	f2	"					25%			12%		49%	13%	100%	Kotulskite-sobolevskite-sudburyite	silicate
"	"	f9	"					73%			20%			7%	100%	Keithconnite-telluropalladinite	silicate
"	"	f5*	"					73%			20%			7%	100%	Keithconnite-telluropalladinite	silicate
"	"	f13	"					66%			29%			5%	100%	Keithconnite-telluropalladinite	silicate
Lanttioja - RT	l35,6-TTK-9	f21	Gabbronorite (pahC)				66%						34%		100%	Sperrylite	silicate
"	"	f12	"					12%			77%		11%		100%	Merenskyite-moncheite-melonite	silicate
"	"	f13	"					19%			81%				100%	Merenskyite-moncheite-melonite	silicate
"	"	f23	"					13%			87%				100%	Merenskyite-moncheite-melonite	BMS
"	"	f26	"					10%			90%				100%	Merenskyite-moncheite-melonite	BMS
"	"	f25	"						66%		34%				100%	Hessite	BMS
Lanttioja - RT	35,8A-TTK-9	f8	Gabbronorite (phCa*)					27%			69%			4%	100%	Merenskyite-moncheite-melonite	silicate
"	"	f9	"					17%			78%			4%	100%	Merenskyite-moncheite-melonite	silicate
Lanttioja - RT	35,8B-TTK-9	f36	Gabbronorite (phCa*)					25%			75%				100%	Merenskyite-moncheite-melonite	BMS
"	"	f35	"					27%			68%			6%	100%	Merenskyite-moncheite-melonite	BMS-contact
"	"	f9	"					25%			65%		5%	5%	100%	Merenskyite-moncheite-melonite	silicate
"	"	f18	"					9%			91%				100%	Merenskyite-moncheite-melonite	BMS-contact
"	"	f41	"					5%			95%				100%	Merenskyite-moncheite-melonite	silicate
"	"	f41	"					4%			96%				100%	Merenskyite-moncheite-melonite	silicate
"	"	f43	"					4%			96%				100%	Merenskyite-moncheite-melonite	silicate
Lanttioja - RT	35.11-TTK-9	f66	Gabbro (pCa*)					2%			95%		3%		100%	Merenskyite-moncheite-melonite	silicate

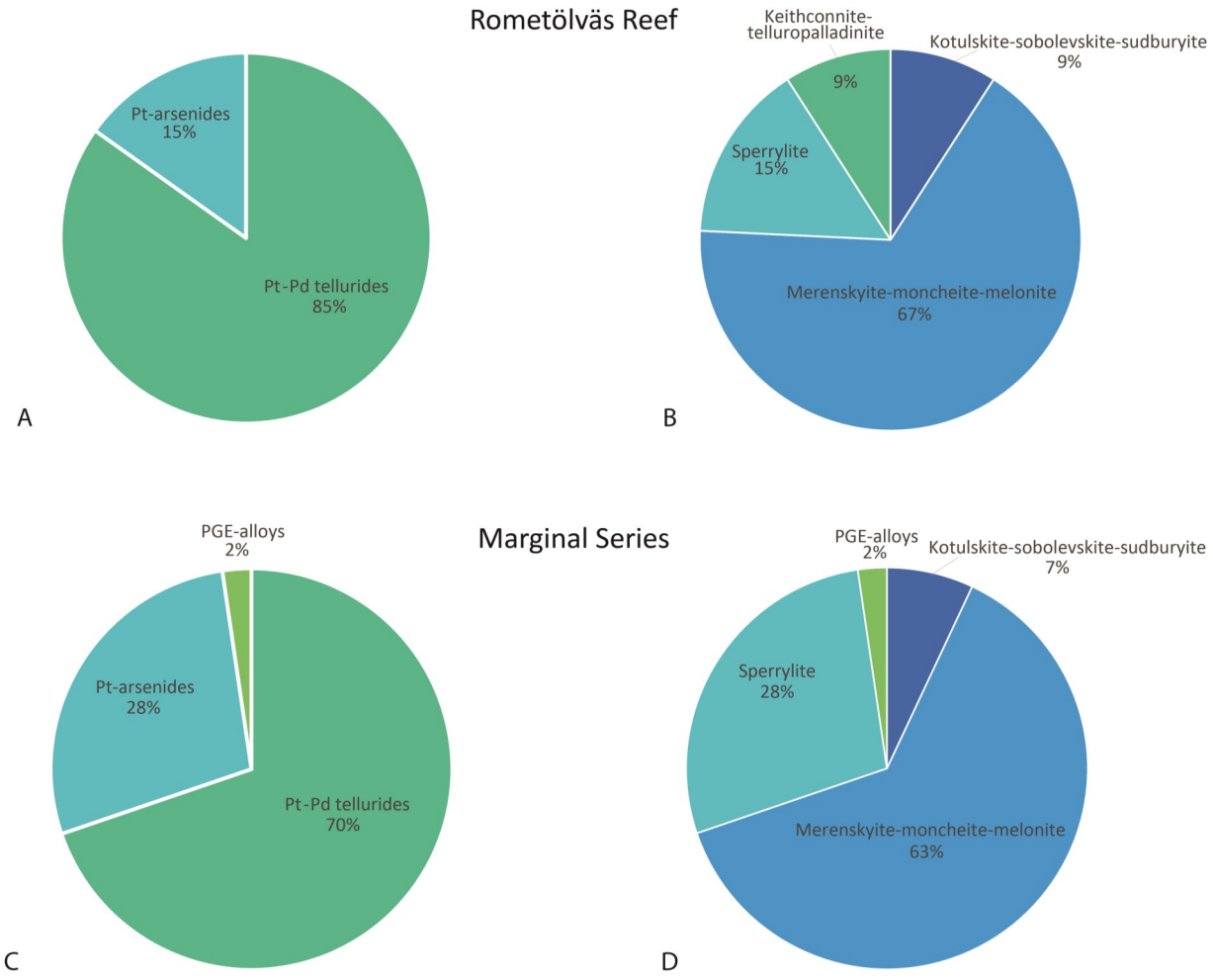

Figure 24. Relative proportions of PGM as categorized by the mineralogy group (presented in a generalized group and a more detailed group), based upon identified number of grains. A-B. PGM classified in the Marginal Series (n = 43). C-D. PGM classified in the Rometölväs Reef (n = 35).

tölväs Reef as a minor (9%) occurrence. In the Marginal Series, one PdAu-alloy grain was identified. Comparing both assemblages, the PdPtTe(Bi) series of merenskyite-moncheite-melonite are most abundant (65%) followed by sperrylite (22%) and kotulskite-sobolevskite-sudburyite (8%). The remaining 5% are keithconnite-telluropalladinite and PGE-alloy. No observations of PGM containing traces of the other platinum-group elements, Ru, Rh, Os and Ir, were made. The dataset of the PGM assemblage were further examined by plotting their chemical compositions plots to visualize any compositional trends. Figure 25 shows the composition of the tellurides identified for each mineralization type, in atomic percentage.

The Rometölväs Reef has a much larger compositional spread compared to the Marginal Series, exhibiting very high Te values, but also containing some compositions with a much higher PGE component. In general, the Bi components are low and no compositions approaching michenerite were identified. The tellurides identified in the Marginal Series plot closer to the merenskyite-moncheite-melonite field, with some occurring in the kotulskite-sobolevskite solid solution series. These grains, much like those in the Rometölväs Reef, are also poor in Bi. As can be seen from the Pd vs. Pt plot displayed in Figure 26, the Rometölväs Reef shows a greater compositional variation in the tellurides compared to the Marginal Series. Moreover, the Bi/Te values are also more diverse in the Rometölväs Reef than the Marginal series, which shows much more focused values (Fig. 27).

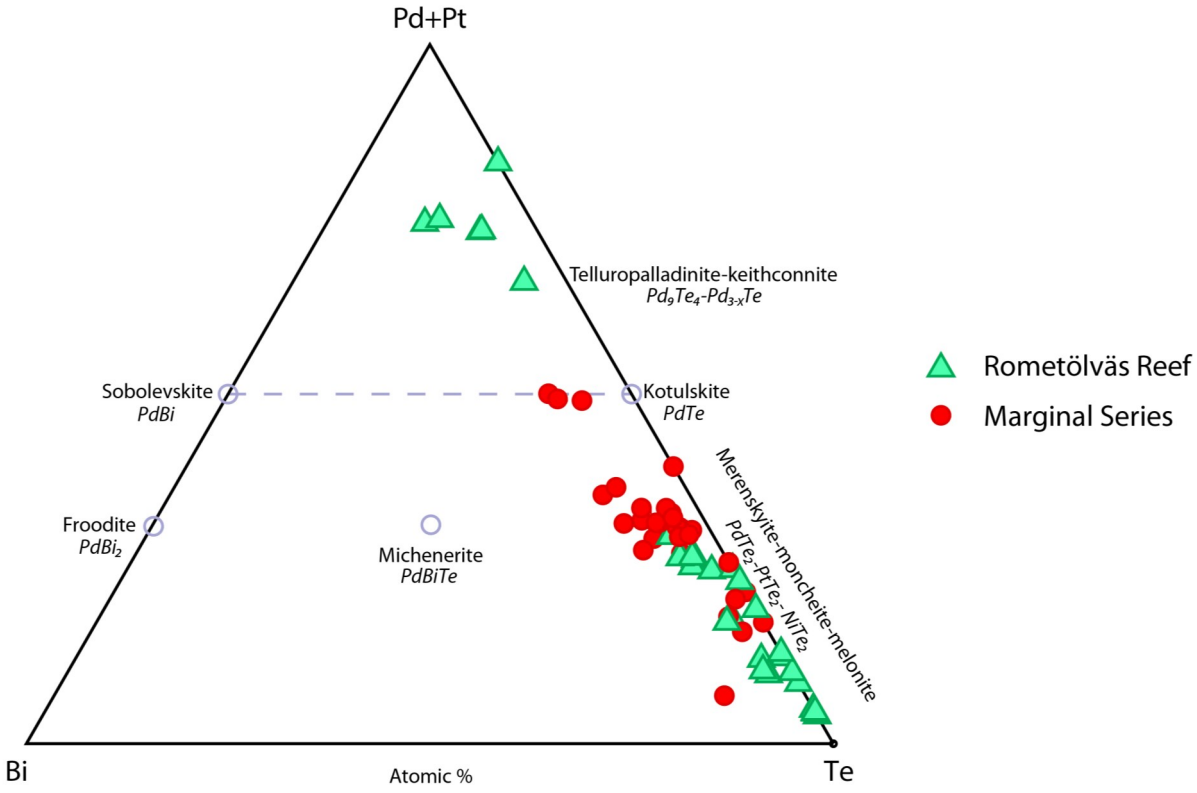

Figure 25. PGE-bearing telluride phases plotted in the Bi-Pd+Pt-Te space. The empty circles represent the stoichiometric composition of the respective mineral. The dotted line illustrates the intermediate members belonging to the sobolevskite-kotulskite solid solution series. Red dots represent the Marginal Series (n = 30), and green triangles represent the Rometölväs Reef (n = 28).

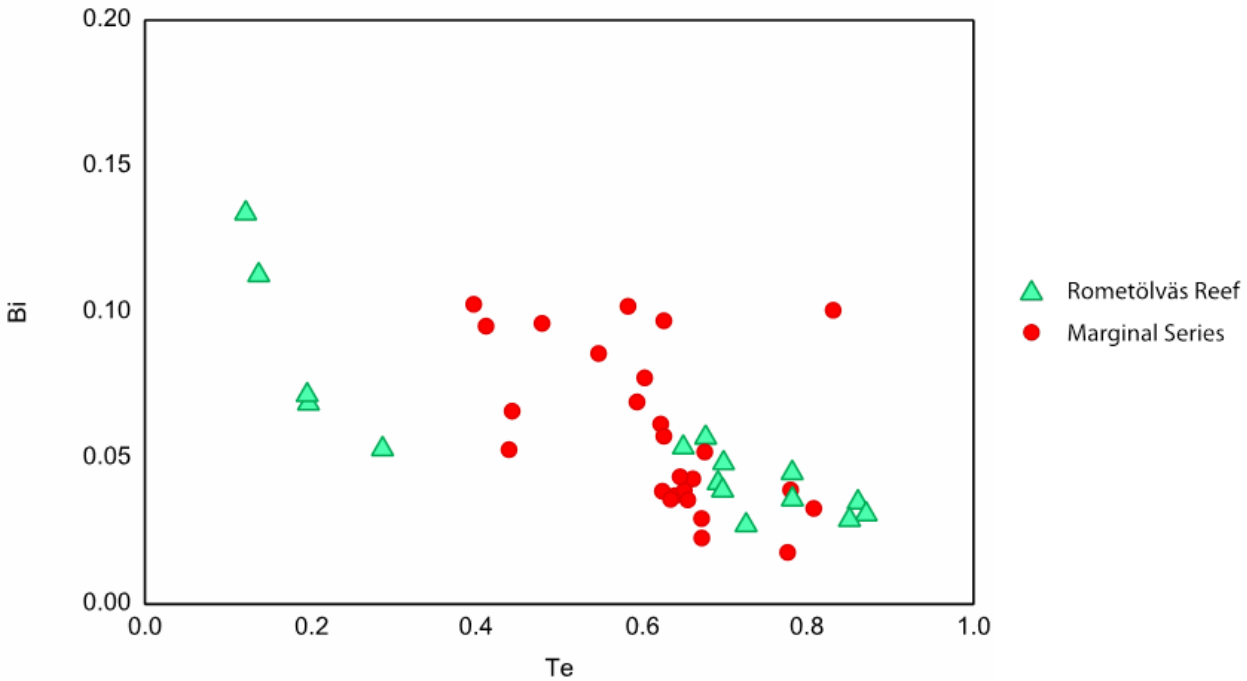

Figure 26. Palladium and platinum contents plotted of analyzed PGE bearing tellurides (%/100). Red dots represent the Marginal Series (n = 30), and green triangles represent the Rometölväs Reef (n = 28).

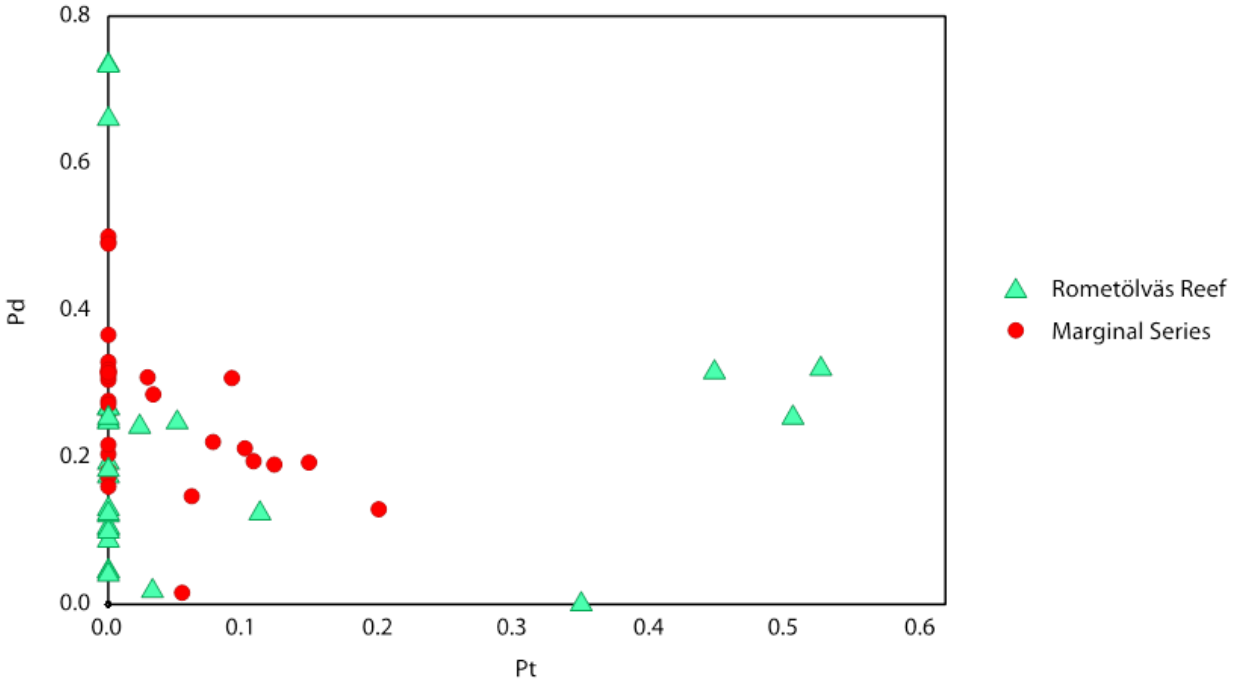

Figure 27. Plot of Bi vs. Te for analyzed PGE bearing tellurides (%/100). Red dots represent the Marginal Series (n = 30), and green triangles represent the Rometölväs Reef (n = 28).

6.2.2 Sulfur isotopes

In-situ $\delta^{34}S$ values of pyrrhotite, chalcopyrite and pyrite from the Rometölväs Reef (45) and the Marginal Series (39) are provided in Table 4. The Rometölväs Reef sulfides range in $\delta^{34}S$ from -0.40‰ to +1.80‰, with a mean of +0.29‰ (Fig. 28). Pyrrhotite and chalcopyrite display similar compositions, whereas pyrite exhibits slightly higher values. Primary sulfides (Po and Ccp) show marginally lower $\delta^{34}S$ values (-0.40‰ to +1.23‰, with a mean of 0.18‰) than remobilized sulfides (Po, Ccp and Py) (-0.24‰ to 1.80‰, with a mean of 0.52‰). All analyzed pyrites are secondary. Remobilized Po and Ccp display a slightly larger $\delta^{34}S$ spread than their primary counterparts. As can be seen in Fig 28, both primary and remobilized sulfides have similar $\delta^{34}S$ values, except for remobilized pyrite, whose $\delta^{34}S$ values are offset towards higher values. The Marginal Series sulfides show a $\delta^{34}S$ range from -0.94‰ to +2.19‰, with a mean of 0.78‰ (Fig. 28). The chalcopyrite and pyrrhotite display – as in the Rometölväs Reef – similar compositions, except that chalcopyrite has a somewhat wider range. Pyrite shows values between +0.65‰ and +1.41‰, slightly lower than the pyrite in the Rometölväs Reef. The primary sulfides (-0.94‰ to +1.90‰, with a mean of 0.61‰) and the remobilized sulfides (-0.60‰ to +2.19‰, with a mean of 0.86‰) are similar in terms of their $\delta^{34}S$ values. Unlike in the Rometölväs Reef, secondary pyrite in the Marginal Series has similar $\delta^{34}S$ values as the primary sulfides.

The data from both the Rometölväs Reef and the Marginal series show $\delta^{34}S$ values near the mantle-like composition, covering a narrow range from -0.94‰ to +2.19‰, with a mean of +0.52‰. On average, the $\delta^{34}S$ values are slightly higher for the Marginal Series with a mean of 0.78‰ compared to the Rometölväs Reef with a mean of 0.52‰. No noticeable correlation is observed between whole-rock sulfur contents and $\delta^{34}S$ values.

Table 4. Results of in-situ LA-ICP-MS isotope analyses of sulfides from the Koillismaa intrusion and whole-rock S concentrations from the Rometölväs Reef (n = 45) and the Marginal Series (n = 39). Abbreviations: Classification of primary (p) and remobilized (r), and uncertain texture (u) sulfides are denoted for chalcopyrite (Ccp), pyrrhotite (Po) and pyrite (Py).

Sample ID	Stratigraphy	Lithology	Spot ID	Texture	Mineral	δ^{34}S ‰ V-CDT	2σ	Wt.% S (WR)
135.6-TTK-99	Lanttioja – Reef	Gabbronorite - pahC	C1-CP1	p	Ccp	0.27	0.13	2.10
”	”	”	C1-PO1	p	Po	0.41	0.09	”
”	”	”	C1-PO2	p	Po	0.37	0.09	”
”	”	”	C2-CP1	p	Ccp	-0.38	0.15	”
”	”	”	C2-CP2	p	Ccp	-0.03	0.13	”
”	”	”	C2-CP3	p	Ccp	0.15	0.14	”
”	”	”	C2-PO1	r	Po	0.04	0.13	”
”	”	”	C2-PO2	p	Po	0.24	0.13	”
135.8B-TTK-99	Lanttioja – Reef	Gabbronorite – phCa*	C1-CP1	r	Ccp	0.36	0.10	1.58
”	”	”	C1-CP2	r	Ccp	0.30	0.13	”
”	”	”	C2-PO1	p	Po	-0.29	0.10	”
”	”	”	C2-PO2	p	Po	0.44	0.11	”
”	”	”	C2-PO3	p	Po	-0.28	0.12	”
”	”	”	C2-PO4	p	Po	-0.04	0.11	”
”	”	”	C3-PO1	r	Po	0.62	0.09	”
”	”	”	C3-PO2	r	Po	0.45	0.10	”
”	”	”	C4-CP1	r	Ccp	-0.17	0.15	”
”	”	”	C4-CP2	r	Ccp	0.48	0.17	”
”	”	”	C4-PO1	p	Po	-0.39	0.10	”
”	”	”	C4-PO2	p	Po	-0.40	0.10	”
137.1-TTK-99	Lanttioja – Reef	Gabbronorite – pahC	C1-PO1	r	Po	-0.11	0.12	1.79
”	”	”	C1-PO2	r	Po	-0.24	0.17	”
”	”	”	C2-CP1	p	Ccp	-0.23	0.15	”
”	”	”	C2-CP2	p	Ccp	-0.22	0.17	”
”	”	”	C3-CP1	p	Ccp	0.32	0.16	”
”	”	”	C3-CP2	p	Ccp	0.41	0.15	”
”	”	”	C5-PO1	p	Po	0.38	0.10	”
”	”	”	C5-PO2	p	Po	0.58	0.10	”
50-TTK-00	Aurinkokallio – Reef	Gabbro – pCa*	C1-PY1	r	Py	1.80	0.14	0.43
”	”	”	C1-PY2	r	Py	1.35	0.11	”
”	”	”	C1-CP1	p	Ccp	1.19	0.17	”
”	”	”	C1-CP2	p	Ccp	1.23	0.18	”
80-TTK-99	Baabelinälkky – Reef	Anorthosite – pC	C1-CP1	p	Ccp	0.43	0.12	1.37
”	”	”	C1-CP2	p	Ccp	0.58	0.12	”
”	”	”	C1-PO1	p	Po	-0.39	0.10	”
”	”	”	C1-PO2	p	Po	-0.35	0.11	”
”	”	”	C1-PO3	p	Po	-0.16	0.09	”
”	”	”	C2-CP1	p	Ccp	0.08	0.11	”
”	”	”	C2-CP2	p	Ccp	0.17	0.11	”
”	”	”	C3-PO1	p	Po	0.71	0.07	”
”	”	”	C4-PO1	p	Po	0.54	0.09	”
82-TTK-00	Rometölväs – Reef	Anorthosite - pCa*	C1-PO1	r	Po	0.53	0.13	1.00
”	”	”	C2-PO1	r	Po	0.99	0.11	”
”	”	”	C2-PO2	r	Po	0.68	0.12	”
”	”	”	C2-PO3	r	Po	0.74	0.12	”

Sample ID	Stratigraphy	Lithology	Spot ID	Texture	Mineral	$\delta^{34}S$ ‰ V-CDT	2 σ	Wt.% S (WR)
257-TTK-00	Soukeli area – MS	Gabbronorite – pbCa	C1-PO1	r	Po	0.84	0.13	0.89
”	”	”	C1-PO2	r	Po	0.83	0.11	”
”	”	”	C2-PO1	u	Po	0.52	0.11	”
”	”	”	C2-PO2	u	Po	0.22	0.13	”
”	”	”	C3-CP1	p	Ccp	1.05	0.15	”
”	”	”	C4-CP1	p	Ccp	0.46	0.14	”
397-TTK-00	Lavotta – MS	Pyroxenite	C1-CP1	p	Ccp	0.27	0.13	0.04
”	”	”	C1-CP2	p	Ccp	0.18	0.14	”
”	”	”	C2-CP1	p	Ccp	-0.94	0.13	”
”	”	”	C3-PO1	p	Po	-0.05	0.11	”
”	”	”	C3-PO2	p	Po	-0.09	0.11	”
400-TTK-00	Soukeli area – MS	Gabbronorite – pbCa	C1-CP1	r	Ccp	1.39	0.12	1.53
”	”	”	C1-CP2	r	Ccp	1.58	0.15	”
”	”	”	C1-PO1	r	Po	1.06	0.10	”
”	”	”	C2-CP1	r	Ccp	0.25	0.12	”
”	”	”	C2-CP2	r	Ccp	0.75	0.12	”
”	”	”	C2-PO1	r	Po	0.76	0.09	”
”	”	”	C2-PO2	r	Po	1.24	0.11	”
”	”	”	C3-PO1	p	Po	1.17	0.12	”
401-TTK-00	Soukeli area – MS	Gabbronorite – pbCa	C1-CP1	r	Ccp	-0.33	0.11	1.76
”	”	”	C2-CP1	r	Ccp	1.26	0.12	”
”	”	”	C3-CP1	r	Ccp	0.22	0.11	”
”	”	”	C4-CP1	r	Ccp	1.12	0.15	”
”	”	”	C7-PO1	p	Po	0.23	0.12	”
”	”	”	C7-PO2	r	Po	-0.60	0.12	”
”	”	”	C8-PO1	r	Po	1.32	0.10	”
”	”	”	C8-PO2	p	Po	1.20	0.13	”
402-TTK-00	Soukeli area – MS	Gabbronorite – pbCa	C1-CP1	p	Ccp	1.90	0.16	1.48
”	”	”	C1-CP2	r	Ccp	2.19	0.27	”
”	”	”	C2-CP1	p	Ccp	0.90	0.15	”
”	”	”	C2-PO1	p	Po	0.38	0.12	”
”	”	”	C3-CP1	u	Ccp	0.39	0.15	”
”	”	”	C5-PO1	p	Po	1.21	0.10	”
”	”	”	C5-PO2	p	Po	1.35	0.10	”
”	”	”	C5-PO3	r	Po	1.38	0.09	”
53-TTK-00	Soukeli area – MS	Gabbronorite	C1-PY1	r	Py	1.32	0.11	0.84
”	”	”	C3-PY1	r	Py	1.33	0.09	”
”	”	”	C5-PY1	r	Py	0.65	0.10	”
”	”	”	C5-PY2	r	Py	1.41	0.12	”

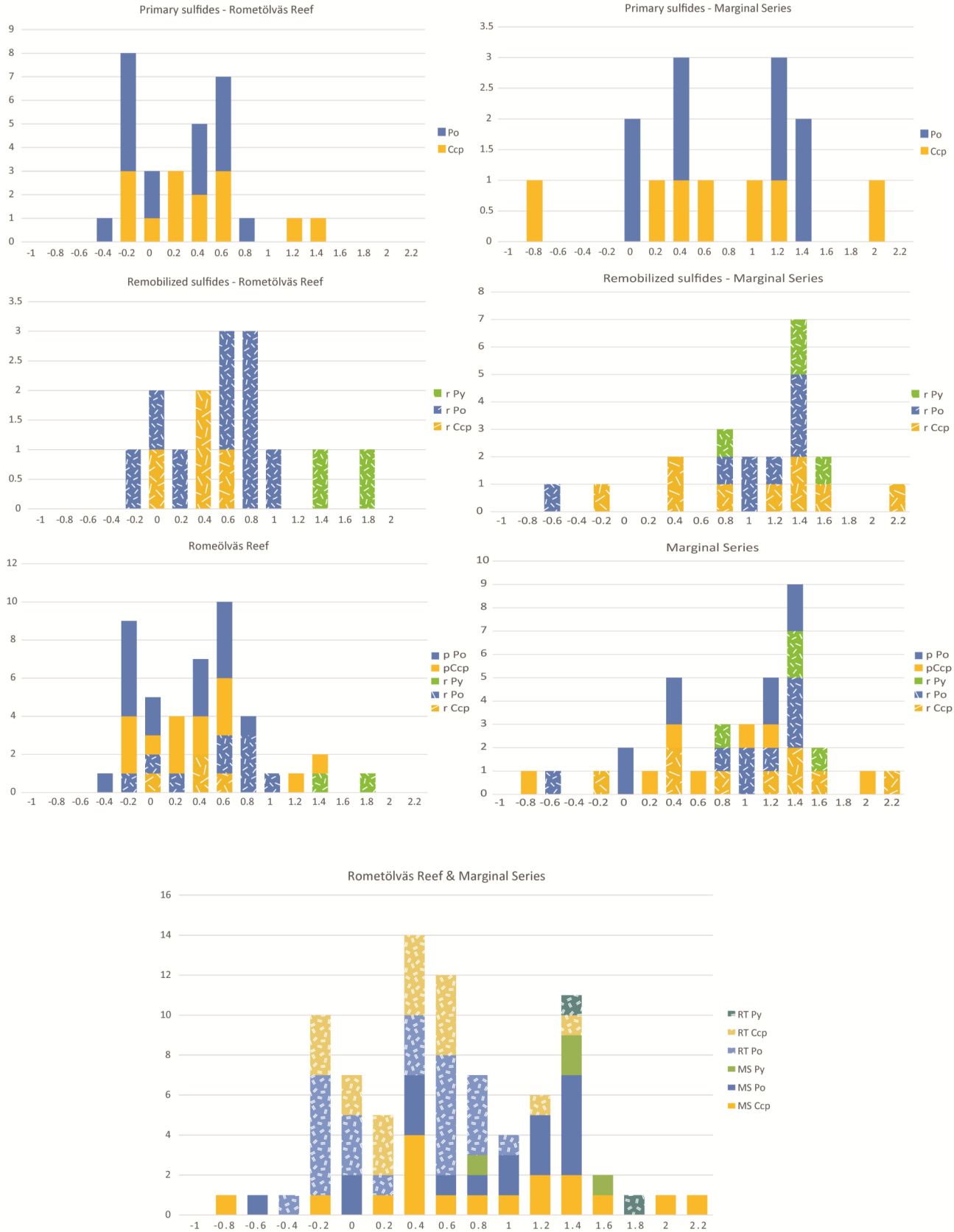

Figure 28. In-situ $\delta^{34}S$ values for primary (p) and remobilized (r) sulfides from the Rometölväs Reef (left); primary – n = 30, remobilized = 15, and the Marginal Series (right); primary = 15, remobilized = 21. Primary sulfides are solid colored, whereas remobilized sulfides are illustrated by a speckled texture. The bottom figure shows the compiled values for both the Rometölväs Reef and the Marginal Series, here the Rometölväs Reef is speckled textured and the Marginal Series solid colored. Abbreviations: Classification of primary (p) and remobilized (r) sulfides are denoted for chalcopyrite (Ccp), pyrrhotite (Po) and pyrite (Py).

7 Discussion

7.1 Petrography

The results of the general and sulfide petrographical study, correlate well with what has previously been described in literature (Alapieti 1982; Lahtinen 1985; Iljina et al. 2001; Karinen 2010; Iljina et al. 2012). The cumulate rocks and sulfide assemblages associated with both mineralization types in the Koillismaa intrusion are commonly observed globally (Naldrett 2004; Maier 2005; Maier & Groves 2011). The petrography is similar to other PGE-bearing intrusions of the Fennoscandian Shield, that also display high amounts of retrograde alteration (Yakovlev et al. 1991; Alapieti & Lahtinen 2002; Iljina & Hanski 2005). Based upon the observed retrograde minerals, it is estimated that the rocks reached upper greenschist facies or lower amphibolite facies (previously determined by Karinen (2010)). The heavily altered and remobilized sulfides of disseminated character is common in many other Fennoscandian Shield intrusions, as will be subsequently discussed. The presence of hydrothermal fluids is evident, in both mineralization types, by the presence of speckled alteration of sulfides and grain reduction, along with the observed remobilized scattered sulfides. The sulfides observed as intergrowths amid hydrosilicates and other secondary minerals further suggest that hydrothermal fluids were present.

7.1.1 Marginal Series

The contact-type mineralization of the Marginal Series is more altered than the reef-type within the layered series, as the outer parts of the intrusion are the most susceptible to external deformation. No xenoliths of the Marginal Series were studied in this MSc-project. Nonetheless, the Marginal Series, consisting of pyroxenites and gabbronorites, seems to be typical of what is often observed in other global layered intrusion (Iljina & Lee 2005; Begg et al. 2010b), such as, the Portimo Complex (Iljina 1994), the East Bull Lake intrusion (Peck et al. 2001), the Lukkulaisvaara intrusion (Semenov et al. 2008) and the Federova-Pansky intrusion (Schissel et al. 2002). They typically display a heterogenous lower marginal series, due to the sialic interaction with the footwall upon formation, that gradually becomes more homogenous upwards.

The Marginal Series of the Koillismaa intrusion is pervasively metamorphosed and sulfides are rather homogenously scattered in the observed samples. No preference to any particular textural association is observed, thus contrasting the mottle-association in the Rometölväs Reef. Furthermore, secondary sulfides are considerably more abundant in the Marginal Series than the Rometölväs Reef.

7.1.2 Rometölväs Reef

The mineralization of the Rometölväs Reef consist of often poikilitic, cumulate anorthosite, gabbronorite and norite rocks, similar to other PGE-bearing intrusions of the Fennoscandian Shield, such as; the Portimo Complex (Iljina 1994), the Lukkulaisvaara intrusion (Semenov et al. 2008) and the Federova-Pansky intrusion (Schissel et al. 2002). It is interesting that the Rometölväs Reef is situated at a megacyclic mineralogical change within the layered series (common for this deposit type, cf. *Section 2.3.2*), where orthopyroxene disappear, and clinopyroxene together with inverted pigeonite make their first appearance, as previously observed by Karinen (2010). The sulfide mineralization is mainly associated with the hydrosilicate mottles, corroborating with Karinen (2010). The mottles and the role of hydrothermal fluids are discussed in a subsequent segment (*Section 7.4*).

7.2 Platinum-group minerals

During analysis, the elements S, Ni, and Fe were not accounted for during the selection of detected EDS spectra, foremost, due to the lack of initial knowledge that PGM could contain these elements. Nonetheless, when measuring the PGM grains the beam was approximately 10 μm in diameter, whereas the average grain size of the grains was 4-5 μm. Because S, Ni and Fe are major components of BMS, the reasoning was to not take these elements into account, as their radiation was potentially backscattered from the hosting BMS and not the PGM grain itself. Sulfur was accounted for among the silicate phases, but no S-bearing components of PGM were detected (correlating with previous studies (Iljina et al. 2001; Kojonen & Iljina 2001; Karinen 2010)). Because Ni was not measured, the mineral melonite ($NiTe_2$) was consequently not accounted for. The data may therefore display higher $PdTe_2$-$PtTe_2$ values than what is true. Acknowledging this when scrutinizing the dataset, this is probably one of the main reasons for the minor offset in the merenskyite-moncheite-melonite solid solution series, compared to previous studies.

Another possible bias may be due to poor resolution while analyzing the PGM. Potential inhomogeneities and/or composite grains could have been undetected and would then give an average composition of a composite grain. No classification of silicate host mineralogy was made, as accurate statistics on silicate-hosts of PGM were not feasible through EDS, due to the high-grade retrograde alteration.

7.2.1.1 Platinum-group mineral hosts

This study observed a predominance of PGM hosted in silicates, and only a minor portion in BMS, for both mineralization types. In the Marginal Series, 81% were hosted in silicates and 14% by sulfides. This correlates very well with previous research from the Kaukua, Kuusijärvi, and Portivaara blocks (Kojonen & Iljina 2001; Iljina et al. 2005; Karinen 2010; Iljina et al. 2012). The study of Alapieti and Piirainen (1984), contrasts with all other research, where PGM in the Kuusijärvi block occur mainly as small inclusions in BMS, especially chalcopyrite.

In the Rometölväs Reef, 71% of the PGM were observed in silicates and 12% in sulfides. Contrasting with the study of Karinen (2010), which observed a lower abundance of PGM hosted in silicates (47%). However, Karinen (2010) included Au and Ag minerals (e.g., hessite and electrum) when compiling his statistics, and therefore the data should be interpreted with caution. Although there is a slight trend to a more common sulfide-host in the Rometölväs Reef in this study, it is nonetheless far away from what was observed by Karinen (2010).

7.2.1.2 Grain size

The grain size of PGM in this study are consistent with previous observations (Iljina et al. 2001; Kojonen & Iljina 2001; Karinen 2010)). However, it should be noted that the trend to smaller grains in the Rometölväs Reef, as described by Karinen (2010), was not observed in this study. The grain size is similar between the two mineralization types, with most grains being <5 μm in length, and the observed average grain size in the Rometölväs Reef is 23,43 μm^2, and 15,93 μm^2 within the Marginal Series. This is comparable to what is observed in other related layered intrusions globally, such as the Federova-Pansky (Schissel et al. 2002), the Merensky Reef (Godel et al. 2007), and the Great Dyke (Coghill & Wilson 1993).

7.2.1.3 Composite grains

In the study of Karinen (2010), the Marginal Series had 6.4% composite grains, whereas the Rometölväs Reef had 23.8% composite grains, contrasting with this study, that identified 11.6% composite grains in the Marginal Series and 2.9% in the Rometölväs Reef. The most obvious reason for the difference is the smaller data set of this study, giving rise to a potential nugget effect. An alternative cause could be that there is a natural heterogeneity in the mineralized zones, which is considered plausible, especially for the Marginal Series, as it is common in other global intrusions. No compositions of composite minerals are given in the study of Karinen (2010), and therefore no comparison with the palladobismuthotellurides of this study could be made. What can be remarked is that in Karinen's study, none of the composite grains are hosted by BMS in the Marginal Series, whereas in the Rometölväs Reef, most of the composite grains are hosted by BMS. The same prevalence is perceived in this study, however, too few composite grains were observed to statistically suggest this. This may be due to a faster cooling rate during primary formation, and/or due to late-stage alteration.

7.2.2 Platinum-group assemblages

The identified PGM assemblages in this study are comparable with previous studies of the Koillismaa intrusion (Alapieti 1982; Iljina et al. 2001; Kojonen & Iljina 2001; Karinen 2010). Comparing this study of the Rometölväs Reef with Karinen (2010), the PGM assemblage is similar, with Pt-Pd tellurides (85% vs. 88%) and Pt-arsenides (15% vs. 19%). The tellurides are Te dominated variants in both studies. The Rometölväs Reef has a larger compositional spread than the Marginal Series in this study, with tellurides exhibiting very high tellurium values and features with higher Pt-Pd components, close to telluropalladinite-keithconnite composition. Karinen (2010) observed a more focused distribution of tellurides with high merenskyite-melonite components, mainly from the Rometölväs Reef, whereas the Marginal Series had lower melonite components. In this study, no melonite components were identified and it is likely that the high Te component observations in the Rometölväs Reef are due to the lack of accounted Ni. If so, the observed grains would align much closer to previous observations (Kojonen & Iljina 2001; Karinen 2010). This could also be due to the presence of composite grains. However, based on the observations of previous studies, it is deemed more likely that the absence of Ni is the main cause of deviation. This is further inferred since previous studies detected higher Ni components in the Rometölväs Reef. Considering that the tellurides identified in this study are offset with higher Te values, this is most likely the reason. This would also partly explain the lack of the high Bi-mineral michenerite, commonly observed in the Rometölväs Reef and as minor occurrences in the Marginal Series, in previous studies (Iljina et al. 2001; Karinen 2010). In this study, no minerals close to a michenerite composition were observed. The high-PGE Pd-Pt bismuthotellurides exhibit Bi-Te ratios close to michenerite. However, this does not explain the exceptionally high Pd and Pt contents and is therefore perplexing. Other larger intrusions, such as the Bushveld Complex, are known to have a heterogeneous PGM assemblage laterally (O'Driscoll & González-Jiménez 2016). However, since a portion of the same sample collection was used in this study as that by Karinen (2010), no great difference, more than a sampling bias should occur. The observed assemblage in the Marginal Series correlates well with the results of Karinen (2010), though the spread is slightly larger in this study. The features cluster in the merenskyite-moncheite-melonite series and the kotulskite-sobolevskite-sudburyite series. The larger spread is interpreted to be due to the missing Ni, as well as the fact that EDS analysis is not as accurate as the microprobe analysis used in previous research (Kojonen & Iljina 2001; Karinen 2010). In previous studies, the merenskyite-component is higher in the Marginal Series, whereas the melonite-component is more dominant in the Rometölväs Reef. This is also observed in this study, with higher Pd/Pt values in the Marginal Series. No sudburyite components were identified in this study, whereas Karinen (2010) observed minor (<2.5 wt.%) Sb components. This study show kotulskite with 10-20 mol.% of the sobolevskite component and sperrylite grains close to their stoichiometry, corresponding with previous studies (Kojonen & Iljina 2001; Karinen 2010). No observation of tra-

ces of Rh or Fe in sperrylite (as seen in Karinen (2010)) were detected in this study. However, much like in previous studies, traces of Pd were identified.

7.2.2.1 Marginal Series

Different areas of the Marginal Series have been studied throughout the years. Because the marginal zone is practically mineralized along strike, albeit with varying PGE grades, a comparison between different blocks is considered eligible. The more centrally investigated areas, such as Kuusijärvi, Lavotta and Rusamo, have higher sulfide contents, whereas the northern Kaukua and Murtolampi blocks have relatively high PGE grades (Iljina 2004). The findings in this study, from the Soukeli area of the Portivaara block, observed 70% Pt-Pd tellurides, 28% Pt arsenides, and 2% PGE alloys. Karinen (2010) examined the same Portivaara block and observed 93% Pt-Pd tellurides and 7% Pt arsenides. Another study, undertaken at the Haukiaho area of the Kuusijärvi block observed 93.6% Pd-Pt tellurides, 6% sperrylite, and minor amounts of PGE cobaltite as inclusions in BMS (Kojonen & Iljina 2001). The predominant tellurides were merenskyite (62%) and Pd-rich melonite (25.3%). Further north at the Kaukua block, the PGM assemblage is reported to be fairly similar (Iljina et al. 2005).

In conclusion, the Marginal Series is dominated by Pd-Pt bismuthotellurides and Pt-arsenides (chiefly sperrylite). PGE-bearing sulfides and alloys are very rare, and the ones identified by (Iljina et al 2012) belong to the braggite-vysotskite series. The PGM mineralogy and hosts, as determined by previous researchers, of the Kaukua, Kuusijärvi, and Portivaara blocks are similar, the data presented in this thesis adhere to that conclusion.

7.2.2.2 Rometölväs Reef

Far fewer studies have focused on the Rometölväs Reef, as the contact-type mineralization of the Marginal series has been of economic interest. The data presented in this thesis are from the Lanttioja area and Mustavaara areas of the Portivaara block, and the Rometölväs area of the Syöte block. The identified PGM assemblage consists of 85% Pt-Pd tellurides and 15% Pt arsenides. This is generally comparable to previous research of the Portivaara and Syöte blocks (areas of Rometölväs, Baabelinälkky, Lanttioja, Välivaara and Mustavaara) observed 88% Pt-Pd tellurides and 12% Pt arsenides (Karinen 2010).

7.2.3 Comparison with similar intrusions

The PGM assemblages and textural settings, that are normally observed in reef- and contact-type mineralization globally, such as the Bushveld Complex (Cawthorn et al. 2002; Godel et al. 2007; Holwell & McDonald 2007) and the Stillwater Complex (Godel & Barnes 2008), (which normally contain high amounts of PGE sulfides and Pt-Fe alloys, and have higher amounts of PGM hosted in BMS), do not seem to be applicable to the Koillismaa intrusion. In the Koillismaa intrusion, Pt-Fe alloys and PGE sulfides are absent in both the Rometölväs Reef and the Marginal Series, which mainly contain palladobismuthotellurides and Pt arsenides.

The PGM assemblages are very similar to those in other PGE deposits of the Fennoscandian Shield, that predominantly consist of Pt and Pd bismuthotellurides, arsenides (commonly sperrylite), and PGE sulfides (Yakovlev et al. 1991); Schissel 2002, and references therein). Generally, there is an observed prevalence of Pd over Pt (Schissel et al. 2002). Yakovlev (1991) stated that the PGM assemblages are, to some extent, affected by metamorphism, and that primary MSS are partially redistributed into arsenides and sulfarsenides. This contrast may be due to metamorphism, where the primary PGE sulfides and Pt-Fe alloys have been altered to the current phases, and a higher portion are remobilized into silicates.

7.2.3.1 Federova-Pansky intrusion

The contact-type mineralization of the western Pansky block of the Federova-Pansky intrusion mainly consists of bismuthotellurides (merenskyite-moncheite-melonite), PGE sulfides (braggite, vysotskite and cooperite (PtS)) and arsenides (sperrylite and hollingsworthite ((Rh,Pt,Pd)AsS))) (Schissel et al. 2002). The typical grain size (0.2 - 5 μm) is very similar to that in the Koillismaa intrusion. Noteworthy is that in the Federova-Pansky intrusion smaller grains are monomineralic, whereas larger grains may be composites of up to three minerals. In the Koillismaa area, this observation is rare in the Marginal Series but more common in the Rometölväs Reef, where composite grains are predominantly associated with BMS (Karinen 2010). Platinum-group minerals in the Federova-Pansky intrusion show a clear association with BMS (>60%), and 20% are hosted by silicates. Moreover, several PGM grains are found at the BMS-contact of remobilized chalcopyrite and secondary silicates (Schissel et al. 2002).

7.2.3.2 Portimo Complex

There are several correlations that can be made between the Portimo Complex and the coeval Koillismaa intrusion. Like Koillismaa, Portimo is composed of several smaller blocks, referred to as the Narkaus, Suhanko and Konttijärvi intrusions. It is also accompanied by a set of mafic dikes (Iljina 1994). The blocks are thought to be dismembered parts of one or two original intrusions that were separated due to tectonic events. The Portimo Complex, much like the Koillismaa intrusion, is heavily deformed and metamorphosed due to Svecokarelian orogenesis (Amelin & Semenov 1996; Iljina & Hanski 2005). The disseminated contact-type mineralization in the Konttijärvi and Ahmavaara intrusions displays similar PGM assemblages (Iljina 1994) to those of the contact-type mineralization in the Koillismaa intrusion. Here, the assemblages are dominated by palladobismuthotelluri-

des and Pt arsenides (sperrylite), lacking PGE sulfides and alloys. However, antimonides are much more common and Pd-Sn minerals are known from both the Konttijärvi and Ahmavaara intrusions (Iljina 1994). According to Iljina (1994), the distribution of PGM in the Konttijärvi intrusion is as follow: 16% in BMS, 8% at BMS-contact, 49% in silicates and 27% in oxides. At Ahmavaara, the corresponding amounts are 39% in BMS, 32% at BMS-contact, 17% in silicates, and 12 % in oxides. The higher amount of PGM associated with BMS compared to the Koillismaa intrusion, could be due to variable degrees of redistribution of PGM into silicates during metamorphism.

The blocks of the Portimo Complex have a marginal series with a variable thickness with the same felsic Archean footwall, cf. Koillismaa. At Narkaus, the marginal series is thinner (10-20 m) compared to those at Suhanko and Konttijärvi (40-80 m & 100-150 m, respectively). Peculiarly, the Portimo Complex hosts fine-grained, granular gabbronorite bodies with length varying from a few centimeters to <100 m. They have been proposed to be autoliths of chilled margin rocks collected by succeeding magma pulses (Iljina 1994). The homogenous cumulates of the Konttijärvi Marginal Series are underlain by what is referred to as a mixing zone, from which more than half of the metal content occurs within "hybrid gabbro", a very heterogeneous mixture of cumulate pyroxenitic rock contaminated by xenoliths and footwall melts. The disseminated mineralized zone is 10-30 m thick along the whole Marginal Series of the Suhanko and Konttijärvi blocks. The mineralization commonly extends into the basement. The PGE content varies but may reach up to >10 ppm at Konttijärvi and Ahmavaara, contrasting to the <2 ppm in most of the Marginal Series of the Suhanko intrusion (Iljina 1994).

Comparing the Rometölväs Reef with the S-K Reef of the Suhanko intrusion, both reefs occur at a stratigraphical position in which Cr- and Mg-rich rocks are overlain by more evolved rocks. The S-K Reef is situated between two megacyclic units, probably representing a different magmatic pulse. The thickness of the S-K Reef varies from <1 m up to several meters. The PGE content is highly erratic, and the reef is thought to be the most sulfide-deficient PGE mineralization in the Portimo Complex with <1 wt.% S. The average Pd-Pt ratio 1.7 but this ratio varies between 0.8 and 3.0, and Pd/Ir between 32.1 and 132 (Iljina 1994). In the Rometölväs Reef, the average Pd/Pt values are approximately 1.0 and the Pd/Pt values vary in the range of 17.9-27.8 (Karinen 2010). Considering the PGM assemblages, all the PGE deposits are nearly identical (Iljina 1994). The host phases vary slightly and for the layered series, the host minerals in the S-K Reef are: BMS 26%, BMS-contact 18%, and silicates 56%, whereas the Rytikangas Reef host phases are: BMS 15%, BMS-contact 21%, and silicates 64%, similar to the Rometölväs Reef, which also has silicates as its dominant PGM host. Common for these reefs is that no PGM are hosted in oxides. Additionally, the mineralogical textures are similar, with PGM mostly displaying anhedral shapes occurring in the interstices of secondary silicates and cracks in primary silicates.

7.2.3.3 Lukkulaisvaara intrusion of the Oulanka Complex

The Oulanka Complex is particularly interesting to compare with the Koillismaa intrusion as they are coeval and were generated by a magma of marianitic-boninitic composition. In the Lukkulaisvaara intrusion of the Oulanka Complex, the main PGE mineralization is related to the presence of potholes (cf. Merensky Reef) and the association of variable-sized, fine-grained gabbronorite bodies (cf. Koillismaa). These bodies are ostensibly concomitant with the potholes and have been proposed to be results of injections of new magma (Glebovitsky et al. 2001; Latypov et al. 2008a; Latypov et al. 2008b). They have a more primary composition and display chilled textures. Metamorphic sulfides occur as fine-grained disseminations and mottled clusters, intergrown with secondary minerals, such as zoisite, scapolite, chlorite, and other hydrosilicates (cf. Koillismaa). The highest PGE grades are related to altered bronzite/gabbronorite veins with a high sulfide content, and in low-sulfide rocks near large fine-grained gabbronorite bodies (Glebovitsky et al. 2001). The PGM assemblage is similar to that of the Koillismaa intrusion, and other Fennoscandian intrusions, such as the Portimo Complex and the Federova-Pansky. The contact-type deposit of the Lukkulaisvaara intrusions is thought to have formed due to metasomatism from tensile deformation during cooling of the intrusion, where the disparities in composition and different compressibility have dictated the hydrothermal processes and consequently the PGE and PGM assemblages (Glebovitsky et al. 2001; Semenov et al. 2008). Additional injections related to the fine-grained bodies may also have played some role in the origin of the mineralization (subsequently discussed in *Section 7.4*), but Semenov et al. (2008) argued that decompression was the dictating factor in forming secondary BMS and PGM, at temperatures below 800°C.

7.2.3.4 East Bull Lake Intrusive Suite

As mentioned above, several intrusions of the Fennoscandian Shield have rather comparable PGM assemblages, although the host phases and mineralization styles vary. Some other areas that may be considered analogous (Schissel et al. 2002; Iljina & Lee 2005) to the TNB and adjacent Kola intrusions, include the contact-type deposits of the 2.48 Ga East Bull Lake Intrusive Suite (EBLIS) in Ontario, Canada (Peck et al. 2001; Easton et al. 2010). The EBLIS is similarly situated alongside Archean and Proterozoic provinces and located within an intracontinental rift zone of the Superior craton, with bimodal magmatism present. Differences are the presence of rocks domina-

ted by gabbroic or leucocratic variants in the EBLIS, contrasting with a higher abundance of more ultramafic rocks in the Fennoscandian region (Alapieti et al. 1990; Alapieti & Lahtinen 2002). The EBLIS hosts disseminated contact-type PGE mineralization in the lower series containing 1-2% S. It occurs as a heterogeneous zone of breccia inside a gabbronorite matrix, thought to be indicative of interaction between magma and footwall (Peck et al. 2001). The lowermost part of the marginal series is dominated by xenoliths of the footwall whereas higher up in the stratigraphy, mafic xenoliths/autoliths become more abundant. The mineralized zone is 20 – 50 m thick and <25km along strike. Much like the Marginal Series of Koillismaa, the Cu-Ni and Pd-Pt ratios are high. However, the overall grades of Pt+Pd are low (<1ppm) (Peck et al. 2001). The PGM assemblage is dominated by Pd tellurides and bismuthides, Pd arsenides and Pt minerals in the form of sperrylite and platarsite (PtAsS) (James et al. 2002). It has been proposed that the mineralization formed due to intense mixing of the footwall and circulating residual magma from multiple magma injections disrupting previously crystallized material, therefore hindering the formation of a chilled margin (Easton et al. 2010). Intriguingly, these characteristics can also be seen in some of the more local intrusions of the Fennoscandian Shield, such as the contact-type mineralizations of the Federova-Pansky intrusion (Schissel et al. 2002) and the Konttijärvi and Ahmavaara of the Portimo Complex (Iljina 1994).

7.2.4 Summary

The PGM assemblages in both the Marginal Series and the Rometölväs Reef are fairly identical, predominantly consisting of various Pt-Pd bismuthotellurides and Pt arsenides. The dominant host-phases of the PGM are silicates, whereas sulfide-related grains are far less common. This contrasts with many of the PGE occurrences among global layered intrusions, such as the Bushveld and the Stillwater complexes, where the PGM assemblages are dominated by PGM sulfides and Fe alloys, and telluride phases are only minor constituents (Cawthorn et al. 2002; Godel et al. 2007; Holwell & McDonald 2007; Godel & Barnes 2008). Furthermore, the contact-style mineralization of the Bushveld Complex (Platreef and Sheba's ridge) is richer in Ni compared to the corresponding deposits of the Fennoscandian Shield (Sharpe et al. 2002; Holwell et al. 2006; Holwell & McDonald 2007). The PGM of the Koillismaa intrusion contain very similar assemblages to other known coeval Fennoscandian PGE mineralizations, including those in the Penikat intrusion (Alapieti & Lahtinen 1986; Maier et al. 2018), the Portimo Complex (Iljina 1994), the Oulanka Complex (Glebovitsky et al. 2001), the Federova-Pansky Complex (Schissel et al. 2002), and the Monchegorsk intrusion (Karykowski et al. 2018). Several of the aforementioned PGE deposits have been proposed to have formed in a low-temperature hydrothermal setting (Alapieti et al. 1990; Yakovlev et al. 1991; Iljina 1994; Semenov et al. 2008). This can in many cases be seen by the presence of hydrothermal sulfides, such as galena, clausthalite, and sphalerite, as well as intergrowth of sulfides with hydrosilicates. In conclusion, the PGM assemblages and host phases are suggested to be generated by hydrothermal fluids, either in a magmatic stage, or during a later stage (e.g., the Svecofennian orogeny), as subsequently discussed in *Section 7.4*.

7.2.5 Enigmas and biases

The way PGM features are reported varies in the literature. Previously, the norm was to report the number of grains of a specific class and thereafter compile percentages based on the observed features in the assemblage. This is also how the different features are reported in this thesis. However, nowadays it is common to report PGM in areal percentages, and then compare these numbers, meaning that if you observe a 100-mm grain and a 10-mm grain, the observed contrast would be 90-10 instead of 50-50. There is thus a higher potential risk for biases when reporting the number of grains in small data sets, as in this study. Depending on the grain cut in the thin section, the actual mineral size could either be over- or underrepresented, which is commonly referred to as a nugget effect. Therefore, in this study, it was deemed more appropriate to report the observed grains in terms of single grains, instead of areal percentage.

7.3 Sulfur isotopes

The $\delta^{34}S$ data obtained from the Rometölväs Reef (-0.40‰ to +1.80‰) and the Marginal Series (from -0.94 to +2.19‰) are mostly within mantle-derived magma values, which are established to be within the range from -2 to +2‰ (Ripley & Li 2003). Values above +2‰ are observed in remobilized chalcopyrite of the Marginal Series. This indicates that there was no significant contribution of crustal sulfur in the generation of these low-sulfide PGE mineralizations. However, the sulfur isotope composition of the country rock is currently unknown, and hence, contamination from an external source cannot be entirely excluded.

7.3.1 Rometölväs Reef

Internal reef-type PGE mineralization, such as the Rometölväs Reef, is generally not associated with external sulfur. Internal reefs, as discussed in *Section 2.7.2.1,* are thought to be derived from the mantle-derived magma without assimilation of country rock. Sulfur-rich deposits, such as Noril'sk (Li et al. 2003), the Duluth Complex (Ripley 1981) and Voisey's Bay (Ripley et al. 1999; Ripley et al. 2002), often exhibit a larger range in $\delta^{34}S$ values (Fig. 7), indicating assimilation of crustal sulfur during their formation. Comparing the $\delta^{34}S$ results of Rometölväs Reef (-0.40‰ to +1.80‰, with a mean of 0.29‰) with those in other worldwide reef-type deposits established to be of magmatic origin, such as the Merensky Reef of the

Bushveld Complex (Penniston-Dorland et al. 2012) or the J-M Reef of the Stillwater Complex (Ripley et al. 2017), reveal similar $\delta^{34}S$ values (Fig. 7). Many intrusions in Fennoscandia, such as the Federova-Pansky (Schissel et al. 2002) and the Portimo Complex (S.H. Yang, pers. comm., 2018), show similar S isotope compositions (Fig. 7). The highest $\delta^{34}S$ values of the Rometölväs Reef (up to +1.80‰) are found in remobilized pyrite, but are still well within the mantle values (Ripley et al. 2003).

No analyses were made of the sulfides from the non-cumulus gabbronorite bodies, which seem to have a connection to the genesis of the Rometölväs Reef (subsequently discussed in *Section 7.4*). However, given that the bulk-rock composition is richer in MgO and Cr, compared to the cumulates, and their resemblance to xenoliths of early magma pulses (Alapieti 1982; Iljina et al. 2001; Karinen 2010), it is unlikely that the sulfides would deviate from the mantle signatures observed in both the reef and contact-type deposits. Similar non-cumulate bodies are encountered in the Lukkulaisvaara intrusion of the Oulanka Complex, where they have been interpreted as xenoliths from earlier magma pulses, interrupted dykes, trapped intercumulus liquids, or as decompression effects from volatile loss (Glebovitsky et al. 2001; Alapieti & Lahtinen 2002; Latypov et al. 2008a; Latypov et al. 2008b; Semenov et al. 2008).

7.3.2 Marginal Series

The contact-type PGE mineralization of the Koillismaa intrusion is thought to represent typical orthomagmatic accumulation of sulfides at the base of the intrusion, which is typical for many intrusions, such as Duluth (Ripley 1981), East Bull Lake (Peck et al. 2001), Portimo (Iljina 1994), Platreef (Holwell et al. 2007; Smith et al. 2016), Lukkulaisvaara (Semenov et al. 2008), Federova-Pansky (Schissel et al. 2002) and Monchegorsk (Bekker et al. 2016). The mineralization has been interpreted to have formed due to sialic crustal contamination by partial melting and assimilation of the Archean basement, triggering sulfide saturation in the melt (Alapieti 1982; Lahtinen 1985; Iljina et al. 2001; Iljina 2004). It is characterized by strong contamination and mixing with melts from the granitoid country rocks, as indicated by the diffusive contact of metasomatized albite-quartz rock, occasionally with patches of meter-thick mafic components (Lahtinen 1985). Further evidence for contamination is provided by the heterogeneity of the Marginal Series, consisting of fragments of partly melted basement rocks and the presence of albite-quartz veins and breccias in the contact gabbro.

The Marginal Series at the Kuusijärvi block was examined by Alapieti & Piirainen (1984), where they reported $\delta^{34}S$ values between +1.3 and +2.0‰, based upon bulk pyrrhotite and chalcopyrite analyses. The results of this study are much alike those of Alapieti and Piirainen (1984), with a difference being that the range of $\delta^{34}S$ is wider, especially to the negative side, displaying $\delta^{34}S$ values of -0.94‰ to +2.19‰. The primary and remobilized sulfides do not differ greatly in terms of the $\delta^{34}S$ range, and no obvious trends are observed other than a few remobilized chalcopyrite grains displaying slightly elevated values.

Normally, contact-type PGE mineralization contains sulfur that is thought to be derived from the country rock (Ripley & Li 2003; Schulz et al. 2010). However, this is not the case with the Koillismaa intrusion, as indicated by the narrow range of mantle-like $\delta^{34}S$ values (-0.94‰ to +2.19‰, with a mean of 0.78‰). The fact that both the primary and remobilized sulfides of the Marginal Series exhibit overlapping $\delta^{34}S$ values suggests that there was no external sulfur contribution during the mineralization process. Comparing the isotope values from the Marginal Series of the Koillismaa intrusion with those from the Platreef (Fig. 6) reveals that the primary sulfide values from the northern Platreef show near mantle-like $\delta^{34}S$ values (-0.7‰ to +2.6‰), but remobilized and basal sulfides (-1.9 to + 11.1‰) clearly show signs of the presence of externally originated sulfur (Holwell et al. 2007). Sharman et al. (2013) showed that sulfides in the southern (Turfspruit & Rietfontein) and northern (Drenthe & Overysel) parts of Platreef have significantly lower $\delta^{34}S$ values (+1.43 to +8.58‰) than the central (Sandsloot & Tweenfontein) parts (+2.74 to +12.7‰) and that there is no preference in $\delta^{34}S$ values between the analyzed BMS. The footwall and xenolith $\delta^{34}S$ values have significantly broader ranges. Calc-silicate rocks in the northern and central part have $\delta^{34}S$ values between +0.7 and +8.2‰, whereas calc-silicate rocks and dolomites in the south vary between +14.7 to +28.7‰. The most extreme values were observed in hornfels (–20.9 to +18.1‰) (Sharman et al. 2013). At Overysel, where the footwall consists of granitoid gneiss, $\delta^{34}S$ in nearly the all primary sulfides in the host rock (feldspathic pyroxenites) is below +2‰ (mean +1.8‰) and the $\delta^{34}S$ values of the footwall vary between +1.5 and +5‰. At Sandsloot, $\delta^{34}S$ in the primary sulfides in feldspathic pyroxenites falls between 0.0 and +2.6‰ (mean 1.8‰) and $\delta^{34}S$ in the footwall consisting of calc-silicates and xenoliths of serpentinized calc-silicates varies between +2.5 and +6.0‰. Chalcopyrite, pyrrhotite and sphalerite in late-stage quartz-feldspar-calcite veins show higher $\delta^{34}S$ of ca. +8‰ (Holwell et al. 2007).

The petrogenesis of the contact-style mineralization - in particular the Platreef - is highly debated. The arguments mainly concern the timing of sulfur saturation in relation to the magma emplacement. One side argues that the mineralization was formed due to sulfur saturation triggered by contamination of country rock material (e.g., (Buchanan et al. 1981). The other side, which is becoming more popular (Lee 1996; Peck et al. 2001; Sharman et al. 2013; Holwell & Keays 2014), suggests that sulfide saturation was reached already before crustal contamination and that the country rocks are of minor importance in generating the contact-type mineralization. Using multiple

sulfur isotopes, Sharman et al. (2013) came to the conclusions that the source of the Platreef crustal is located in a restricted horizon in the footwall (Duitschland Formation). However, the input was minor in the formation of the mineralization. Rather, the assimilation of crustal sulfur diluted the original PGE-rich sulfide melt, which had already reached sulfur saturation prior to the magma emplacement.

One possible reason to the near-zero $\delta^{34}S$ values observed in the Koillismaa intrusion may be the fact that most contact-type reefs, such as the Platreef, are associated with sedimentary country rocks whereas the Koillismaa intruded into Archean granitoid gneisses. To my knowledge, there are no sulfur isotope data available from the basement granitoid gneisses in the Koillismaa region. The Federova-Pansky intrusion basement rocks are also granite-gneisses, with $\delta^{34}S$ values ranging from -2.0 to -0.5‰ (Schissel et al. 2002), thus being noticeably lower than in the mineralized intrusion (−0.2 to +1.4 ‰). Furthermore, according to Schissel et al. (2002), the high S/Se ratios of 1000 - 5000 indicate magmatic sulfur. The same is observed at Overysel, where the footwall consists of granitoid gneiss; nearly all primary sulfides in the host rock (feldspathic pyroxenites) have $\delta^{34}S$ values below +2‰ (mean +1.8‰) and the $\delta^{34}S$ values of the footwall varies between +1.5 and +5‰ (Holwell et al. 2007).

The δ^{34S} data does not exclude the possibility that some hydrothermal processes or assimilation of the country rock occurred during or after the formation of the Marginal Series, as occurred in Duluth (Ripley 1981), East Bull Lake (Peck et al. 2001), Portimo (Iljina 1994), Platreef (Holwell et al. 2007; Smith et al. 2016), Lukkulaisvaara (Semenov et al. 2008), Federova-Pansky (Schissel et al. 2002) and Monchegorsk (Bekker et al. 2016). In fact, all these occurrences of contact-type mineralization show clear signs of crustal assimilation, containing xenoliths of country rocks, breccias, etc. However, whether crustal sulfur was involved in a primary or secondary phase (through metamorphism and hydrothermal activity, e.g., the Svecokarelian Orogeny), is not possible to confirm without $\delta^{34}S$ data from the country rocks. Nevertheless, the $\delta^{34}S$ signatures of both primary and secondary sulfides strongly suggest that that the sulfur is derived from the mantle.

As is common with Archean rocks, the country rocks may display mantle-like $\delta^{34}S$ signatures (Farquhar & Wing 2003; Ripley & Li 2003), as discussed in *Section 3.2-3.3*. If the country rocks were to display near-zero $\delta^{34}S$ values, the supposition of mantle-derived $\delta^{34}S$ signatures in the intrusion may be incorrect. This was the case with the Monchegorsk pluton, whose $\delta^{34}S$ has a magmatic signature. However, when analyzing the sulfides for multiple isotopes, it was discovered that there is a significant contribution of external sulfur (Bekker et al. 2016). Similarly, in the komatiite-hosted Ni-Cu-(PGE) Vaara deposit, south east of the Koillismaa intrusion, $\delta^{34}S$ data indicate a magmatic source though $\Delta^{33}S$ reveals significant assimilation of crustal sulfur (Konnunaho et al. 2013). The Vaara deposit, however, is not a layered intrusion and the country rocks contain metasediments, contrasting with the granitoids in the Koillismaa region. The closest comparable intrusion is the Portimo Complex, to the north-west of Koillismaa, where unpublished data of sulfides show near-zero $\Delta^{33}S$ values (S.H. Yang, pers. comm., 2018). This indicates a mantle origin for sulfur without any crustal sulfur contamination. As both the Portimo and Koillismaa intrusions are of the same age, formed during the same magmatic event and have the same type of Archean basement (i.e. the Tornio-Näränkävaara belt) (Iljina & Hanski 2005; Iljina et al. 2015), it is probable that the Koillismaa intrusion did not assimilate significant amounts of sulfur during crustal contamination.

In conclusion, based on the obtained $\delta^{34}S$ data, it is inferred that crustal sulfur played no significant role in the generation of the PGE mineralization of the Koillismaa intrusion. It is concluded that no external sulfur triggered sulfur saturation of the melt during the formation of the Marginal Series. Rather, sialic contamination by partial melting of the felsic basement may have caused sulfur saturation via lowering the sulfur solubility and precipitation of sulfide liquid. This has been suggested for the Noril'sk deposit, in Siberia (Barnes & Lightfoot 2005). Another possible cause of sulfur saturation could have been a change in oxygen fugacity, in response to assimilation of oxygen-rich rocks. However, because the basement is largely anhydrous, this process is deemed unlikely.

7.4 Genetic concepts

So far, I have addressed the fact that the PGE mineralization shows clear signs of hydrothermal fluids processes, and that the Svecofennian orogeny may have significantly altered both BMS and PGM assemblages. Subsequently, the primary mineralization processes related to the formation of the Koillismaa intrusion and the possible influence of hydrothermal fluids will be discussed.

The role of hydrothermal fluids

Hydrothermal fluids are most likely the cause of the heavily remobilized and altered sulfides in both mineralization types. The Svecofennian orogeny was proposed by Alapieti (1982) as the cause of the extensive displacement of the intrusion into the presently observed blocks of the complex. It is probable that fluids were present during a deformational event. I suggest this to be the main cause of the observed disseminated remobilized grains and retrograde alteration. This does, however, not exclude the fact that the sulfides could have been transported via deuteric fluids upon initial formation, in accordance with a metasomatic model (cf. *Section 2.6.2*). If a hydrothermal formation of the Rometölväs Reef is real, it is difficult to distinguish this from an orthomagmatic petrogenesis based

upon petrography, as secondary metamorphic events may have altered and remobilized the minerals.

Fluid and melt inclusions studies, as well in situ trace elements of primary and secondary sulfides could possibly distinguish between a primary hydrothermal origin and a late-stage secondary event that overprinted a primary orthomagmatic mineralization. The fact that the sulfides in the Rometölväs Reef are predominantly located in mottles, that also contain minerals of incompatible elements of the rocks, could be signs of the presence of a primary hydrothermal fluid. However, it could also simply be that they are just heavily altered due to the interstitial minerals being more prone to disintegration, and/or the fact that the sulfides could act as oxidation-catalysts. Conversely, this does not explain the mottle-textured mineralization associated with the microgabbronorites of the Rometölväs Reef and is therefore improbable. The presence of hydrothermal fluids is evident from the observed hydrosilicates and remobilized scattered sulfides. However, at what stage and to which extent fluids were present is difficult to interpret.

The role of noncumulus bodies

The presence of noncumulus bodies within layered intrusions, as in the Koillismaa intrusion, is also present in some of the Fennoscandian Shield intrusions. Noncumulus bodies like this have been reported in; the Monchegorsk intrusion (Sharkov & Smolkin 1998; Dedeev et al. 2002), the Akanvaara intrusion (Mutanen 1997), the Portimo Complex (Iljina 1994) and the Lukkulaisvaara intrusion (Glebovitsky et al. 2001; Latypov et al. 2008a; Latypov et al. 2008b). Some common characteristics of the bodies are that they occur mainly in noritic-gabbronoritic rocks. They are varied sized lenticular-ellipsoidal bodies and are observed both conformable as well as somewhat concordant in respect to the surrounding cumulate layering. The bodies contrast their surrounding cumulate rocks, in that they are fine-grained and more primitive, with higher MgO-, Cr- and An- content, while also having lower incompatible elements. Moreover, they are often zoned, grading from quenched margins to poikilitic interiors.

In both Koillismaa and Lukkulaisvaara, the noncumulus bodies are associated with PGE mineralization, and have been suggested to be preserved portions of later magma pulses (although the processes are controversial (Latypov et al. 2008a)). The bodies from both intrusions share many common features, such as; fine-grained textures indicative of supercooling, a distinct compositional contrast from the cumulate rocks, and the presence of irregular mottles of the cumulate rocks in close association with the bodies (Alapieti & Piirainen 1984; Glebovitsky et al. 2001; Iljina 2004; Latypov et al. 2008b; Latypov et al. 2008a; Karinen 2010).

Karinen (2010), suggested that the bodies of the Koillismaa intrusion were late magma injections that intruded laterally along a semi-consolidated magma chamber. He argued that the magma of the bodies was fluid-saturated upon entry and were formed related to supercooling from degassing induced crystallization, related to internal volatile loss (also proposed by Latypov et al. (2008a,b) for the Lukkulaisvaara intrusion) which would explain the textures and may provide PGE-rich fluids to the cumulate rocks. Karinen (2010) argued that because the presence of mottles and mineralization are directly linked to the microgabbronorites, the microgabbronorites must therefore be the source of PGE.

I suggest that the bodies were emplaced along the model proposed by Latypov et al. (2008a) for the Lukkulaisvaara intrusions; as horizontal sills into the cumulate pile, and due to volatile loss induced supercooling; the sills crystallized faster than the semi-consolidating cumulate pile, which caused dismembering of the sills into the now observed dispersed bodies. I suggest that the microgabbronorites are responsible for the formation of the mottled textures. Speculatively, the source could have been a lower stage magma chamber upgraded in PGE, similar to what was proposed by Cawthorn et al. (2005); Naldrett et al. (2009). However, to which extent the bodies sourced PGE is irresolute. If the microgabbronorites were formed due to volatile loss, these fluids would provide a good source for hydrothermal percolation of sulfides.

Karinen (2010) argued against an orthomagmatic model, saying that even though the Rometölväs Reef is at a compositional chemical contrast in the layered series, the metasomatic models are more likely. He reasoned that other reversal units below the reef would be more suitable for PGE reefs and that the presence of higher Cl values in apatites beneath the reef indicates percolation (among other things, cf. Karinen (2010)). It is possible that the microgabbronorites reached a natural horizon at the megacyclic unit that the Rometölväs Reef is situated at and thus, were unable to reach higher up in stratigraphy. Karinen (2010) argued that the cumulate rocks controlled the location of the fluid-saturation horizon during formation of the reef. However, since similar horizons have PGE reefs in both the Portimo Complex and the Penikat intrusion (Iljina et al. 2015). The argument that the chemical contrast is not suitable for an orthomagmatic reef is, in my opinion, invalid. Additionally, could these bodies provide enough ore and fluid source to allow percolation and formation of the whole reef?

Another hypothesis is that the reef could have formed along the model of Maier et al. (2016), with cumulate sulfide-mushes slumping, and the mottles observed in the Rometölväs could be signs of fluid percolation and not mineralization. It could be that that microgabbronorite bodies are nothing more than an oddity, that were responsible for the mottles and that the location of the reef is just a coincidence. After all, the microgabbronorites of the Portimo Complex are not believed to be responsible for the internal reef mineralization. However, I am not sure that I believe in

the coincidence that the microgabbronorites just happen to be positioned along a major PGE reef, without any genetic connection.

If percolation of fluids were responsible of the reef formation, as "hinted" by the Cl-rich apatites below the reef, and the mottle-associated mineralization. A "traditional" metasomatic model along the one of Godel et al. (2008), could also be plausible as a large amount of magma needs to be sourced, in order to form the reef. Still, many arguments against the metasomatic models persist (cf. *Section 2.6.2*). For example, it does not explain how a percolating fluid would form a horizontally homogenous reef, with a different underlying distance to the footwall.

In terms of the contact-type mineralization, no metasomatic models are considered, as the fluids would have no source of underlying cumulate rock to percolate and collect metals from. The contact-type is believed to have formed due to sialic contamination from the country rock, during emplacement. The signs of hydrothermal alteration, as is evident from the petrography, is instead thought to have formed solely during a later-stage metamorphic event, presumably the Svecofennian orogeny.

It is deemed unlikely that the microgabbronorites had the same type of influence over the Marginal Series as they did with the Rometölväs Reef. If deuteric fluids were involved they were probably only responsible for the petrogenesis of the Rometölväs Reef, this as the close relationship with microgabbronorites provide a possible fluid source.

8 Conclusions

The aim of this study was - besides giving a review of PGE mineralization in layered intrusions - to present new information of the Koillismaa intrusions Cu-Ni PGE mineralization in the layered- and marginal series, in order to try and elucidate the origin of PGE mineralization. The two main questions sought to be answered were:

1). Was external crustal sulfur involved in the formation of PGE sulfide mineralization?
2). Were hydrothermal processes involved during the formation of PGE mineralization?

The results of this study are listed below:

- The sulfide petrography is similar to other PGE-bearing intrusions of the Fennoscandian Shield. The sulfide assemblages of both the Marginal Series and the Rometölväs Reef consist of chalcopyrite, pyrrhotite, pentlandite, and minor additions of pyrite, and are solely disseminated in character. Most sulfides are heavily altered and display a speckled porous appearance, moreover, significant grain reduction and remobilization of sulfides are observed in all samples. Both primary and secondary remobilized sulfides are observed and remobilized sulfides are predominant in both mineralization types.
- Both mineralization types are distinctly associated with hydrosilicates. The primary sulfides of Rometölväs Reefs sulfides are commonly located in mottles, whereas the Marginal Series does not show a preference in sulfide textural relationship.
- The PGM assemblages in both the Marginal Series and the Rometölväs Reef are fairly identical, predominantly consisting of various Pt-Pd bismuthotellurides and Pt arsenides. The PGM were, in order of abundance 1. merenskyite-moncheite-melonite ($PdTe_2$-$PtTe_2$-$NiTe_2$), 2. sperrylite ($PtAs_2$), (3) kotulskite-sobolevskite-sudburyite (PdTe-PdBi-PdSb), and (4) keithconnite-telluropalladinite ($Pd_{3-x}Te$-Pd_9Te_4) in the Rometölväs Reef, and 1) merenskyite-moncheite-melonite, 2) sperrylite, (3) kotulskite-sobolevskite-sudburyite, and 4) PGE-alloy in the Marginal Series. This is similar to other coeval Fennoscandian PGE mineralizations, that are suggested to have formed in a low-temperature hydrothermal setting, but contrasts with many of the PGE occurrences among global layered intrusions which are dominated by PGM sulfides and Fe alloys.
- The dominant host-phase of the PGM are silicates, whereas sulfide-related grains are far less common. Also similar to other Fennoscandian PGE mineralizations, suggested to have formed in a hydrothermal setting.
- The $\delta^{34}S$ data obtained from the Rometölväs Reef and the Marginal Series for both primary and secondary sulfides, suggests that crustal sulfur played no role in the generation of the PGE mineralization of the Koillismaa intrusion. During the formation of the Marginal Series, sialic contamination by partial melting of the felsic basement may have caused sulfur saturation via lowering sulfur solubility and the precipitation of sulfide liquid. However, the $\delta^{34}S$ values of the country rock is currently unknown, and hence, contamination from an external sulfur source cannot be entirely excluded.
- The PGM assemblages and host phases are suggested to be generated by hydrothermal fluids, either in a late magmatic stage, and/or later-stage, during the Svecofennian orogeny.
- The Rometölväs Reef is suggested to have formed from a primary metasomatic event, in association with the microgabbronoritic bodies. On the other hand, the Marginal Series is suggested to have formed in an orthomagmatic setting due to sialic contamination triggering

sulfur saturation of the primary magma, during interaction with the footwall. Further implied by the xenolithic textures and contact melt, as well as the results of the sulfur isotope data presented in this study.

9 Further studies

- In-situ trace elements on BMS, as originally intended to be published in this study, could potentially elucidate the primary metasomatic influence of mineralization. While there have been no previous studies on the PGE trace elements in fluid process-related PGE deposits, the BMS should show different characteristics from an orthomagmatic signature. Presumably, BMS would display a lower PGE-content and different trace element patterns in a metasomatic setting. A mass-balance estimation based on previous bulk rock PGE data and new obtained in-situ analyses, would show how much PGE is hosted in BMS and PGM, respectively. This would help to separate a late-stage metamorphic event from the primary formation.
- Detailed petrographic studies of the relationship between the microgabbronorites and the cumulate rocks with focus on melting textures, coupled with fluid and melt inclusions would elucidate the fluid and melt composition.
- Sulfur isotopes of the country rock are needed to confidently rule out crustal sulfur during contact-type mineralization. Either the conventional ^{34}S or mass independent ^{33}S system.
- The observation of PGM and sulfides in hydrosilicates textures implies that hydrothermal fluids mobilized BMS and PGM. The composition of the fluid, and the source is unknown. Thus, fluid inclusions could possibly further explain the origin of mineralization.

10 Acknowledgements

I would like to thank Shenghong Yang at the University of Oulu, for supervision and for proposing this project. A special thank you to Tuomo Karinen, for providing sample material and acting as a field guide during my visit to the Koillismaa region. The facilities of the Finnish Geoscience Laboratory (SGL) in GTK, Espoo, and the help and support of Yann Lahaye, Hugh O'Brien and Marja Lehtonen. A special thank you to Eero Hanski at the University of Oulu, for additional supervision. Moreover, I would like to thank my supervisor Anders Scherstén at Lund University, for encouragement and supervision. Additionally, I would like to thank my examiner Ulf Söderlund of Lund University, for additional constructive feedback. Finally, a thank you to all my colleagues at the fifth floor for making this experience enjoyable.

This project was funded by the K.H. Renlund foundation.

11 References

Abzalov, M. Z. & Both, R. A., 1997: The Pechenga Ni-Cu deposits, Russia: Data on PGE and Au distribution and sulphur isotope compositions. Mineralogy and Petrology 61, 119-143.

Alapieti, T., 1982: The Koillismaa layered igneous complex, Finland : its structure, mineralogy and geochemistry, with emphasis on the distribution of chromium. Espoo : Geologinen tutkimuslaitos, 1982.

Alapieti, T., Hugg, R. & Piirainen, T., 1979: Structure, Mineralogy, and Chemistry of the Syöte Section in the Early Proterozoic Koillismaa Layered Intrusion, Northeastern Finland. Geologinen tutkimuslaitos.

Alapieti, T. & Lahtinen, J., 1986: Stratigraphy, petrology, and platinum-group element mineralization of the early Proterozoic Penikat layered intrusion, northern Finland. Economic Geology 81, 1126-1136.

Alapieti, T. & Piirainen, T., 1984: Cu-Ni-PGE mineralization in the marginal series of the early Proterozoic Koillismaa layered igneous complex, northeast Finland. Sulphide deposits in mafic and ultramafic rocks: proceedings of IGCP Projects 161, 123-131.

Alapieti, T. T., Filén, B. A., Lahtinen, J. J., Lavrov, M. M., Smolkin, V. F. & Voitsekhovsky, S. N., 1990: Early Proterozoic layered intrusions in the northeastern part of the Fennoscandian Shield. Mineralogy and Petrology 42, 1-22.

Alapieti, T. T. & Lahtinen, J. J., 2002: Platinum-group element mineralization in layered intrusions of northern Finland and the Kola Peninsula, Russia. the Geology, Geochemistry, Mineralogy and Mineral Beneficiation of Platinum-Group Elements, Edited by LJ Cabri. Canadian Institute of Mining, Metallurgy, and Petroleum, this volume, 507-546.

Alard, O., Griffin, W. L., Lorand, J. P., Jackson, S. E. & O'reilly, S. Y., 2000: Non-chondritic distribution of the highly siderophile elements in mantle sulphides. Nature 407, 891.

Allègre, C. J., 2008: Isotope Geology. Cambridge University Press.

Amelin, Y. V. & Semenov, V. S., 1996: Nd and Sr isotopic geochemistry of mafic layered intrusions in the eastern Baltic shield: implications for the evolution of Paleoproterozoic continental mafic magmas. Contributions to Mineralogy and Petrology 124, 255-272.

Armitage, P. E. B., Mcdonald, I., Edwards, S. J. & Manby, G. M., 2002: Platinum-group element mineralization in the Platreef and calc-silicate footwall at Sandsloot, Potgietersrus District, South Africa. Applied Earth Science 111, 36-45.

Augé, T., Cocherie, A., Genna, A., Armstrong, R., Guerrot, C., Mukherjee, M. M. & Patra, R. N., 2003: Age of the Baula PGE mineralization (Orissa, India) and its implications concerning the Singhbhum Archaean nucleus. Precambrian Research 121, 85-101.

Ballhaus, C. G. & Stumpfl, E. F., 1986: Sulfide and platinum mineralization in the Merensky Reef: evidence from hydrous silicates and fluid inclusions.

Contributions to Mineralogy and Petrology 94, 193-204.

Barnes, S., Osborne, G. A., Cook, D., Barnes, L., Maier, W. & Godel, B., 2011: The Santa Rita Nickel Sulfide Deposit in the Fazenda Mirabela Intrusion, Bahia, Brazil: Geology, Sulfide Geochemistry, and Genesis. Economic Geology 106, 183.

Barnes, S.-J., Cox, R. A. & Zientek, M., 2006: Platinum-group element, gold, silver and base metal distribution in compositionally zoned sulfide droplets from the Medvezky Creek Mine, Noril'sk, Russia. Contributions to Mineralogy

Petrology 152, 187-200.

Barnes, S.-J. & Lightfoot, P., 2005: Formation of Magmatic Nickel-Sulfide Ore Deposits and Processes Affecting Their Copper and Platinum-Group Element Contents. Economic Geology 100, 179-213.

Barnes, S.-J. & Maier, W. 2002a: Platinum-group element distributions in the Rustenburg Layered Suite of the Bushveld Complex, South Africa. In L. Cabri (ed.): The geology, geochemistry, mineralogy and mineral beneficiation of platinum-group elements, 431-458. Canadian Institute of Mining, Metallurgy and Petroleum.

Barnes, S.-J. & Maier, W. D., 1999: The fractionation of Ni, Cu and the noble metals in silicate and sulphide liquids. Short Course Notes-Geological Association of Canada 13, 69-106.

Barnes, S.-J. & Maier, W. D., 2002b: Platinum-group Elements and Microstructures of Normal Merensky Reef from Impala Platinum Mines, Bushveld Complex. Journal of Petrology 43, 103-128.

Barnes, S.-J., Melezhik, V. A. & Sokolov, S. V., 2001: The composition and mode of formation of the Pechenga nickel deposits, Kola Peninsula, northwestern Russia. The Canadian Mineralogist 39, 447-471.

Barnes, S.-J., Naldrett, A. J. & Gorton, M. P., 1985: The origin of the fractionation of platinum-group elements in terrestrial magmas. Chemical Geology 53, 303-323.

Barnes, S.-J., Savard, D., Bédard, L. P. & Maier, W., 2009: Selenium and sulfur concentrations in the Bushveld Complex of South Africa and implications for formation of the platinum-group element deposits. Mineralium Deposita 44, 647.

Barnes, S. J. & Liu, W., 2012: Pt and Pd mobility in hydrothermal fluids: Evidence from komatiites and from thermodynamic modelling. Ore Geology Reviews 44, 49-58.

Bayanova, T., Ludden, J. & Mitrofanov, F., 2009: Timing and duration of Palaeoproterozoic events producing ore-bearing layered intrusions of the Baltic Shield: metallogenic, petrological and geodynamic implications. Geological Society, London, Special Publications 323, 165-198.

Begg, G. C., Hronsky, J. A., Arndt, N. T., Griffin, W. L., O'reilly, S. Y. & Hayward, N., 2010a: Lithospheric, cratonic, and geodynamic setting of Ni-Cu-PGE sulfide deposits. Economic Geology 105, 1057-1070.

Begg, G. C., Hronsky, J. a. M., Arndt, N. T., Griffin, W. L., O'reilly, S. Y. & Hayward, N., 2010b: Lithospheric, Cratonic, and Geodynamic Setting of Ni-Cu-PGE Sulfide Deposits. Economic Geology 105, 1057-1070.

Bekker, A., Grokhovskaya, T. L., Hiebert, R., Sharkov, E. V., Bui, T. H., Stadnek, K. R., Chashchin, V. V. & Wing, B. A., 2016: Multiple sulfur isotope and mineralogical constraints on the genesis of Ni-Cu-PGE magmatic sulfide mineralization of the Monchegorsk Igneous Complex, Kola Peninsula, Russia. Mineralium Deposita 51, 1035-1053.

Bekker, A., Holland, H., Wang, P.-L., Rumble Iii, D., Stein, H., Hannah, J., Coetzee, L. & Beukes, N., 2004: Dating the rise of atmospheric oxygen. Nature 427, 117.

Bockrath, C., Ballhaus, C. & Holzheid, A., 2004: Fractionation of the Platinum-Group Elements During Mantle Melting. Science 305, 1951.

Boudreau, A. & Mccallum, I., 1986: Investigations of the Stillwater Complex; III, The Picket Pin Pt/Pd deposit. Economic Geology 81, 1953-1975.

Boudreau, A. & Mccallum, I., 1992: Concentration of platinum-group elements by magmatic fluids in layered intrusions. Economic Geology 87, 1830-1848.

Boudreau, A. E., 1994: Mineral segregation during crystal aging in two-crystal, two-component systems. South African Journal of Geology 97, 473-485.

Boudreau, A. E., 2008: Modeling the Merensky Reef, Bushveld Complex, Republic of South Africa. Contributions to Mineralogy and Petrology 156, 431-437.

Brenan, J. M. & Andrews, D., 2001: High-temperature stability of laurite and Ru–Os–Ir alloy and their role in PGE fractionation in mafic magmas. The Canadian Mineralogist 39, 341-360.

Brooks, C. K. & Gleadow, A. J. W., 1977: A fission-track age for the Skaergaard intrusion and the age of the East Greenland basalts. Geology 5, 539-540.

Brownscombe, W., Herrington, R., Wilkinson, J., J Berry, A., Coppard, J., Ihlenfeld, C., Klatt, S., Hartshorne, C., Boyce, A. & Taylor, R. 2013: Geochemistry of the Sakatti magmatic Cu-Ni-PGE deposit, northern Finland. In Proceedings of the 12th Biennial SGA Meeting on Mineral Deposit Research for a High-Tech World, 12-15.

Buchanan, D., Nolan, J., Suddaby, P., Rouse, J., Viljoen, M. & Davenport, J., 1981: The genesis of sulfide mineralization in a portion of the Potgietersrus Limb of the Bushveld Complex. Economic Geology 76, 568-579.

Butler, J., 2012: Platinum 2012. Royston, Hertfordshire, England. 60 pp.

Cabri, L., 1992: The Distribution of Trace Precious Metals in Minerals and Mineral Products. Mineralogical Magazine 56:3, 289-308.

Cabri, L., 2002: The platinum-group minerals. The geology, geochemistry, mineralogy and mineral beneficiation of platinum-group elements. 13-129 pp.

Campbell, I. H. & Naldrett, A. J., 1979: The in-

fluence of silicate:sulfide ratios on the geochemistry of magmatic sulfides. Economic Geology 74, 1503-1506.

Campbell, I. H., Naldrett, A. J. & Barnes, S. J., 1983: A Model for the Origin of the Platinum-Rich Sulfide Horizons in the Bushveld and Stillwater Complexes. Journal of Petrology 24, 133-165.

Canfield, D., 2001: Biogeochemistry of sulfur isotopes. Reviews in Mineralogy

Geochemistry 43, 607-636.

Capobianco, C. J. & Drake, M. J., 1990: Partitioning of ruthenium, rhodium, and palladium between spinel and silicate melt and implications for platinum group element fractionation trends. Geochimica et Cosmochimica Acta 54, 869-874.

Cawthorn, R., Barnes, S., Ballhaus, C. & Malitch, K., 2005: Platinum group element, chromium and vanadium deposits in mafic and ultramafic rocks. Platinum group element, chromium and vanadium deposits in mafic and ultramafic rocks 100th Anniversary Volume, 215-249.

Cawthorn, R. G., Lee, C. A., Schouwstra, R. P. & Mellowship, P., 2002: Relationship between PGE and PGM in the Bushveld Complex. The Canadian Mineralogist 40, 311-328.

Coghill, M. B. & Wilson, A., 1993: Platinum-Group Minerals in the Selukwe Subchamber, Great Dyke, Zimbabwe: Implications for PGE Collection Mechanisms and Post-Formational Redistribution. Mineralogical Magazine 57, 613-633.

Craig, J. R., Vaughan, D. J. & Hagni, R. D., 1981: Ore microscopy and ore petrography. Wiley New York.

Crocket, J. H., 2002: Platinum-group element geochemistry of mafic and ultramafic rocks. Canadian Institute of Mining, Metallurgy and Petroleum 54, 177 -210.

Davey, S., Bleeker, W., Kamo, S., Ernst, R. & Cousens, B., 2018: Trace element geochemistry and Sm-Nd isotopes of 2.1 ga mafic magmatism in the Karelia-Kola, Wyoming and Superior cratons. Nordic Geoscience Winter Meeting Copenhagen, Demark.

Dedeev, A., Khashkovskaya, T. & Galkin, A., 2002: PGE mineralization of the Monchegorsk layered mafic–ultramafic intrusion of the Kola Peninsula. The geology, geochemistry, mineralogy

mineral beneficiation of platinum-group elements. Canadian Institute of Mining 54, 569-577.

Ding, T., Valkiers, S., Kipphardt, H., De Bièvre, P., Taylor, P. D. P., Gonfiantini, R. & Krouse, R., 2001: Calibrated sulfur isotope abundance ratios of three IAEA sulfur isotope reference materials and V-CDT with a reassessment of the atomic weight of sulfur. Geochimica et Cosmochimica Acta 65, 2433-2437.

Ding, X., Ripley, E. & Li, C., 2009: Multiple S Isotopic Study of the Eagle Ni-Cu-PGE magmatic Deposit, Northern Michigan, USA. AGU Fall Meeting Abstracts.

Easton, R., Jobin-Bevans, L. S. & James, R. S., 2010: Geological Guidebook to the Paleoproterozoic East Bull Lake Intrusive Suite Plutons at East Bull Lake, Agnew Lake and River Valley, Ontario: A Field Trip for the 11th International Platinum Symposium. Ontario Geological Survey.

Ebel, D. & Naldrett, A., 1996: Fractional crystallization of sulfide ore liquids at high temperature. Economic Geology 91, 607-621.

Enkovaara, A., Härme, M. & Väyrynen, H., 1953: Bedrock map of Oulu and Tornio areas. Geological map of Finland 1: 400 000. Geological Survey of Finland, Helsinki.

Farquhar, J., Bao, H. & Thiemens, M., 2000: Atmospheric influence of Earth's earliest sulfur cycle. Science 289, 756-758.

Farquhar, J. & Wing, B. A., 2003: Multiple sulfur isotopes and the evolution of the atmosphere. Earth and Planetary Science Letters 213, 1-13.

Finnigan, C. S., Brenan, J. M., Mungall, J. E. & Mcdonough, W., 2008: Experiments and models bearing on the role of chromite as a collector of platinum group minerals by local reduction. Journal of Petrology 49, 1647-1665.

Fonseca, R. O. C., Campbell, I. H., O'neill, H. S. C. & Allen, C. M., 2009: Solubility of Pt in sulphide mattes: Implications for the genesis of PGE-rich horizons in layered intrusions. Geochimica et Cosmochimica Acta 73, 5764-5777.

Garuti, G. & Rinaldi, R., 1986: Mineralogy of melonite-group and other tellurides from the Ivrea-Verbano basic complex, western Italian Alps. Economic Geology 81, 1213-1217.

Gervilla, F. & Kojonen, K., 2002: The platinum-group minerals in the upper section of the Keivitsansarvi Ni–Cu–PGE deposit, northern Finland. The Canadian Mineralogist 40, 377-394.

Gilbert, S. E., Danyushevsky, L. V., Rodemann, T., Shimizu, N., Gurenko, A., Meffre, S., Thomas, H., Large, R. R. & Death, D., 2014: Optimisation of laser parameters for the analysis of sulphur isotopes in sulphide minerals by laser ablation ICP-MS. Journal of Analytical Atomic Spectrometry 29, 1042-1051.

Glebovitsky, V. A., Semenov, V. S., Belyatsky, B. V., Koptev-Dvornikov, E. V., Pchelintseva, N. F., Kireev, B. S. & Koltsov, A. B., 2001: The Structure of the Lukkulaisvaara Intrusion, Oulanka Group, Northern Karelia: Petrological Implications. The Canadian Mineralogist 39, 607-637.

Godel, B. 2015: Platinum-group element deposits in layered intrusions: recent advances in the understanding of the ore forming processes. In Layered Intrusions, 379-432. Springer.

Godel, B. & Barnes, S.-J., 2008: Image analysis and composition of platinum-group minerals in the JM Reef, Stillwater Complex. Economic Geology 103, 637-651.

Godel, B., Barnes, S.-J. & Maier, W., 2006: 3-D Distribution of Sulphide Minerals in the Merensky Reef (Bushveld Complex, South Africa) and the J-M Reef (Stillwater Complex, USA) and their Relationship to Microstructures Using X-Ray Computed Tomo-

graphy. Journal of Petrology 47, 1853-1872.

Godel, B., Barnes, S.-J. & Maier, W., 2007: Platinum-Group Elements in Sulphide Minerals, Platinum-Group Minerals, and Whole-Rocks of the Merensky Reef (Bushveld Complex, South Africa): Implications for the Formation of the Reef. Journal of Petrology 48.

Godel, B., Maier, W. & Barnes, S.-J., 2008: Platinum-Group Elements in the Merensky and J-M Reefs: A Review of Recent Studies. Geological Society of India 72, 595-608.

Goldhaber, M. & Kaplan, I., 1975: Controls and consequences of sulfate reduction rates in recent marine sediments. Soil Science 119, 42-55.

Grinenko, L., 1985: Sources of sulfur of the nickeliferous and barren gabbro-dolerite intrusions of the northwest Siberian platform. International Geology Review 27, 695-708.

Groves, D. I., Ho, S. E., Rock, N. M., Barley, M. E. & Muggeridge, M. T., 1987: Archean cratons, diamond and platinum: Evidence for coupled long-lived crust-mantle systems. Geology 15, 801-805.

Groves, D. I., Vielreicher, R. M., Goldfarb, R. J. & Condie, K. C., 2005: Controls on the heterogeneous distribution of mineral deposits through time. Geological Society, London, Special Publications 248, 71-101.

Hamlyn, P. R. & Keays, R., 1986: Sulfur saturation and second-stage melts; application to the Bushveld platinum metal deposits. Economic Geology 81, 1431-1445.

Hanley, J. J., 2005: The aqueous geochemistry of the platinum-group elements (PGE) in surficial, low-T hydrothermal and high-T magmatic-hydrothermal environments. Exploration for Platinum-group element deposits 35, 35-56.

Hanski, E. 2015: Synthesis of the Geological Evolution and Metallogeny of Finland In R. Lahtinen & H. O'Brien (eds.): Mineral Deposits of Finland, 39-71. Elsevier.

Hanski, E., Huhma, H., Smolkin, V. F. & Vaasjoki, M., 1990: The age of the ferropicritic volcanics and comagmatic Ni-bearing intrusions at Pechenga, Kola Peninsula, USSR. Bull. Geol. Soc. Finland 62, 123-133.

Hanski, E., Walker, R. J., Huhma, H. & Suominen, I., 2001: The Os and Nd isotopic systematics of c. 2.44 Ga Akanvaara and Koitelainen mafic layered intrusions in northern Finland. Precambrian Research 109, 73-102.

Harmer, R. E. & Sharpe, M. R., 1985: Field relations and strontium isotope systematics of the marginal rocks of the eastern Bushveld Complex. Economic Geology 80, 813-837.

Helmy, H. M., 2005: Melonite group minerals and other tellurides from three Cu–Ni–PGE prospects, Eastern Desert, Egypt. Ore Geology Reviews 26, 305-324.

Helmy, H. M., Ballhaus, C., Berndt, J., Bockrath, C. & Wohlgemuth-Ueberwasser, C., 2007: Formation of Pt, Pd and Ni tellurides: experiments in sulfide–telluride systems. Contributions to Mineralogy and Petrology 153, 577-591.

Hiemstra, S. A., 1979: The role of collectors in the formation of the platinum deposits in the Bushveld Complex. Canadian Mineralogist 17, 469-482.

Holwell, D. A., Boyce, A. J. & Mcdonald, I., 2007: Sulfur Isotope Variations within the Platreef Ni-Cu-PGE Deposit: Genetic Implications for the Origin of Sulfide Mineralization. Economic Geology 102, 1091-1110.

Holwell, D. A., Boyce, A. J. & Mcdonald, I., 2008: Sulfur Isotope Variations within the Platreef Ni-Cu-PGE Deposit: Genetic Implications for the Origin of Sulfide Mineralization. Economic Geology 102, 1091.

Holwell, D. A. & Keays, R. R., 2014: The formation of low-volume, high-tenor magmatic PGE-Au sulfide mineralization in closed systems: evidence from precious and base metal geochemistry of the Platinova Reef, Skaergaard Intrusion, East Greenland. Economic Geology 109, 387-406.

Holwell, D. A. & Mcdonald, I., 2006: Petrology, geochemistry and the mechanisms determining the distribution of platinum-group element and base metal sulphide mineralisation in the Platreef at Overysel, northern Bushveld Complex, South Africa. Mineralium Deposita 41, 575.

Holwell, D. A. & Mcdonald, I., 2007: Distribution of platinum-group elements in the Platreef at Overysel, northern Bushveld Complex: a combined PGM and LA-ICP-MS study. Contributions to Mineralogy and Petrology 154, 171-190.

Holwell, D. A., Mcdonald, I. & Armitage, P., 2006: Platinum-group mineral assemblages in the Platreef at the Sandsloot Mine, northern Bushveld Complex, South Africa. Mineralogical Magazine 70, 83-101.

Huhma, H., Cliff, R. A., Perttunen, V. & Sakko, M., 1990: Sm−Nd and Pb isotopic study of mafic rocks associated with early Proterozoic continental rifting: the Peröpohja schist belt in northern Finland. Contributions to Mineralogy and Petrology 104, 369-379.

Huhma, H., Mänttäri, I., Peltonen, P., Kontinen, A., Halkoaho, T., Hanski, E., Hokkanen, T., Hölttä, P., Juopperi, H. & Konnunaho, J., 2012: The age of the Archaean greenstone belts in Finland. Geological Survey of Finland, Special Paper 54, 74-175.

Huhma, H., O'brien, H., Lahaye, Y. & Mänttäri, I. 2011: Isotope geology and Fennoscandian lithosphere evolution. In Geoscience for Society: 125th Anniversary Volume, 35-48.

Hulston, J. R. & Thode, H. G., 1965a: Cosmic-ray-produced S36 and S33 in the metallic phase of iron meteorites. Journal of Geophysical Research 70, 4435-4442.

Hulston, J. R. & Thode, H. G., 1965b: Variations in the S33, S34, and S36 contents of meteorites and their relation to chemical and nuclear effects. Journal of Geophysical Research 70, 3475-3484.

Iljina, M., 1994: The Portimo layered igneous complex: with emphasis on diverse sulphide and platinum-

group element deposits. University of Oulu Oulu, Finland.

Iljina, M., 2004: Tutkimustyöselostus valtausalueilla Koskiaho 1-2, Kuusi 4-23, Maaselkä 1-14, Murto 1-2 sekä Portti 1-37 Pudasjärven, Taivalkosken ja Posion kunnissa suoritetusta tutkimuksesta vuosina 1996-2002 - Mineral exploration report of relinquished claims of Koskiaho 1-2, Kuusi 4-23, Maaselkä 1-14, Murto 1-2 and Portti 1-37. 25 pp.

Iljina, M., Duke, C. & Hinzer, J., 2012: A Technical Review of the Läntinen Koillismaa Project. Finland for Finore Mining Inc NI 43–101 Technical Report.

Iljina, M. & Hanski, E. 2005: Layered mafic intrusions of the Tornio—Näränkävaara belt. In M. J. Lehtinen, P. A. Nurmi & O. T. Rämö (eds.): Precambrian Geology of Finland Key to the Evolution of the Fennoscandian Shield, 101-137.

Iljina, M., Heikura, P. & Salmirinne, H., 2005: The Haukiaho and Kaukua PGE-Cu-Ni-Au prospects in the Koillismaa Layered Igneous Complex, Finland.

Iljina, M., Karinen, T. & E. Räsänen, J., 2001: The Koillismaa Layered Igneous Complex, general geology, structural development and related sulphide and platinum-group element mineralization.

Iljina, M., Maier, W. D. & Karinen, T. 2015: PGE-(Cu-Ni) Deposits of the Tornio-Näränkävaara Belt of Intrusions (Portimo, Penikat, and Koillismaa). In Mineral Deposits of Finland, 133-164. Elsevier.

Iljina, M. J. & Lee, C. A. 2005: PGE deposits in the marginal series of layered intrusions. In Exploration for platinum group element deposits, 75-96.

Irvine, T. 1976: Crystallization sequences in the Muskox intrusion and other layered intrusions—II. Origin of chromitite layers and similar deposits of other magmatic ores. In Chromium: its Physicochemical Behavior and Petrologic Significance, 991-1020. Elsevier.

James, R., Jobin-Bevans, S., Easton, R., Wood, P., Hrominchuk, J., Keays, R. & Peck, D., 2002: Platinum -group element mineralization in Paleoproterozoic basic intrusions in central and Northeastern Ontario, Canada. The geology, geochemistry, mineralogy and mineral beneficiation of platinum-group elements. Canadian Institute of Mining, Metallurgy and Petroleum, Spec 54, 339-365.

Jenner, F. E., O'neill, H. S. T. C., Arculus, R. J. & Mavrogenes, J. A., 2010: The Magnetite Crisis in the Evolution of Arc-related Magmas and the Initial Concentration of Au, Ag and Cu. Journal of Petrology 51, 2445-2464.

Johnston, D. T., 2011: Multiple sulfur isotopes and the evolution of Earth's surface sulfur cycle. Earth-Science Reviews 106, 161-183.

Karinen, T., 1998: Posion Kuusijärven alueen stratigrafia ja rakennegeologia. Pro gradu-tutkielma. Oulun yliopisto, geotieteiden laitos 8.

Karinen, T., 2010: The Koillismaa Intrusion, Northeastern Finland: Evidence for the PGE Reef Forming Processes in the Layered Series. Geological Survey of Finland.

Karinen, T. & Iljina, M., 2009: Structural history of the western part of the Koillismaa Layered Igneous Complex.

Karykowski, B. T., Maier, W. D., Groshev, N. Y., Barnes, S.-J., Pripachkin, P. V., Mcdonald, I. & Savard, D., 2018: Critical Controls on the Formation of Contact-Style PGE-Ni-Cu Mineralization: Evidence from the Paleoproterozoic Monchegorsk Complex, Kola Region, Russia. Economic Geology 113, 911-935.

Kerr, A. & Leitch, A. M., 2005: Self-Destructive Sulfide Segregation Systems and the Formation of High-Grade Magmatic Ore Deposits. Economic Geology 100, 311-332.

Kojonen, K. & Iljina, M., 2001: Platinum-Group Minerals in the Early Proterozoic Kuusijärvi Marginal Series, Koillismaa Layered Igneous Complex, Northeastern Finland.

Konnunaho, J., Halkoaho, T., Hanski, E. & Törmänen, T. 2015: Komatiite-Hosted Ni-Cu-PGE Deposits in Finland. In R. Lahtinen & H. O'Brien (eds.): Mineral Deposits of Finland, 93-131. Elsevier.

Konnunaho, J., Hanski, E., Bekker, A., Halkoaho, T., Hiebert, R. & Wing, B., 2013: The Archean komatiite-hosted, PGE-bearing Ni–Cu sulfide deposit at Vaara, eastern Finland: evidence for assimilation of external sulfur and post-depositional desulfurization. Mineralium Deposita 48, 967-989.

Kruger, F. J., Kinnaird, J. A., Nex, P. A. & Cawthorn, R. G., 2002: Chromite is the key to PGE. 9th International Platinum Symposium. Abstract and Program. 21-25 pp.

Kuivasaari, T., Torppa, A., ÄIkäS, O. & Eilu, P. 2012: Otanmäki V-Ti-Fe. In P. Eilu (ed.): Mineral Deposits and Metallogeny of Fennoscandia, 272–275. Geological Survey of Finland.

Kullerud, G., 1969: Phase relations in the Cu-Fe-S, Cu-Ni-S and Fe-Ni-S system. Magmatic ore deposits, 323-343.

Lahtinen, J., 1985: PGE-bearing copper-nickel occurrences in the marginal series of the Early Proterozoic Koillismaa layered intrusion, northern Finland. Nickel-copper deposits of the Baltic Shield Scandinavian Caledonides. Geological Survey of Finland. Bulletin 333, 161-178.

Lambert, D. D., Foster, J. G., Frick, L. R., Ripley, E. M. & Zientek, M., 1998: Geodynamics of magmatic Cu-Ni-PGE sulfide deposits; new insights from the Re -Os isotope system. Economic Geology 93, 121-136.

Latypov, R., Chistyakova, S. Y. & Alapieti, T., 2008a: Fine-grained mafic bodies as preserved portions of magma replenishing layered intrusions: the Nadezhda gabbronorite body, Lukkulaisvaara intrusion, Fennoscandian Shield, Russia. Mineralogy and Petrology 92, 165-209.

Latypov, R., Chistyakova, S. Y. & Alapieti, T., 2008b: PGE reefs as an in situ crystallization phenomenon: the Nadezhda gabbronorite body, Lukkulaisvaara layered intrusion, Fennoscandian Shield,

Russia. Mineralogy and Petrology 92, 211-242.

Lauri, L., 2004: Petrogenesis of felsic igneous rocks associated with the Paleoproterozoic Koillismaa layered igneous complex, Finland.

Lee, C. 1996: A review of mineralization in the Bushveld Complex and some other layered intrusions. In Developments in Petrology, 103-145. Elsevier.

Li, C., Ripley, E., Maier, W. & Gomwe, T., 2002a: Olivine and sulfur isotopic compositions of the Uitkomst Ni–Cu sulfide ore-bearing complex, South Africa: evidence for sulfur contamination and multiple magma emplacements. Chemical Geology 188, 149-159.

Li, C. & Ripley, E. M., 2005: Empirical equations to predict the sulfur content of mafic magmas at sulfide saturation and applications to magmatic sulfide deposits. Mineralium Deposita 40, 218-230.

Li, C., Ripley, E. M., Maier, W. D. & Gomwe, T. E. S., 2002b: Olivine and sulfur isotopic compositions of the Uitkomst Ni–Cu sulfide ore-bearing complex, South Africa: evidence for sulfur contamination and multiple magma emplacements. Chemical Geology 188, 149-159.

Li, C., Ripley, E. M. & Naldrett, A. J., 2003: Compositional variations of olivine and sulfur isotopes in the Noril'sk and Talnakh intrusions, Siberia: implications for ore-forming processes in dynamic magma conduits. Economic Geology 98, 69-86.

Li, C., Ripley, E. M., Oberthür, T., Miller, J. D. & Joslin, G. D., 2008a: Textural, mineralogical and stable isotope studies of hydrothermal alteration in the main sulfide zone of the Great Dyke, Zimbabwe and the precious metals zone of the Sonju Lake Intrusion, Minnesota, USA. Mineralium Deposita 43, 97-110.

Li, Z. X., Bogdanova, S. V., Collins, A. S., Davidson, A., De Waele, B., Ernst, R. E., Fitzsimons, I. C. W., Fuck, R. A., Gladkochub, D. P., Jacobs, J., Karlstrom, K. E., Lu, S., Natapov, L. M., Pease, V., Pisarevsky, S. A., Thrane, K. & Vernikovsky, V., 2008b: Assembly, configuration, and break-up history of Rodinia: A synthesis. Precambrian Research 160, 179-210.

Lightfoot, P., Naldrett, A. & Hawkesworth, C., 1984: The geology and geochemistry of the Waterfall Gorge section of the Insizwa Complex with particular reference to the origin of the nickel sulfide deposits. Economic Geology 79, 1857-1879.

Locmelis, M., Melcher, F. & Oberthür, T., 2010: Platinum-group element distribution in the oxidized main sulfide zone, Great Dyke, Zimbabwe. Mineralium Deposita 45, 93-109.

Lorand, J.-P. & Alard, O., 2001: Platinum-group element abundances in the upper mantle: new constraints from in situ and whole-rock analyses of Massif Central xenoliths (France). Geochimica et Cosmochimica Acta 65, 2789-2806.

Lorand, J.-P., Luguet, A., Alard, O., Bezos, A. & Meisel, T., 2008a: Abundance and distribution of platinum-group elements in orogenic lherzolites; a case study in a Fontete Rouge lherzolite (French Pyrénées). Chemical Geology 248, 174-194.

Lorand, J. P., Luguet, A. & Alard, O., 2008b: Platinum-Group Elements: A New Set of Key Tracers for the Earth's Interior. Elements 4, 247-252.

Luolavirta, K., Hanski, E., Maier, W., Lahaye, Y., O'brien, H. & Santaguida, F., 2018: In situ strontium and sulfur isotope investigation of the Ni-Cu-(PGE) sulfide ore-bearing Kevitsa intrusion, northern Finland. Mineralium Deposita.

Macnamara, J. & Thode, H. G., 1950: Comparison of the Isotopic Constitution of Terrestrial and Meteoritic Sulfur. Physical Review 78, 307-308.

Maier, W. D., 2005: Platinum-group element (PGE) deposits and occurrences: Mineralization styles, genetic concepts, and exploration criteria. Journal of African Earth Sciences 41, 165-191.

Maier, W. D. 2015: Geology and Petrogenesis of Magmatic Ni-Cu-PGE-Cr-V Deposits: An Introduction and Overview. In Mineral Deposits of Finland, 73-92. Elsevier.

Maier, W. D. & Barnes, S.-J., 1999: Platinum-group elements in silicate rocks of the lower, critical and main zones at Union Section, western Bushveld Complex. Journal of Petrology 40, 1647-1671.

Maier, W. D. & Barnes, S.-J., 2003: Platinum-group elements in the Boulder Bed, western Bushveld Complex, South Africa. Mineralium Deposita 38, 370-380.

Maier, W. D., Barnes, S.-J., Gartz, V. & Andrews, G., 2003: Pt-Pd reefs in magnetitites of the Stella layered intrusion, South Africa: A world of new exploration opportunities for platinum group elements. Geology 31, 885-888.

Maier, W. D., Barnes, S.-J. & Groves, D. I., 2013: The Bushveld Complex, South Africa: formation of platinum–palladium, chrome- and vanadium-rich layers via hydrodynamic sorting of a mobilized cumulate slurry in a large, relatively slowly cooling, subsiding magma chamber. Mineralium Deposita 48, 1-56.

Maier, W. D., Barnes, S.-J., Sarkar, A., Ripley, E., Li, C. & Livesey, T., 2010: The Kabanga Ni sulfide deposit, Tanzania: I. Geology, petrography, silicate rock geochemistry, and sulfur and oxygen isotopes. Mineralium Deposita 45, 419-441.

Maier, W. D. & Groves, D. I., 2011: Temporal and spatial controls on the formation of magmatic PGE and Ni–Cu deposits. Mineralium Deposita 46, 841-857.

Maier, W. D., Halkoaho, T., Huhma, H., Hanski, E. & Barnes, S. J., 2018: The Penikat Intrusion, Finland: Geochemistry, Geochronology, and Origin of Platinum –Palladium Reefs. Journal of Petrology 59, 967-1006.

Maier, W. D., Karykowski, B. T. & Yang, S.-H., 2016: Formation of transgressive anorthosite seams in the Bushveld Complex via tectonically induced mobilisation of plagioclase-rich crystal mushes. Geoscience Frontiers 7, 875-889.

Maier, W. D., Määttää, S., Yang, S., Oberthür, T., Lahaye, Y., Huhma, H. & Barnes, S. J., 2015: Composition of the ultramafic–mafic contact interval of the

Great Dyke of Zimbabwe at Ngezi mine: Comparisons to the Bushveld Complex and implications for the origin of the PGE reefs. Lithos 238, 207-222.

Mavrogenes, J. A. & O'neill, H. S. C., 1999: The relative effects of pressure, temperature and oxygen fugacity on the solubility of sulfide in mafic magmas. Geochimica et Cosmochimica Acta 63, 1173-1180.

Mcclay, K. R. & Campbell, I. H., 2009: The structure and shape of the Jimberlana Intrusion, Western Australia, as indicated by an investigation of the Bronzite Complex. Geological Magazine 113, 129-139.

Mcdonough, W. F. & Sun, S. S., 1995: The composition of the Earth. Chemical Geology 120, 223-253.

Mitrofanov, F., Митрофанов, Ф. П., Малич, К. Н., Баянова, Т. Б., Корчагин, А. У. & Жиров, Д. В., 2012: Comparison of East-Scandinavian and Norilsk large plume mafic igneous provinces of PGE ores. Вестник Мурманского государственного технического университета 15.

Mungall, J., 2013: Geochemistry of Magmatic Ore Deposits. 195-218 pp.

Mungall, J. E., 2002: Kinetic Controls on the Partitioning of Trace Elements Between Silicate and Sulfide Liquids. Journal of Petrology 43, 749-768.

Mungall, J. E. 2014: Geochemistry of Magmatic Ore Deposits In K. K. Turekian (ed.): Treatise on Geochemistry (Second Edition), 195-218. Elsevier.

Mungall, J. E. & Naldrett, A., 2008: Ore deposits of the platinum-group elements. Elements 4, 253-258.

Mutanen, T., 1997: Geology and ore petrology of the Akanvaara and Koitelainen mafic layered intrusions and the Keivitsa-Satovaara layered complex, northern Finland. Geological Survey of Finland.

Mutanen, T. & Huhma, H., 2001: U-Pb geochronology of the Koitelainen, Akanvaara and Keivitsa layered intrusions and related rocks. Special Paper-Geological Survey of Finland, 229-246.

Müller, W., Shelley, M., Miller, P. & Broude, S., 2009: Initial performance metrics of a new custom-designed ArF Excimer LA-ICP-MS system coupled to a two-volume laser-ablation cell. Journal of Analytical Atomic Spectrometry 24, 209-214.

Naldrett, A., 2010: Secular Variation of Magmatic Sulfide Deposits and Their Source Magmas. Economic Geology 105, 669-688.

Naldrett, A. & Lehmann, J. 1988: Spinel non-stoichiometry as the explanation for Ni-, Cu-and PGE-enriched sulphides in chromitites. In Geo-platinum 87, 93-109. Springer.

Naldrett, A. J., 2004: Magmatic Sulfide Deposits: Geology, Geochemistry and Exploration. Springer.

Naldrett, A. J., Gasparrini, E. C., Barnes, S., Von Gruenewaldt, G. & R. Sharpe, M., 1986: The upper critical zone of the Bushveld Complex and the origin of merensky-type ores. Economic Geology 81, 1105-1117.

Naldrett, A. J. & Von Gruenewaldt, G., 1989: Association of platinum-group elements with chromitite in layered intrusions and ophiolite complexes. Economic Geology 84, 180-187.

Naldrett, A. J., Wilson, A., Kinnaird, J. & Chunnett, G., 2009: PGE Tenor and Metal Ratios within and below the Merensky Reef, Bushveld Complex: Implications for its Genesis. Journal of Petrology 50, 625-659.

O'driscoll, B. & González-Jiménez, J., 2016: Petrogenesis of the Platinum-Group Minerals. 489-578 pp.

Osbahr, I., 2012: Platinum-group element distribution in base-metal sulfides of the Merensky Reef and UG2 from the eastern and western Bushveld Complex, South Africa. Mineralium Deposita.

Osbahr, I., Klemd, R., Oberthür, T., Brätz, H. & Schouwstra, R., 2013: Platinum-group element distribution in base-metal sulfides of the Merensky Reef from the eastern and western Bushveld Complex, South Africa. Mineralium Deposita 48, 211-232.

Osbahr, I., Krause, J., Bachmann, K. & Gutzmer, J., 2015: Efficient and Accurate Identification of Platinum-Group Minerals by a Combination of Mineral Liberation and Electron Probe Microanalysis with a New Approach to the Offline Overlap Correction of Platinum-Group Element Concentrations. Microscopy and Microanalysis 21, 1080-1095.

Pagé, P., Barnes, S.-J., Bédard, J. H. & Zientek, M. L., 2012: In situ determination of Os, Ir, and Ru in chromites formed from komatiite, tholeiite and boninite magmas: implications for chromite control of Os, Ir and Ru during partial melting and crystal fractionation. Chemical Geology 302, 3-15.

Park, Y. R., Ripley, E. M., Miller Jr, J. D., Li, C., Mariga, J. & Shafer, P., 2004: Stable isotopic constraints on fluid-rock interaction and Cu-PGE-S redistribution in the Sonju Lake intrusion, Minnesota. Economic Geology 99, 325-338.

Pearson, G., Irvine, G. J., Ionov, D., Boyd, F. R. & Dreibus, G. E., 2004: Re-Os isotope systematics and platinum group element fractionation during mantle melt extraction: a study of massif and xenolith peridotite suites. Chemical Geology 208, 29-59.

Peck, D. C., Keays, R. R., James, R. S., Chubb, P. T. & Reeves, S. J., 2001: Controls on the Formation of Contact-Type Platinum-Group Element Mineralization in the East Bull Lake Intrusion. Economic Geology 96, 559-581.

Penniston-Dorland, S., A. Mathez, E., A. Wing, B., Farquhar, J. & Kinnaird, J., 2012: Multiple sulfur isotope evidence for surface-derived sulfur in the Bushveld Complex. Earth and Planetary Science Letters 337, 236–242.

Penniston-Dorland, S., A. Wing, B., Nex, P., Kinnaird, J., Farquhar, J., Brown, M. & Sharman, E., 2008: Multiple sulfur isotopes reveal a magmatic origin for the Platreef platinum group element deposit, Bushveld Complex, South Africa. Geology 36.

Peregoedova, A., Barnes, S.-J. & Baker, D., 2004: The formation of Pt–Ir alloys and Cu–Pd-rich sulfide melts by partial desulfurization of Fe–Ni–Cu sulfides: results of experiments and implications for natural

systems. Chemical Geology 208, 247-264.

Piirainen, T., Hugg, R., Aario, R., ForsströM, L., Ruotsalainen, A. & Koivumaa, S., 1978: Koillismaan malmikriittisten alueiden tutkimusprojektin loppuraportti 1976: The report of the Koillismaa Research Project. Geological Survey of Finland.

Piirainen, T., Hugg, R., Isohanni, M. & Juopperi, A., 1974: On the geotectonics and ore forming processes in the basic intrusive belts of Kemi—Suhanko, and Syote—Narankavaara, northern Finland. Bull. Geol. Soc. Finland 46, 93-104.

Piispanen, R. & Tarkian, M., 1984: Cu-Ni-PGE mineralization at Rometölväs, Koillismaa layered igneous complex, Finland. Mineralium Deposita 19, 105 -111.

Pracejus, B., 2015: The ore minerals under the microscope: an optical guide. Elsevier.

Prevec, S. A., 1997: Magmatic ore deposits of the Sudbury igneous complex. Institute on Lake Superior Geology— Proceedings of the 43rd annual meeting, Sudbury, Ontario, Canada, May 6–11, 1997. Sudbury, Ontario, Canada, Institute on Lake Superior Geology,. 33 pp.

Ripley, E. M., 1981: Sulfur isotopic studies of the Dunka Road Cu-Ni deposit, Duluth Complex, Minnesota. Economic Geology 76, 610-620.

Ripley, E. M., 1983: Sulfide mineralogy and sulfur isotope geochemistry of layered sills in the Deer Lake Complex, Minnesota. Mineralium Deposita 18, 3-15.

Ripley, E. M. & Li, C., 2003: Sulfur isotope exchange and metal enrichment in the formation of magmatic Cu-Ni-(PGE) deposits. Economic Geology 98, 635.

Ripley, E. M. & Li, C., 2013: Sulfide Saturation in Mafic Magmas: Is External Sulfur Required for Magmatic Ni-Cu-(PGE) Ore Genesis? Economic Geology 108, 45-58.

Ripley, E. M., Li, C. & Shin, D., 2002: Paragneiss assimilation in the genesis of magmatic Ni-Cu-Co sulfide mineralization at Voisey's Bay, Labrador: $\delta^{34}S$, $\delta^{13}C$, and Se/S evidence. Economic Geology 97, 1307-1318.

Ripley, E. M., Lightfoot, P. C., Li, C. & Elswick, E. R., 2003: Sulfur isotopic studies of continental flood basalts in the Noril'sk region: Implications for the association between lavas and ore-bearing intrusions. Geochimica et Cosmochimica Acta 67, 2805-2817.

Ripley, E. M., Park, Y.-R., Li, C. & Naldrett, A. J., 1999: Sulfur and oxygen isotopic evidence of country rock contamination in the Voisey's Bay Ni–Cu–Co deposit, Labrador, Canada. Lithos 47, 53-68.

Ripley, E. M., Sarkar, A. & Li, C., 2005: Mineralogic and stable isotope studies of hydrothermal alteration at the Jinchuan Ni-Cu deposit, China. Economic Geology 100, 1349-1361.

Ripley, E. M., Wernette, B. W., Ayre, A., Li, C., Smith, J. M., Underwood, B. S. & Keays, R. R., 2017: Multiple S isotope studies of the Stillwater Complex and country rocks: An assessment of the role of crustal S in the origin of PGE enrichment found in the J-M Reef and related rocks. Geochimica et Cosmochimica Acta 214, 226-245.

Rollinson, H. R., 2014: Using geochemical data: evaluation, presentation, interpretation. Routledge.

Rowell, W. F. & Edgar, A. D., 1986: Platinum-group element mineralization in a hydrothermal Cu-Ni sulfide occurrence, Rathbun Lake, northeastern Ontario. Economic Geology 81, 1272-1277.

Schissel, D., Tsvetkov, A. A., P. Mitrofanov, F. & Korchagin, A. U., 2002: Basal Platinum-Group Element Mineralization in the Federov Pansky Layered Mafic Intrusion, Kola Peninsula, Russia. Economic Geology 97, 1657-1677.

Schouwstra, R., Kinloch, E. D. & Lee, C. A., 2000: A Short Geological Review of the Bushveld Complex. Platinum Metals Review 44, 33-39.

Schulz, K. J., Chandler, V. W., Nicholson, S. W., Piatak, N., Seal, R. R., Woodruff, L. G. & Zientek, M. L., 2010: Magmatic sulfide-rich nickel-copper deposits related to picrite and (or) tholeiitic basalt dike-sill complexes: A preliminary deposit model. US Department of the Interior, US Geological Survey.

Schwarcz, H. P., 1973: Sulfur Isotope Analyses of Some Sudbury, Ontario, Ores. Canadian Journal of Earth Sciences 10, 1444-1459.

Scoon, R. N. & Teigler, B., 1994: Platinum-group element mineralization in the critical zone of the western Bushveld Complex; I, Sulfide poor-chromitites below the UG-2. Economic Geology 89, 1094-1121.

Seal, R. R., 2006: Sulfur Isotope Geochemistry of Sulfide Minerals. Reviews in Mineralogy and Geochemistry 61, 633.

Seat, Z., Beresford, S. W., Grguric, B. A., Gee, M. M. & Grassineau, N. V., 2009: Reevaluation of the role of external sulfur addition in the genesis of Ni-Cu-PGE deposits: Evidence from the Nebo-Babel Ni-Cu-PGE deposit, West Musgrave, Western Australia. Economic Geology 104, 521-538.

Semenov, S. V., Glebovitsky, V. A., Kol'tsov, A. B., Semenov, V. S., Korneev, S. I. & Savatenkov, V. M., 2008: Metasomatic processes in the Lukkulaisvaara layered intrusion, Russia, and formation of low-sulfide PGE mineralization. Geology of Ore Deposits 50, 249.

Sharkov, E. & Smolkin, V., 1998: Palaeoproterozoic layered intrusions of the Russian part of the Fennoscandian Shield: a review. Transactions of the Institutions of Mining

Metallurgy, Section B: Applied Earth Science 107, B23-B38.

Sharman, E. R., Penniston-Dorland, S. C., Kinnaird, J. A., Nex, P. a. M., Brown, M. & Wing, B. A., 2013: Primary origin of marginal Ni-Cu-(PGE) mineralization in layered intrusions: Δ³³S evidence from The Platreef, Bushveld, South Africa. Economic Geology 108, 365.

Sharpe, M., Crous, S., Gain, S., Chunnett, G. & Lee, C., 2002: Sheba's Ridge—an unconventional setting for Platreef, UG2 and Merensky-style PGE

BMS deposits in the Bushveld Complex. Abstr. 9th Int Platinum Symposium, Billings, Montana. 407-408 pp.

Silver, P. G., Fouch, M. J., Gao, S. S. & Schmitz, M., 2004: Seismic anisotropy, mantle fabric, and the magmatic evolution of Precambrian southern Africa. South African Journal of Geology 107, 45-58.

Smith, J. W., Holwell, D. A., Mcdonald, I. & Boyce, A. J., 2016: The application of S isotopes and S/Se ratios in determining ore-forming processes of magmatic Ni–Cu–PGE sulfide deposits: A cautionary case study from the northern Bushveld Complex. Ore Geology Reviews 73, 148-174.

Telenvuo, B., 2016: Cumulus stratigraphy and cryptic variation in the north-western part of the Näränkävaara layered intrusion. University of Oulu. 83 pp.

Urey, H. C., 1947: The thermodynamic properties of isotopic substances. Journal of the Chemical Society (Resumed), 562-581.

Vermaak, C., 1976: The Merensky Reef; thoughts on its environment and genesis. Economic Geology 71, 1270-1298.

Von Gruenewaldt, G., 1979: A review of some recent concepts of the Bushveld Complex, with particular reference to sulfide mineralization. 233-256 pp.

Wager, L. R. & Brown, G. M., 1967: Layered igneous rocks. WH Freeman.

Watkinson, D. H. & Melling, D. R., 1992: Hydrothermal origin of platinum-group mineralization in low -temperature copper sulfide-rich assemblages, Salt Chuck Intrusion, Alaska. Economic Geology 87, 175-184.

Wendlandt, R. F., 1982: Sulfide saturation of basalt and andesite melts at high pressures and temperatures. American Mineralogist 67, 877-885.

Willmore, C., Boudreau, A. & Kruger, F., 2000a: The halogen geochemistry of the Bushveld Complex, Republic of South Africa: implications for chalcophile element distribution in the lower and critical zones. Journal of Petrology 41, 1517-1539.

Willmore, C. C., Boudreau, A. E. & Kruger, F. J., 2000b: The Halogen Geochemistry of the Bushveld Complex, Republic of South Africa: Implications for Chalcophile Element Distribution in the Lower and Critical Zones. Journal of Petrology 41, 1517-1539.

Wohlgemuth-Ueberwasser, C. C., Fonseca, R. O. C., Ballhaus, C. & Berndt, J., 2013: Sulfide oxidation as a process for the formation of copper-rich magmatic sulfides. Mineralium Deposita 48, 115-127.

Wood, S., 2002: The aqueous geochemistry of the platinum-group elements with applications to ore deposits. The geology, geochemistry, mineralogy and mineral beneficiation of platinum-group elements 54, 211-249.

Yakovlev, Y. N., Mitrofanov, F. P., Razhev, S. A., Veselovsky, N. N., Distler, V. & Grokhovskaya, T., 1991: Mineralogy of PGE in the mafic-ultramafic massifs of the Kola region. Mineralogy and Petrology 43, 181-192.

Zientek, M. L., Loferski, P. J., Parks, H. L., Schulte, R. F. & Seal Ii, R. R., 2017: Platinum-group elements. In: K. J. Schulz, J. H. DeYoung Jr, R. R. Seal Ii & D. C. Bradley (eds.) Professional Paper. Reston, VA. 106 pp.

12 Appendix

Appendix I

Nomenclature

In this thesis, the nomenclature of cumulate rocks, established by Irvine (1982); Mathison (1987) is used. The cumulus terminology as reviewed in Irvine (1982), describes a cumulate as a framework of touching minerals formed in an igneous rock due to fractional crystallization. The fractionated minerals are labeled cumulus crystals. Cumulus crystals are typically euhedral to subhedral in their form and "cemented" by texturally later crystallized intercumulus liquid that originally was in interstices of cumulates. No formational implications are to be derived by this purely textural classification. Cumulates are divided into three groups based on the abundance of postcumulus minerals in relation to cumulate crystals. (1) Orthocumulates contain approx. 25–50 vol.% of intercumulus minerals in the rock and cumulate crystals are generally euhedral. (2) Mesocumulates contain approximately 7–25 vol.% of intercumulus minerals and cumulus grains adjoin somewhat in shared contact boundaries. (3) Adcumulates contain the least amount of intercumulus minerals, 0-7 vol. %, and have a primary presence of shared grain boundaries (Irvine 1982; Irvine 1987). When intercumulus minerals in a cumulate rock visually enclose numerous cumulus crystals, the intercumulus crystals are termed oikocrysts and are said to have a poikilitic texture. Small crystals occurring as inclusions in the oikocryst are called chadacrysts (Mathison 1987). Furthermore, when discussing and describing cumulates, abbreviations are used based upon Irvine (1982). The cumulus minerals are listed and abbreviated in correspondence to their modal abundance. Karinen (2010) described the Koillismaa Intrusion using this classification with some modification, by also denoting intercumulus minerals. Because most of the material used and discussed in this work are based upon Karinen (2010), I have chosen to do so as well. The classification is listing the cumulus minerals in descending order of abundance and mentioning the intercumulus mineral after the symbol C. An example of this would be bCa*, describing a poikilitic bronzite cumulate with intercumulus augite. The asterisk symbol indicates that the rock has a poikilitic texture. The metamorphic mineralogy is generally omitted in the names, because the interest is in the primary mineralogy and not later stage modifications. It should be stated that while the Koillismaa Intrusion has undergone greenschist to lower amphibolite metamorphism and contain a lot of metamorphic alteration products, pseudomorphs normally retain the original cumulus textures, thus primary cumulate phases are documented (Karinen 2010). When possible, the abbreviations for minerals follow those suggested by Whitney & Evans (2010).

Additionally, in *Segment 4.2*, the symbol "*" is used to note that the cited reference is available in Finnish only. The referenced sources are commonly used among fellow researchers, and although, I have not been able to read the articles, it is out of respect to the original contributors, that they should be credited regardless.

Appendix II

Thin sections used during research from the Rometölväs Reef and the Marginal Series

A. **Thin section: 4-TTK-00**
Stratigraphy: Rometölväs Reef
Area: Syöte block – Pikku-Syöte
Rock type: Gabbro
Texture: Poikilitic plagioclase cumulate with intercumulus clinopyroxene

B. **Thin section: 39.3-TTK-00**
Stratigraphy: Rometölväs Reef
Area: Portivaara block - Mustavaara
Rock type: Gabbronorite
Texture: plagioclase clinopyroxene and orthopyroxene cumulate

C. **Thin section: 50-TTK-00**
Stratigraphy: Rometölväs Reef
Area: Syöte block – Aurinkokallio
Rock type: Gabbro
Texture: Poikilitic plagioclase cumulate with intercumulus clinopyroxene

D. **Thin section: 77.2-TTK-00**
Stratigraphy: Rometölväs Reef
Area: Syöte block – Rometölväs
Rock type: Anorthosite
Texture: Poikilitic plagioclase cumulate with intercumulus clinopyroxene

E. **Thin section: 80-TTK-99**
Stratigraphy: Rometölväs Reef
Area: Portivaara block – Baabelinälkky
Rock type: Anorthosite
Texture: plagioclase cumulate

F. **Thin section: 82-TTK-00**
Stratigraphy: Rometölväs Reef
Area: Syöte block – Rometölväs
Rock type: Anorthosite
Texture: Poikilitic plagioclase cumulate with intercumulus clinopyroxene

G. **Thin section: 135.6-TTK-99**
Stratigraphy: Rometölväs Reef
Area: Portivaara block – Lanttioja
Rock type: Gabbronorite
Texture: plagioclase, clinopyroxene and orthopyroxene cumulate

H. **Thin section: 135.8A-TTK-99**
Stratigraphy: Rometölväs Reef
Area: Portivaara block – Lanttioja
Rock type: Gabbronorite
Texture: Poikilitic plagioclase and orthopyroxene cumulate with intercumulus clinopyroxene

I. **Thin section: 135.8B-TTK-99**
Stratigraphy: Rometölväs Reef
Area: Portivaara block – Lanttioja
Rock type: Gabbronorite
Texture: Poikilitic plagioclase and orthopyroxene cumulate with intercumulus clinopyroxene

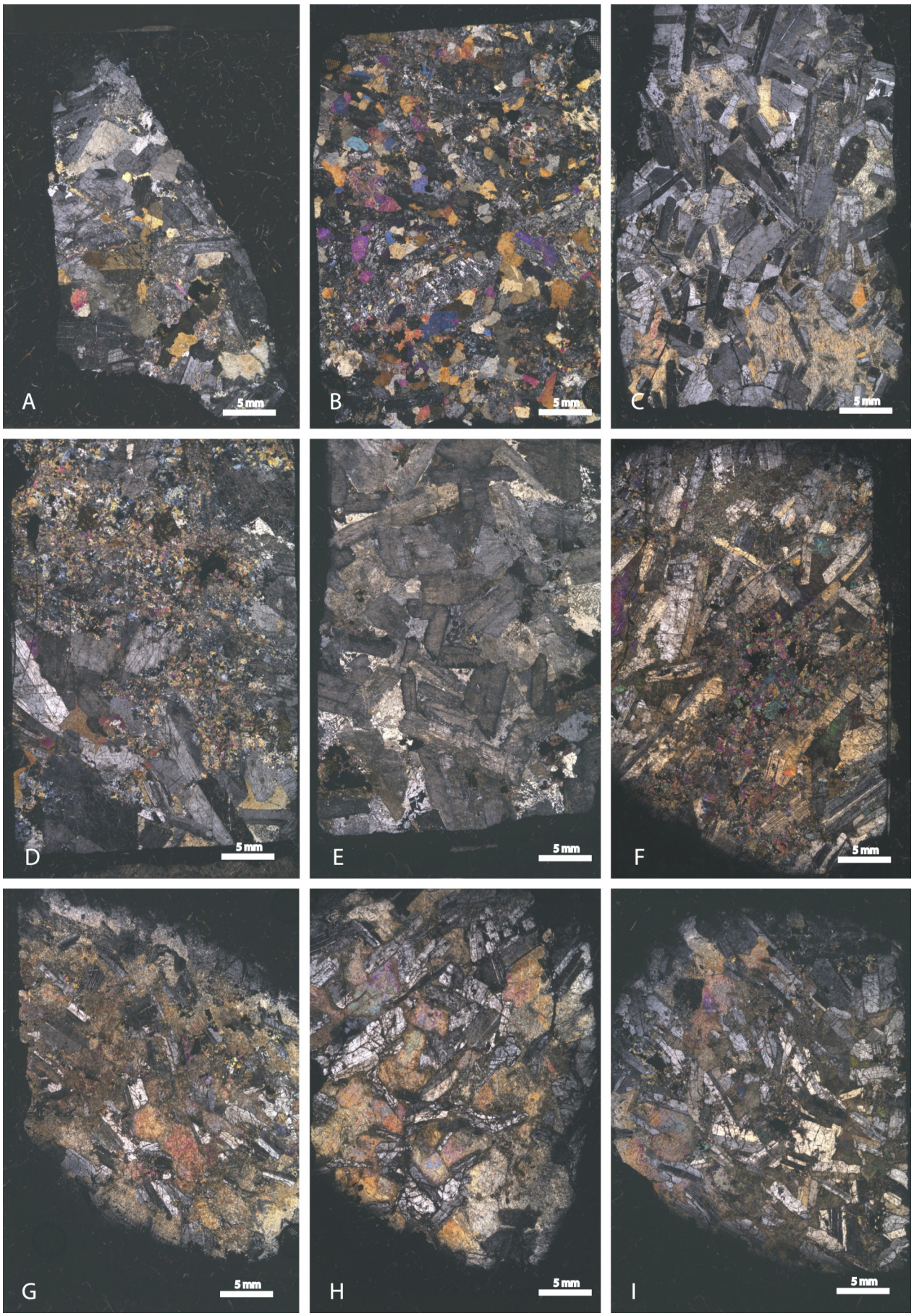
A
5 mm
B
5 mm
C
5 mm
D
5 mm
E
5 mm
F
5 mm
G
5 mm
H
5 mm
I
5 mm

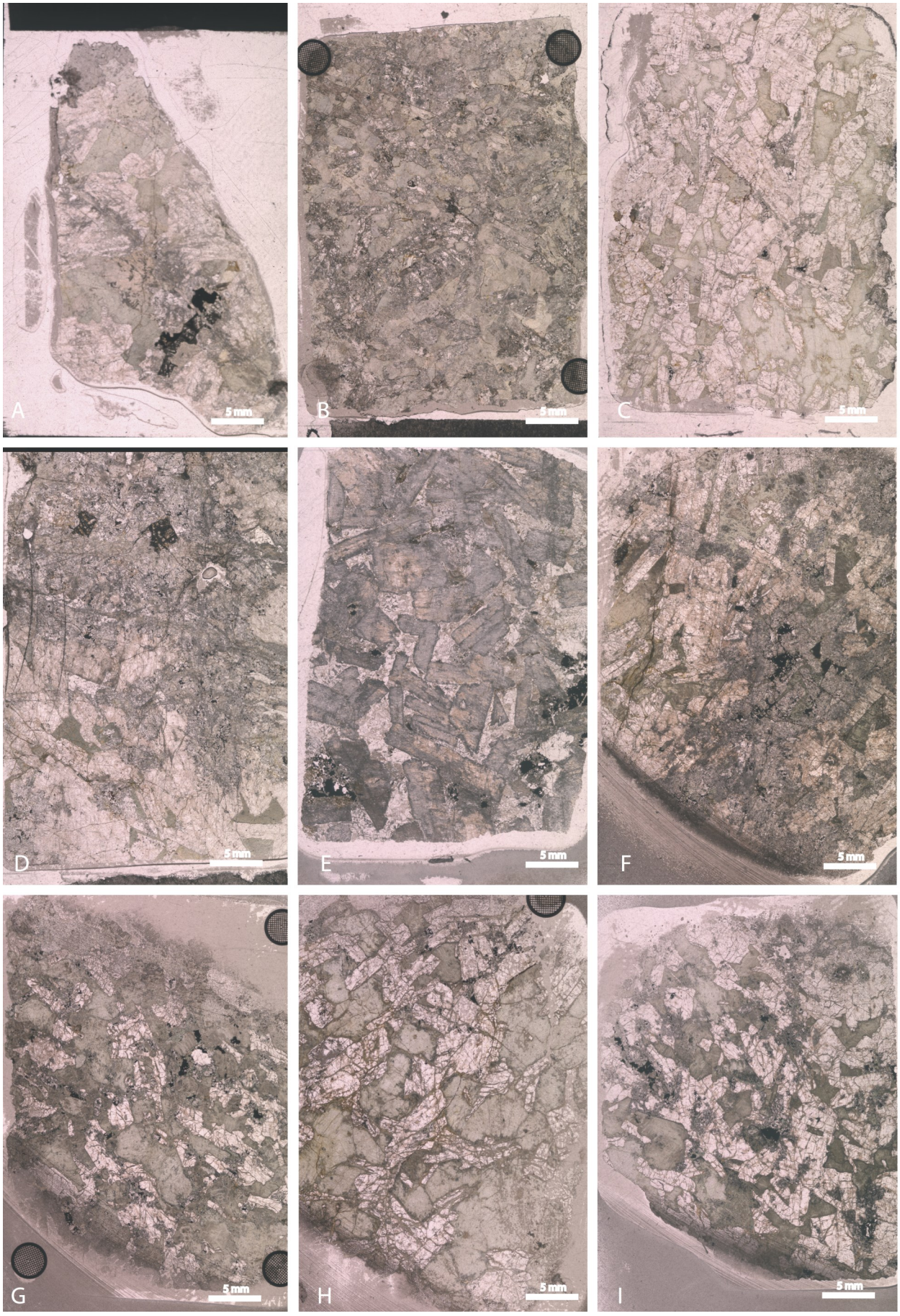
A
5 mm
B
5 mm
C
5 mm
D
5 mm
E
5 mm
F
5 mm
G
5 mm
H
5 mm
I
5 mm

A. **Thin section: 11-TTK-00**
Stratigraphy: Marginal Series - LZMSa
Area: Portivaara block - Soukeli
Rock type: Gabbronorite
Texture: Plagioclase and orthopyroxene cumulate with intercumulus clinopyroxene

B. **Thin section: 53-TTK-00**
Stratigraphy: Marginal Series - LZMSb
Area: Portivaara block - Soukeli
Rock type: Gabbronorite
Texture:

C. **Thin section: 257-TTK-00**
Stratigraphy: Marginal Series - LZMSa
Area: Portivaara block - Soukeli
Rock type: Gabbronorite
Texture: Plagioclase and orthopyroxene cumulate with intercumulus clinopyroxene

D. **Thin section: 261-TTK-00**
Stratigraphy: Marginal Series - LZMSb
Area: Portivaara block - Soukeli
Rock type: Gabbronorite
Texture: Plagioclase and orthopyroxene cumulate with intercumulus clinopyroxene

E. **Thin section: 264-TTK-00**
Stratigraphy: Marginal Series - UZMSa
Area: Portivaara block - Soukeli
Rock type: Pyroxenite
Texture: n.d

F. **Thin section: 397-TTK-00**
Stratigraphy: Marginal Series - UZMSa
Area: Portivaara block - Lavotta
Rock type: Pyroxenite
Texture: n.d

G. **Thin section: 400-TTK-00**
Stratigraphy: Marginal Series - LZMSa
Area: Portivaara block - Soukeli
Rock type: Gabbronorite
Texture: plagioclase and orthopyroxene cumulate with intercumulus clinopyroxene

H. **Thin section: 401-TTK-00**
Stratigraphy: Marginal Series - LZMSb
Area: Portivaara block - Soukeli
Rock type: Gabbronorite
Texture: plagioclase and orthopyroxene cumulate with intercumulus clinopyroxene

I. **Thin section: 402-TTK-00**
Stratigraphy: Marginal Series - LZMSb
Area: Portivaara block - Soukeli
Rock type: Gabbronorite
Texture: plagioclase and orthopyroxene cumulate with intercumulus clinopyroxene

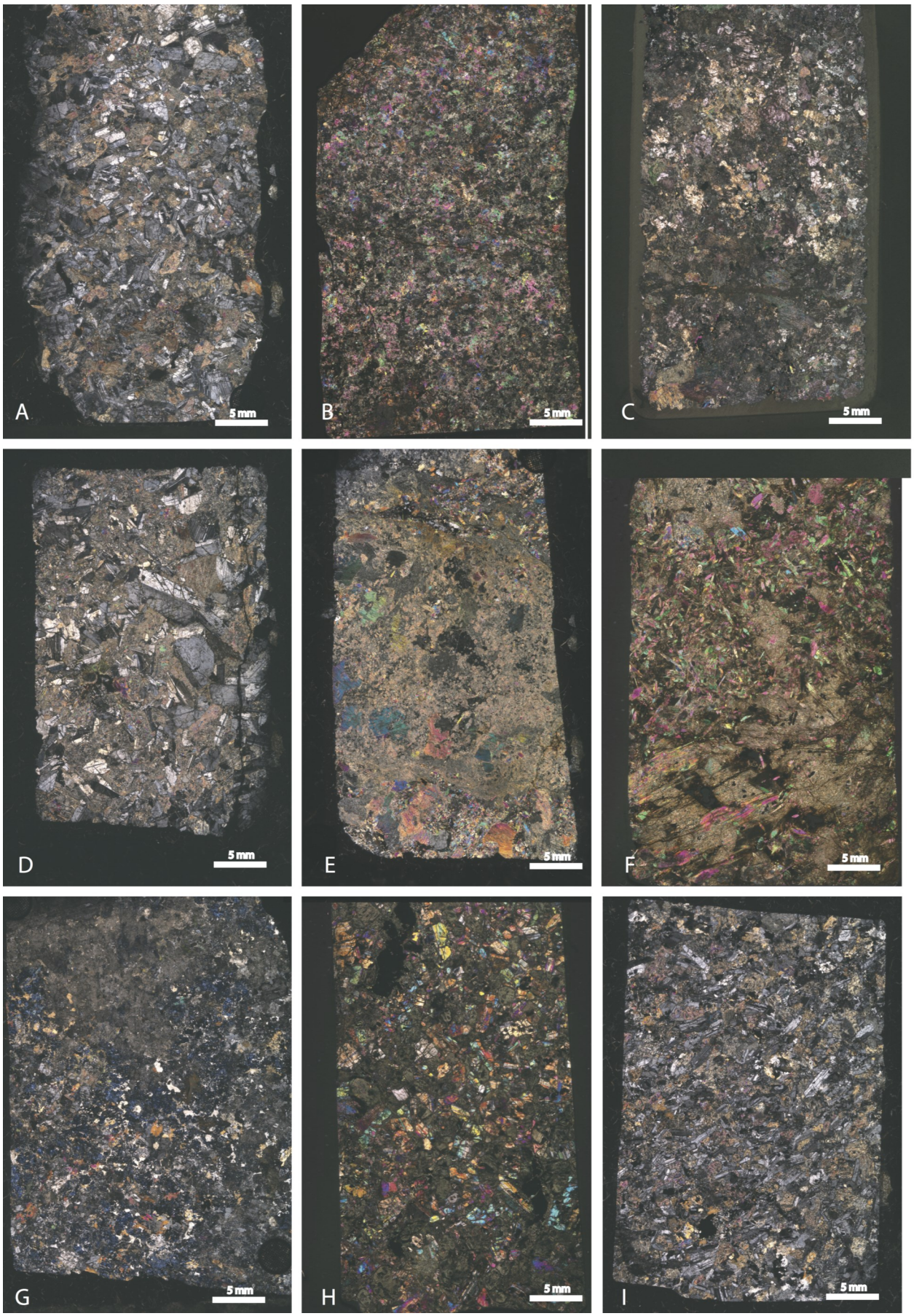
A
5 mm
B
5 mm
C
5 mm
D
5 mm
E
5 mm
F
5 mm
G
5 mm
H
5 mm
I
5 mm

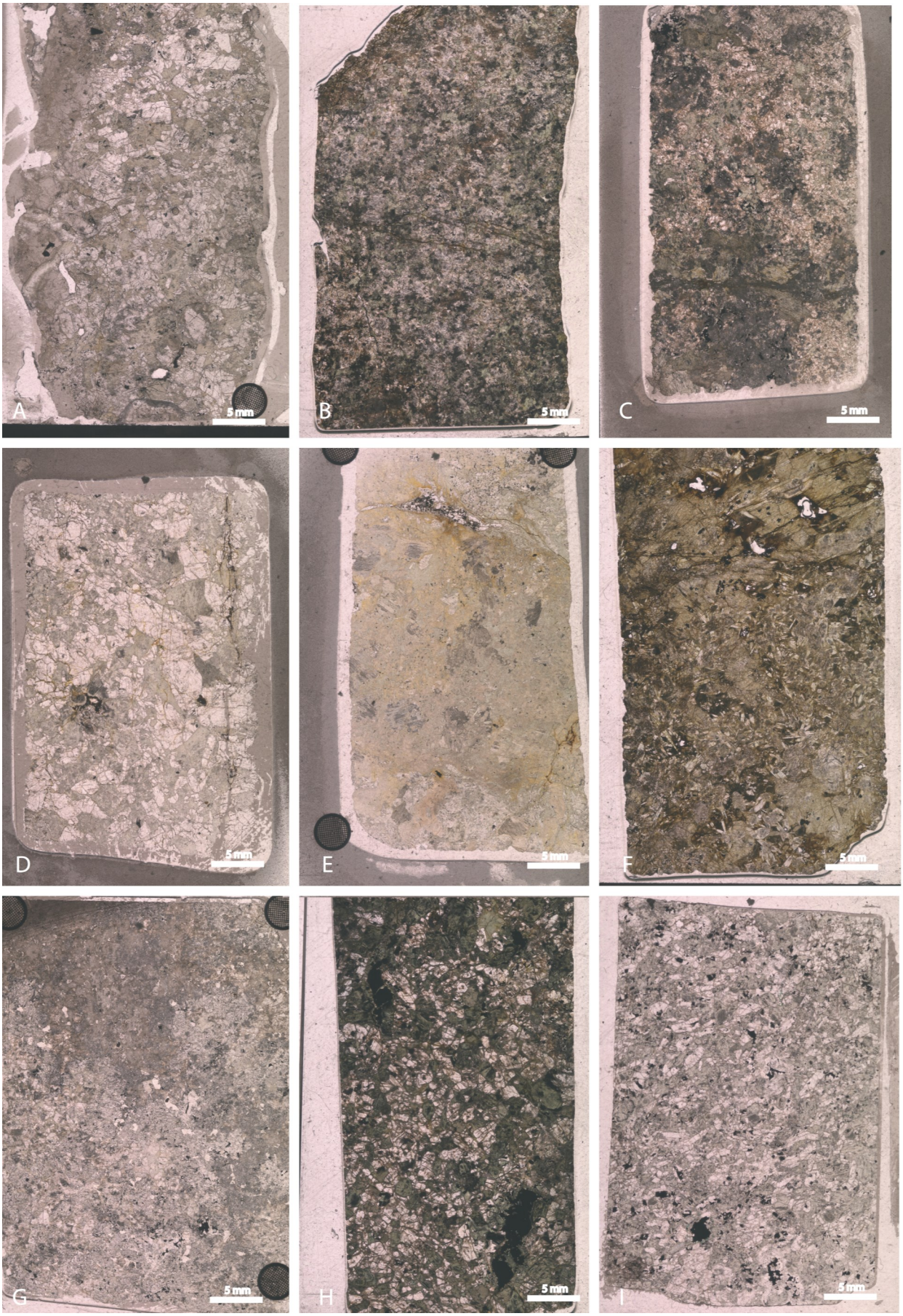
A
5 mm
B
5 mm
C
5 mm
D
5 mm
E
5 mm
F
5 mm
G
5 mm
H
5 mm
I
5 mm

A. **Thin section: 135.11-TTK-99**
Stratigraphy: Rometölväs Reef
Area: Portivaara block - Lanttioja
Rock type: Gabbro
Texture: Poikilitic plagioclase cumulate with intercumulus clinopyroxene

B. **Thin section: 137.1-TTK-99**
Stratigraphy: Rometölväs Reef
Area: Portivaara block - Välivaara
Rock type: Gabbronorite
Texture: Plagioclase, clinopyroxene and orthopyroxene cumulate

C. **Thin section: 83-TTK-99**
Stratigraphy: Rometölväs Reef
Area: Syöte block - Rometölväs
Rock type: Gabbronorite
Texture: non-cumulus

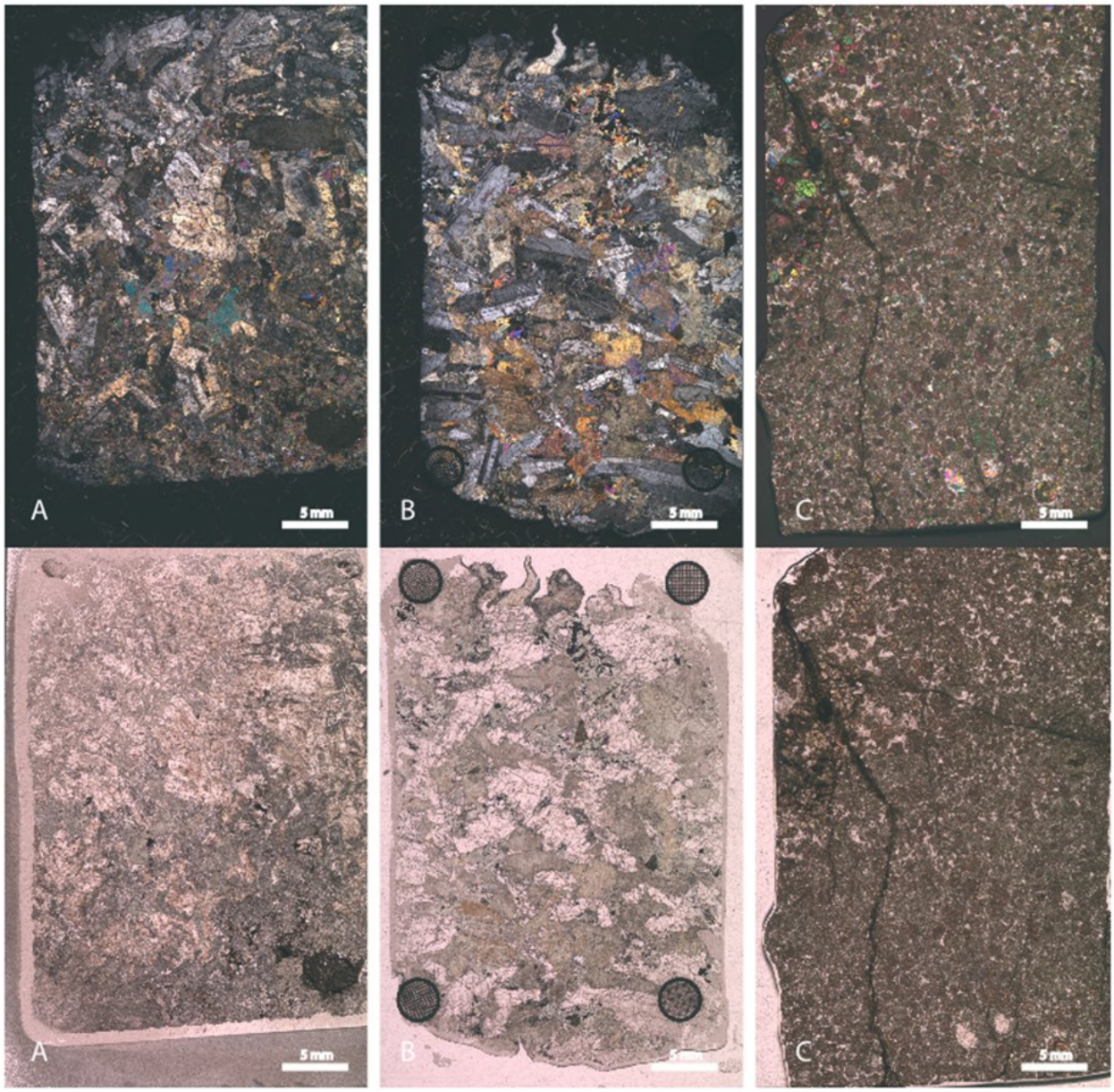

Appendix III

Grain size analyses of platinum-group minerals from SEM-EDS using INCA-software.

Thin Section	Source	Feature	Area (sq. µm)	ECD (µm)	Length (µm)
257-TTK-00	MS	5	3.29	2.05	3.14
		6	3.84	2.21	2.67
		8	12.08	3.92	4.69
		14	11.53	3.83	4.32
		26	3.29	2.05	2.67
		28	14.82	4.34	4.97
		29	72.45	9.60	22.20
		30	19.76	5.02	7.63
		32	4.39	2.36	3.05
		35	3.84	2.21	2.67
		38	5.49	2.64	3.70
		39	3.29	2.05	2.67
		40	2.20	1.67	2.34
400-TTK-00	MS	15	6.04	2.77	3.99
		18	32.38	6.42	8.67
		21	191.01	15.60	25.23
402-TTK-00	MS	3	23.60	5.48	7.03
		6	8.78	3.34	3.99
		8	6.59	2.90	4.32
		9	4.39	2.36	3.05
		19	2.20	1.67	2.10
		20	1.65	1.45	2.10
		30	7.68	3.13	3.99
261-TTK-00	MS	30	12.08	3.92	4.69
264-TTK-00	MS	10	3.29	2.05	2.67
		15	4.39	2.36	3.31
		16	1.65	1.45	2.10
11- TTK-00	MS	1	10.98	3.74	5.39
		4	2.20	1.67	2.10
		6	5.49	2.64	3.31
		9	10.43	3.64	5.64
		13	30.74	6.26	9.04
		14	3.84	2.21	2.67
		15	12.08	3.92	4.97

Thin Section	Source	Feature	Area (sq. µm)	ECD (µm)	Length (µm)
39.3- TTK-00	RT	2	4.39	2.36	3.05
		3	1.65	1.45	2.10
		4	2.74	1.87	2.34
		5	3.29	2.05	2.67
		9	2.20	1.67	2.10
		10	12.08	3.92	4.97
		11	6.04	2.77	4.69
		12	12.62	4.01	4.74
		13	13.17	4.10	6.37
135.6- TTK-99	RT	4	4.39	2.36	3.05
		12	4.94	2.51	3.31
		13	19.76	5.02	7.41
		21	15.92	4.50	6.63
		23	2.20	1.67	2.10
		24	3.29	2.05	3.31
		25	5.49	2.64	4.32
		26	1.65	1.45	2.10
135.8A- TTK-99	RT	8	4.94	2.51	3.31
		9	8.23	3.24	4.69
135,8B- TTK-99	RT	9	3.29	2.05	2.67
		18	12.08	3.92	6.11
		35	5.49	2.64	3.70
		36	12.08	3.92	5.64
		41	3.29	2.05	2.67
		43	15.92	4.50	7.03
		44	395.20	22.43	43.98
135.11- TTK-99	RT	66	4.39	2.36	3.05
82- TTK-00	RT	47	21.41	5.22	7.41
		50	58.73	8.65	11.50
		57	51.05	8.06	9.94
		72	85.08	10.41	18.40
		73	1.65	1.45	2.10
		1	13.17	4.10	5.34
		4	6.04	2.77	3.70
		5	2.20	1.67	2.34

Appendix IV

Representative LA-ICP-MS spots of base-metal sulfides chosen for analysis of sulfur isotopes. Grains of pyrrhotite, chalcopyrite and pyrite were ablated at a spatial resolution of 40 µm in diameter, as is illustrated by the red circle.

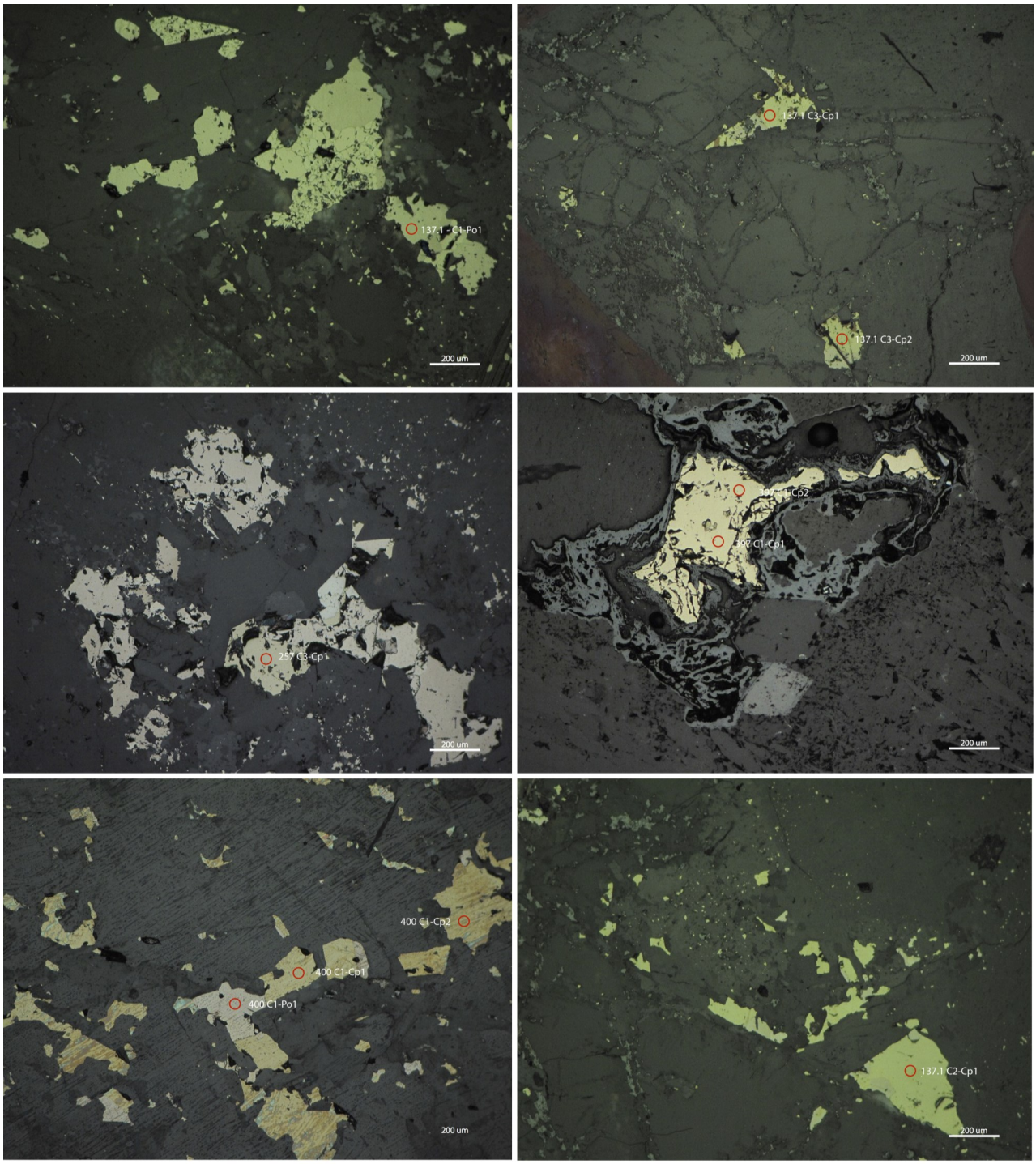

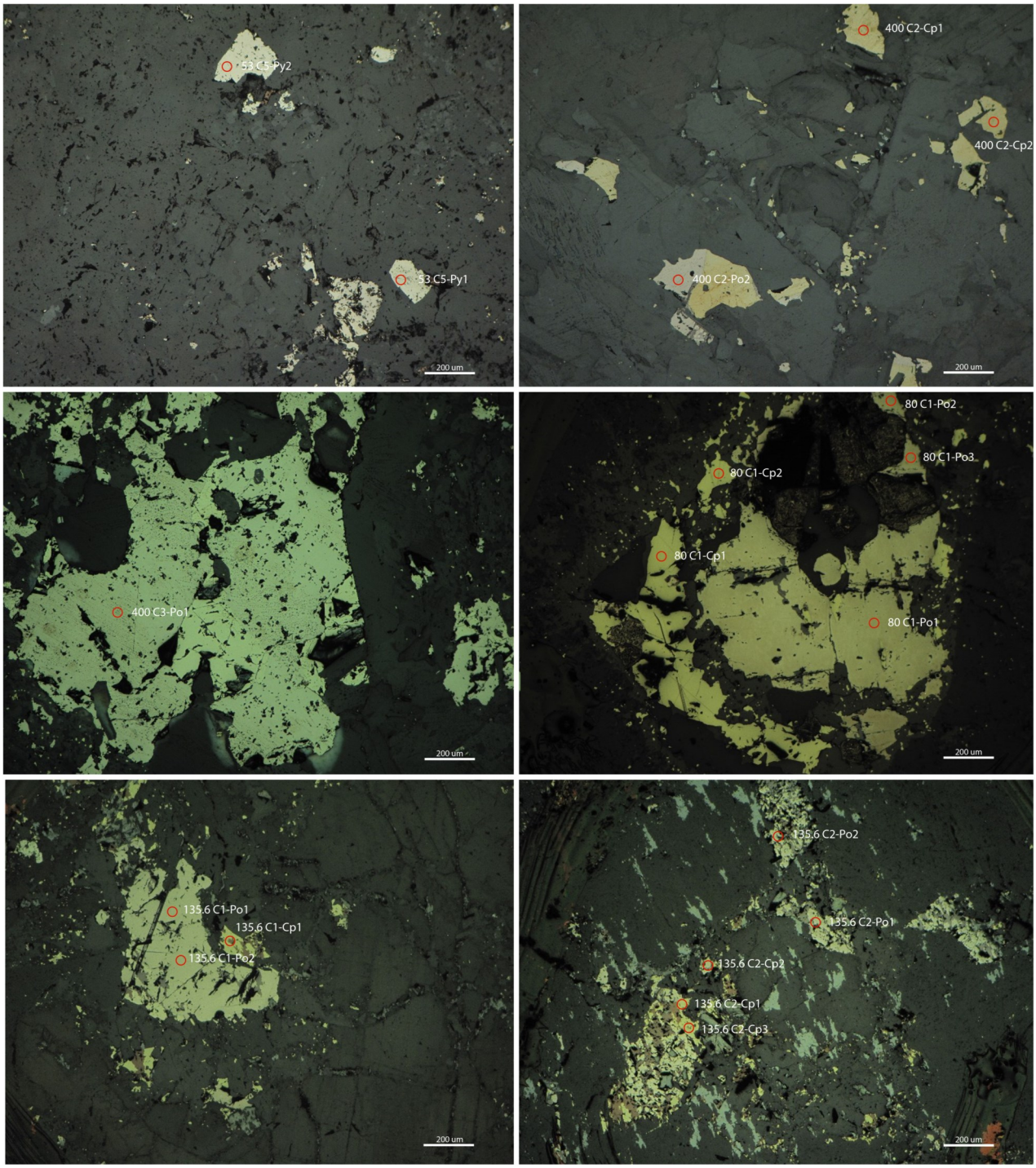
52 C5-Py2
53 C5-Py1
200 um
400 C2-Cp1
400 C2-Cp2
400 C2-Po2
200 um
400 C3-Po1
200 um
80 C1-Po2
80 C1-Po3
80 C1-Cp2
80 C1-Cp1
80 C1-Po1
200 um
135.6 C1-Po1
135.6 C1-Cp1
135.6 C1-Po2
200 um
135.6 C2-Po2
135.6 C2-Po1
135.6 C2-Cp2
135.6 C2-Cp1
135.6 C2-Cp3
200 um

Appendix V

Nano-particulate pressed powder tablets for LA-ICP-MS

Additionally, a sample-processing and measurement protocol of nano-particulate pressed powder tablets for LA-ICP-MS is presented subsequently. This protocol was developed at GTK for producing undiluted nano-particulate pressed powder tablets. The objective of the procedure was to manufacture in-house standards suitable for LA-ICP-MS work. Besides the interest of GTK to be able to create in-house standards, the idea was to create a PGE-standard to be used during my laser ablation analysis of BMS. However, due to time-constraints the development of a nanopellet standard were not done by the date of analysis, instead, a reference standard was purchased from Université du Québec á Chicoutimi, Canada.

Unfortunately, the analytical laser ablation data of the PGE trace elements in BMS was not received during the writing of this thesis, and therefore this data, which was intended to be the principal part of this thesis is absent. This data is intended to be subsequently publicized.

2019-07-28

Nano-particulate pressed powder tablets for LA-ICP-MS

Sample-processing and measurement protocol

Jon Gustafsson

LUND UNIVERSITY

UNIVERSITY OF OULU

Introduction

In order to understand many geochemical and petrological processes, access to good analytical data is essential, especially regarding trace elements and ultra-trace elements, which require very low detection values. Over the last 10 - 20 years, major progress has been made in this field, especially in the usage of LA-ICP-MS, in various fields of research, continuously improving accuracy, precision and lower limit of detection (Koch and Günther 2011).

One of the major hindrances for progression of laser ablation analysis, is the available standard reference material (RM), from which to calibrate the LA-ICP-MS. Adequate matrix-matched RM and non-matrix matched (i.e. glass) RM, are still somewhat scarce and those available and classified as certified reference material (CRM) are often expensive to acquire. The reference material needs to be homogenous enough to establish exact values of trace and ultra-trace elements on a micro-scale and the matrix need to match with the samples analyzed. The risks with non-matrix matched calibration, is that it may lead to a bias. Due to the fact that many elements, when ablated, may be differently distributed in terms of size and region (Flamigni et al. 2012; Kroslakova and Günther 2007). Thus, a non-matrix matched reference material is not utilizing all the improvements made for the LA-ICP-MS over the years, to its full potential. In terms of geochemical appliances, there is a large collection of CRM available from suppliers connected to databases, such as GeoReM (Geological and Environmental Reference Materials Database). However, most of these samples come in the form of medium to fine grained powders and are therefore seldom suitable for trace elements or isotope studies. Natural minerals in larger quantities, homogenous enough to be certified as CRM are incredibly rare and difficult to acquire (Garbe-Schönberg and Müller 2014). There are some natural volcanic glasses distinguished as CRM, but these are uncommon (Ulrich and Kamber Balz 2013). Synthetically made materials are very difficult to produce to a CRM-standard. According to Garbe-Schönberg and Müller (2014), there are four commonly used methods for producing adequate reference material suitable for laser ablation analysis. 1) Synthesis of minerals, 2) acquiring natural minerals with adequate homogeneity, 3) vitrification of pulverized samples, and 4) manufacturing pressed powder pellets (PPP) from either natural or synthetic material. The three aforementioned methods all have their drawbacks (cf., Garbe-Schönberg and Müller 2014; Peters and Pettke 2017). The methods all have the same objective, which is that the sample material should be pulverized and adequately homogenized, to ensure satisfactory representativeness, by also increasing the relative surface of the material (Peters and Pettke 2017).

The idea of using a pelletized powder standard was first endeavored by Gray (1985), since then, many researchers have continued to optimize and advance methods of making PPP for the appliance of measuring trace element in LA-ICP-MS (e.g., Arrowsmith 1987; Mukherjee et al. 2013; Zhu et al. 2013). These authors used a binder to cope with the natural in-cohesiveness of the sample material. The usage of a binder is solely to increase the durability and cohesion of the pellet, thereby also producing a more stable and reproducible laser ablation signal. Common for many of the methods involving binders (e.g. polyvinyl alcohol, cellulose, spectroblend and collagen hydrolysate) is that they often show bad repeatability and inhomogeneity (Peters and Pettke 2017). Some researchers have successfully created PPP without binding agents (e.g., Garbe-Schönberg and Müller 2014; Imai 1990). Garbe-Schönberg and Müller (2014), drastically improved the quality of PPP by creating nanoparticulate sized pellets, without the addition of a binder. By wet-milling the samples in a planetary ball mill, the duo produced a grain size by one order of magnitude smaller than the previous commercial standard, $d_{50} < 1.5$ mm. This method for manufacturing PPP was further refined by Peters and Pettke (2017).

Protocol

The development of this sample processing and measurement protocol, took place in May 2017 and February 2018 at GTK facilities in Espoo, Helsinki. A trial for testing methods aimed at producing undiluted Nano-particulate pressed powder tablets without addition of any binder by applying wet-milling protocols using a planetary ball mill. The objective of the procedure was to obtain ultra-fine sample powders for pelleting, with an average grain size small enough that grain-to-grain heterogeneity is no longer detected during LA-ICP-MS recording. The protocol below is largely based on the protocol used by Peters and Pettke (2017), some of the differences include changed parameters and settings to account for the different equipment used, as well as the absence of a binder during pelleting.

When using highly siliceous sample material, this method proved inadequate in producing a cohesive pellet and therefore a binder is needed. Silica-poor sample material displayed good cohesiveness through this method. At the time of writing, no systematic evaluation via laser ablation has been made.

Material & Equipment

Material and equipment needed during work:

- Powder-free gloves
- Paper sheets
- Lab-cleaning wipes
- Ultrapure water
- Ethanol
- Spoon
- PFA-beakers or ceramic bowls
- PFA-sieve
- Parafilm
- Weighing paper
- Pipette
- Pair of tweezers

- Heating plate
- High-precision scale
- Ultrasonic bath
- Compressed air
- Agate mortar and pestle

- Planetary ball mill (Fritsch Pulverisette 7 premium line)
- 10x agate milling balls (ø 10mm)
- Hydraulic press (Perkin-Elmer)

Preparations

Before initiating the loading of the vials, make sure that the working surface is clean, preferably by wiping the surface with ethanol and cover the working area with sheets of paper. Powder-free gloves should be used during the whole procedure, to avoid contamination. Make sure the surface of the scale is clean and clean the 20 mL agate vials with ethanol and compressed air.

Each vial is then loaded with ten agate milling balls (ø10mm) weighing 15 grams in total, using a clean spoon. 1 gram of sample is measured using weighing paper and then added on top of the balls in the vial. Next, 2,5 mL of ultraclean water is gently added via a pipette, making sure that no dust from the sample is lost. *(It may be worthwhile reversing this step by adding the water before the sample for this reason. However, the user's manual suggests adding the sample before any additional liquid)*. This results in a ball-to-powder ratio (BPR) of ~ 15 and a water-to-powder ratio (WPR) of 2.5, which is desirable.

Carefully attach and close the lid of the vial, before loading it into the planetary ball mill. Make sure that each vial is correctly mounted before commencing milling. *(Note that there must always be two vials of similar weight mounted into the planetary ball mill, to assure adequate counter balance during operation.)*

Milling

Total milling time should be 45 min (i.e., 15 cycles) at 600 Hz, divided into intervals of three-minute milling, followed by 1 min of cooling. With the direction of rotation alternating, for each milling interval.

Sample recovery

Demount the vials from the planetary ball mill and bring them to your already prepared working surface. Place the vial on a paper sheet and gently remove the lid. *(Note, the sample residue on the lid should not be sampled, since the gasket of the lid abrades during milling, making it a potential source of contamination).*

Transfer the milling balls using a clean spoon into a PFA-sieve, placed onto a PFA-beaker. Rinse the balls with small amounts ultraclean water. Remove the sieve and then rinse the milling balls using ethanol to remove the leftover residue, and then place the sieve with the balls aside.

Stir the slurry in the vial by gently shaking it to promote suspension of the particles. Collect the slurry in the vial using a pipette and transfer it into a PFA-beaker or a ceramic bowl. Small amounts of ultraclean water can be added to optimize the extraction of the sample from the vial. The amount of water needed will greatly depend on

the sample material, as some samples, e.g. sulfides, will be stickier and more adhesive.

Note, depending on the amount of water needed to rinse the balls in the sieve, the slurry collected in the PFA-beaker could potentially also collected and used, together with the sample slurry in the vial. When using a larger vial this is possible, but it has not been tested using the smaller 20 mL vials available.

Drying of sample

Place the PFA-beaker or ceramic bowl containing the sample on a heating plate, at 70° C, under a fume hood until the sample is dry (approx. 5-7 hours).

When dried, cover the beaker or bowl with a parafilm making sure it is properly sealed. Bounce the beaker on the table to fracture the solidified sample and ease extraction. The sample is then rehomogenized using an agate mortar and pestle, ultimately to be stored in an appropriate container. *(The homogenization procedure may potentially be skipped).*

Cleaning procedure

Clean the vial, lid and gasket using ultrapure water and wipes. Already, when removing the lid of the vial during sample recovery, rinse the lid with ultrapure water, in order to remove the majority of the residue (removing the residue when the vials are dry is significantly harder).

After having wiped of the vial, lid and gasket using ultrapure water, clean with compressed air and then wipe them again, using ethanol and subsequently compressed air.

The milling balls still remaining in the sieve, are rinsed over a sink using ultraclean water and ethanol until the draining liquid is clear. Transfer the balls into a clean PFA-beaker filled with ultraclean water and ethanol (10:1 ratio) and let sit in an ultrasonic bath for 5 minutes. Rinse the balls once again with ultraclean water, and place them on a few wipes and let dry, before transferring them into a clean beaker.

Once the aforementioned cleaning procedure has been completed. The vials are then cleaned by milling of synthetic quarts, using the same parameters as for the milling of the sample. Add 1 gram of quartz together with the used milling balls, while adding 2,5 mL of ultraclean water. Cleaning is done by milling at 600hz for 5 cycles, divided into intervals of 3 min milling, followed by 1 min of cooling, with reversal between each cycle. In the meantime, clean the beaker and sieve using ultrapure water, ethanol and compressed air.

This whole cleaning process may be repeated up to three more times, each with new synthetic quartz added. Whether such a thorough procedure is necessary depends on the similarity of the samples being processed. For similar milling materials, one run of quartz milling is enough. After the final milling step, clean the equipment as previously described in the first section, apart from a 15-minute ultrasonic bath, instead of 5 minutes.

Pelletizing

Clean the pelletizing equipment using ethanol and compressed air before and after pelletizing.

Measure 200 - 300 mg (depending on desirable pellet thickness) of the sample using weighing paper into a separate PFA-container. Add the sample into the pellet jig, insert the jig carefully into the press and press for 30 minutes, at 10 tonnes of pressure.

Finally, gently detach the equipment from the press and very carefully remove the pressed pellet using clean set of tweezers. Store the pellet in a sample container.

Flow scheme

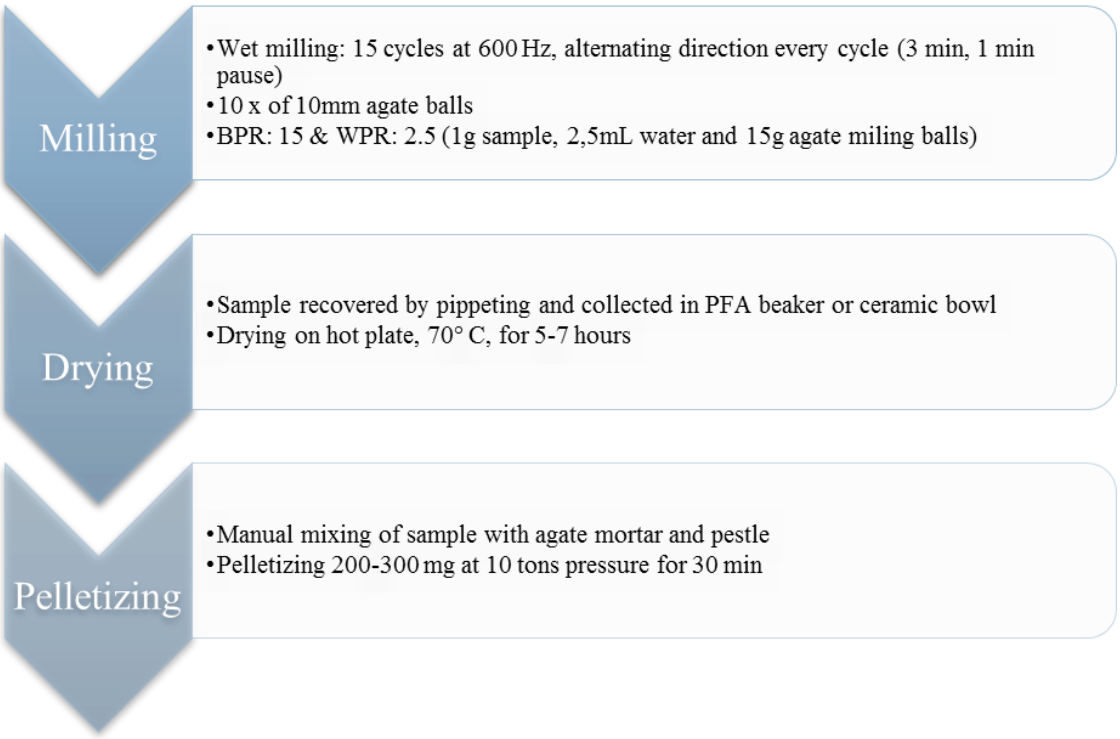

References

Arrowsmith P (1987) Laser ablation of solids for elemental analysis by inductively coupled plasma mass spectrometry Analytical Chemistry 59:1437-1444 doi:10.1021/ac00137a014

Flamigni L, Koch J, Günther D (2012) Experimental and theoretical investigations about the vaporization of laser-produced aerosols and individual particles inside inductively-coupled plasmas — Implications for the extraction efficiency of ions prior to mass spectrometry Spectrochimica Acta Part B: Atomic Spectroscopy 76:70-76 doi:https://doi.org/10.1016/j.sab.2012.07.016

Garbe-Schönberg D, Müller S (2014) Nano-particulate pressed powder tablets for LA-ICP-MS Journal of Analytical Atomic Spectrometry 29:990-1000 doi:10.1039/C4JA00007B

Gray L, Alan (1985) Solid Sample Introduction by Laser Ablation for Inductively Coupled Plasma Mass Spectrometry vol 110. doi:10.1039/an9851000551

Imai N (1990) Quantitative analysis of original and powdered rocks and mineral inclusions by laser ablation inductively coupled plasma mass spectrometry Analytica Chimica Acta 235:381-391 doi:https://doi.org/10.1016/S0003-2670(00)82097-8

Koch J, Günther D (2011) Review of the State-of-the-Art of Laser Ablation Inductively Coupled Plasma Mass Spectrometry Applied Spectroscopy 65:155A-162A doi:10.1366/11-06255

Kroslakova I, Günther D (2007) Elemental fractionation in laser ablation-inductively coupled plasma-mass spectrometry: evidence for mass load induced matrix effects in the ICP during ablation of a silicate glass Journal of Analytical Atomic Spectrometry 22:51-62 doi:10.1039/B606522H

Mukherjee Pk, P. Khanna P, Saini NK (2013) Rapid Determination of Trace and Ultra-Trace Level Elements in Diverse Silicate Rocks in Pressed Powder Pellet Targets by LA-ICP-MS using a Matrix Independent Protocol vol 38. doi:10.1111/j.1751-908X.2013.012015.x

Peters D, Pettke T (2017) Evaluation of Major to Ultra Trace Element Bulk Rock Chemical Analysis of Nanoparticulate Pressed Powder Pellets by LA-ICP-MS Geostandards and Geoanalytical Research 41:5-28 doi:10.1111/ggr.12125

Ulrich T, Kamber Balz S (2013) Natural Obsidian Glass as an External Accuracy Reference Material in Laser Ablation-Inductively Coupled Plasma-Mass Spectrometry Geostandards and Geoanalytical Research 37:169-188 doi:10.1111/j.1751-908X.2012.00189.x

Zhu Y, Hioki A, Chiba K (2013) Quantitative analysis of the elements in powder samples by LA-ICP-MS with PMMA powder as the binder and Cs as the internal standard Journal of Analytical Atomic Spectrometry 28:301-306 doi:10.1039/C2JA30279A

Tidigare skrifter i serien ”Examensarbeten i Geologi vid Lunds universitet”:

521. Önnervik, Oscar, 2017: Ooider som naturliga arkiv för förändringar i havens geokemi och jordens klimat. (15 hp)
522. Nilsson, Hanna, 2017: Kartläggning av sand och naturgrus med hjälp av resistivitetsmätning på Själland, Danmark. (15 hp)
523. Christensson, Lisa, 2017: Geofysisk undersökning av grundvattenskydd för planerad reservvattentäkt i Mjölkalånga, Hässleholms kommun. (15 hp)
524. Stamsnijder, Joaen, 2017: New geochronological constraints on the Klipriviersberg Group: defining a new Neoarchean large igneous province on the Kaapvaal Craton, South Africa. (45 hp)
525. Becker Jensen, Amanda, 2017: Den eocena Furformationen i Danmark: exceptionella bevaringstillstånd har bidragit till att djurs mjukdelar fossiliserats.(15 hp)
526. Radomski, Jan, 2018: Carbonate sedimentology and carbon isotope stratigraphy of the Tallbacken-1 core, early Wenlock Slite Group, Gotland, Sweden. (45 hp)
527. Pettersson, Johan, 2018: Ultrastructure and biomolecular composition of sea turtle epidermal remains from the Campanian (Upper Cretaceous) North Sulphur River of Texas. (45 hp)
528. Jansson, Robin, 2018: Multidisciplinary perspective on a natural attenuation zone in a PCE contaminated aquifer. (45 hp)
529. Larsson, Alfred, 2018: Rb-Sr sphalerite data and implications for the source and timing of Pb-Zn deposits at the Caledonian margin in Sweden. (45 hp)
530. Balija, Fisnik, 2018: Stratigraphy and pyrite geochemistry of the Lower–Upper Ordovician in the Lerhamn and Fågelsång -3 drill cores, Scania, Sweden. (45 hp)
531. Höglund, Nikolas, 2018: Groundwater chemistry evaluation and a GIS-based approach for determining groundwater potential in Mörbylånga, Sweden. (45 hp)
532. Haag, Vendela, 2018: Studie av mikrostrukturer i karbonatslagkäglor från nedslagsstrukturen Charlevoix, Kanada. (15 hp)
533. Hebrard, Benoit, 2018: Antropocen – vad, när och hur? (15 hp)
534. Jancsak, Nathalie, 2018: Åtgärder mot kusterosion i Skåne, samt en fallstudie av erosionsskydden i Löderup, Ystad kommun. (15 hp)
535. Zachén, Gabriel, 2018: Mesosideriter – redogörelse av bildningsprocesser samt SEM-analys av Vaca Muertameteoriten. (15 hp)
536. Fägersten, Andreas, 2018: Lateral variability in the quantification of calcareous nannofossils in the Upper Triassic, Austria. (15 hp)
537. Hjertman, Anna, 2018: Förutsättningar för djupinfiltration av ytvatten från Ivösjön till Kristianstadbassängen. (15 hp)
538. Lagerstam, Clarence, 2018: Varför svalde svanödlor (Reptilia, Plesiosauria) stenar? (15 hp)
539. Pilser, Hannes, 2018: Mg/Ca i bottenlevande foraminiferer, särskilt med avseende på temperaturer nära 0°C. (15 hp)
540. Christiansen, Emma, 2018: Mikroplast på och i havsbotten - Utbredningen av mikroplaster i marina bottensediment och dess påverkan på marina miljöer. (15 hp)
541. Staahlnacke, Simon, 2018: En sammanställning av norra Skånes prekambriska berggrund. (15 hp)
542. Martell, Josefin, 2018: Shock metamorphic features in zircon grains from the Mien impact structure - clues to conditions during impact. (45 hp)
543. Chitindingu, Tawonga, 2018: Petrological characterization of the Cambrian sandstone reservoirs in the Baltic Basin, Sweden. (45 hp)
544. Chonewicz, Julia, 2018: Dimensionerande vattenförbrukning och alternativa vattenkvaliteter. (15 hp)
545. Adeen, Lina, 2018: Hur lämpliga är de geofysiska metoderna resistivitet och IP för kartläggning av PFOS? (15 hp)
546. Nilsson Brunlid, Anette, 2018: Impact of southern Baltic sea-level changes on landscape development in the Verkeån River valley at Haväng, southern Sweden, during the early and mid Holocene. (45 hp)
547. Perälä, Jesper, 2018: Dynamic Recrystallization in the Sveconorwegian Frontal Wedge, Småland, southern Sweden. (45 hp)
548. Artursson, Christopher, 2018: Stratigraphy, sedimentology and geophysical assessment of the early Silurian Halla and Klinteberg formations, Altajme core, Gotland, Sweden. (45 hp)
549. Kempengren, Henrik, 2018: Att välja den mest hållbara efterbehandlingsmetoden vid sanering: Applicering av beslutsstödsverktyget SAMLA. (45 hp)
550. Andreasson, Dagnija, 2018: Assessment of using liquidity index for the approximation of undrained shear strength of clay tills in Scania. (45 hp)
551. Ahrenstedt, Viktor, 2018: The Neoproterozoic Visingsö Group of southern Sweden: Lithology, sequence stratigraphy and

provenance of the Middle Formation. (45 hp)

552. Berglund, Marie, 2018: Basaltkuppen - ett spel om mineralogi och petrologi. (15 hp)
553. Hernnäs, Tove, 2018: Garnet amphibolite in the internal Eastern Segment, Sveconorwegian Province: monitors of metamorphic recrystallization at high temperature and pressure during Sveconorwegian orogeny. (45 hp)
554. Halling, Jenny, 2019: Characterization of black rust in reinforced concrete structures: analyses of field samples from southern Sweden. (45 hp)
555. Stevic, Marijana, 2019: Stratigraphy and dating of a lake sediment record from Lyngsjön, eastern Scania - human impact and aeolian sand deposition during the last millennium. (45 hp)
556. Rabanser, Monika, 2019: Processes of Lateral Moraine Formation at a Debris-covered Glacier, Suldenferner (Vedretta di Solda), Italy. (45 hp)
557. Nilsson, Hanna, 2019: Records of environmental change and sedimentation processes over the last century in a Baltic coastal inlet. (45 hp)
558. Ingered, Mimmi, 2019: Zircon U-Pb constraints on the timing of Sveconorwegian migmatite formation in the Western and Median Segments of the Idefjorden terrane, SW Sweden. (45 hp)
559. Hjorth, Ingeborg, 2019: Paleomagnetisk undersökning av vulkanen Rangitoto, Nya Zeeland, för att bestämma dess utbrottshistoria. (15 hp)
560. Westberg, Märta, 2019: Enigmatic worm-like fossils from the Silurian Waukesha Lagerstätte, Wisconsin, USA. (15 hp)
561. Björn, Julia, 2019: Undersökning av påverkan på hydraulisk konduktivitet i förorenat område efter in situ-saneringsförsök. (15 hp)
562. Faraj, Haider, 2019: Tolkning av georadarprofiler över grundvattenmagasinet Verveln - Gullringen i Kalmar län. (15 hp)
563. Bjermo, Tim, 2019: Eoliska avlagringar och vindriktningar under holocen i och kring Store Mosse, södra Sverige. (15 hp)
564. Langkjaer, Henrik, 2019: Analys av Östergötlands kommande grundvattenresurser ur ett klimtperspektiv - med fokus på förstärkt grundvattenbildning. (15 hp)
565. Johansson, Marcus, 2019: Hur öppet var landskapet i södra Sverige under Atlantisk tid? (15 hp)
566. Molin, Emmy, 2019: Litologi, sedimentologi och kolisotopstratigrafi över krita–paleogen-gränsintervallet i borrningen Limhamn-2018. (15 hp)
567. Schroeder, Mimmi, 2019: The history of European hemp cultivation. (15 hp)
568. Damber, Maja, 2019: Granens invandring i sydvästa Sverige, belyst genom pollenanalys från Skottenesjön. (15 hp)
569. Lundgren Sassner, Lykke, 2019: Strandmorfologi, stranderosion och stranddeposition, med en fallstudie på Tylösand sandstrand, Halland. (15 hp)
570. Greiff, Johannes, 2019: Mesozoiska konglomerat och Skånes tektoniska utveckling. (15 hp)
571. Persson, Eric, 2019: An Enigmatic Cerapodian Dentary from the Cretaceous of southern Sweden. (15 hp)
572. Aldenius, Erik, 2019: Subsurface characterization of the Lund Sandstone – 3D model of the sandstone reservoir and evaluation of the geoenergy storage potential, SW Skåne, South Sweden. (45 hp)
573. Juliusson, Oscar, 2019: Impacts of subglacial processes on underlying bedrock. (15 hp)
574. Sartell, Anna, 2019: Metamorphic paragenesis and P-T conditions in garnet amphibolite from the Median Segment of the Idefjorden Terrane, Lilla Edet. (15 hp)
575. Végvári, Fanni, 2019: Vulkanisk inverkan på klimatet och atmorsfärcirkulationen: En litterarurstudie som jämför vulkanism på låg respektive hög latitud. (15 hp)
576. Gustafsson, Jon, 2019: Petrology of platinum-group element mineralization in the Koillismaa intrusion, Finland. (45 hp)

LUNDS UNIVERSITET

Geologiska institutionen
Lunds universitet
Sölvegatan 12, 223 62 Lund